



**POLITECNICO**  
MILANO 1863

**SCUOLA DI INGEGNERIA CIVILE, AMBIENTALE E TERRITORIALE**

**Laurea Magistrale in Ingegneria per l'Ambiente e il Territorio**

# **Assessment of the geothermal economic potential in the sedimentary basins of the Netherlands**

Supervisors: Dr Marco BINOTTI  
Dr Paola BOMBARDA  
Prof. Dr Martin O. SAAR  
Dr Daniel VOGLER  
Dr Benjamin ADAMS

Selene CREMONESI  
884098

Academic Year 2018–2019



---

---

*Quali sono i vostri sogni? Che cosa desiderate voi? Fare l'ingegnere?  
È giusto: ciò deve servire alla vostra vita materiale.  
Ma, e poi? Oltre la carne vi è in voi l'intelligenza, il cuore, la fantasia,  
che vogliono esser soddisfatte.  
Oltre l'ingegnere vi è in voi il cittadino, lo scienziato, l'artista. [...]  
Prima di essere ingegneri voi siete uomini.*

Francesco De Sanctis, *Prolusione letta nell'Istituto Politecnico di Zurigo*, 1856

---

---

## Acknowledgements

This thesis project was designed and carried out during my exchange experience (May 2019 – December 2019) at the Geothermal Energy and Geofluids (GEG) Research Group at ETH, Zurich. Thank you, Martin, for having hosted me in your amazing team. I am deeply grateful to Daniel for having accepted my application and guided me through the research process. I have learnt a lot from you also about teamwork, focus and purpose. Thank you very much. I feel obliged to Ben for all the advice and the punctual supervising activity. All those hours spent breaking down the tasks, evaluating strategies and solutions have taught me a smart method to address any kind of problems. Thanks to all the people at GEG this experience has been very empowering also beyond the academic level.

Then I want to acknowledge the invaluable supervision of Dr Binotti and Dr Bombarda, thanks to whom the analysis has been enriched by a case-specific power plant optimization as well. I am very grateful for all the knowledge you have shared with me and the time spent discussing together.

I dedicate this work to my family, you are the most supportive people I could have ever asked for.

---

# Table of Contents

<b>ACKNOWLEDGEMENTS .....</b>	<b>IV</b>
<b>TABLE OF CONTENTS .....</b>	<b>V</b>
<b>TABLE OF FIGURES .....</b>	<b>VII</b>
<b>ABSTRACT .....</b>	<b>X</b>
<b>EXTENDED ABSTRACT IN ITALIAN .....</b>	<b>XII</b>
<b>CHAPTER 1 INTRODUCTION .....</b>	<b>15</b>
1.1 GEOTHERMAL ENERGY IN SEDIMENTARY BASINS .....	20
1.2 DIRECT USE OF LOW-TEMPERATURE GEOTHERMAL SOURCES .....	21
1.3 ELECTRICITY GENERATION FROM LOW-TEMPERATURE GEOTHERMAL SOURCES .....	22
1.4 LEVELIZED COST OF ENERGY AS AN ECONOMIC METRIC .....	24
1.5 RESOURCE ASSESSMENT AND ECONOMIC POTENTIAL METHODS .....	24
<b>CHAPTER 2 CASE STUDY AND MODELLING TOOLS .....</b>	<b>31</b>
2.1 THE NETHERLANDS ENERGY FRAMEWORK .....	32
2.2 THERMOGIS DATASET .....	33
2.3 DOUBLET-CALC1D .....	37
2.4 GEOPHIRES .....	39
<b>CHAPTER 3 METHODOLOGY .....</b>	<b>47</b>
3.1 WORKFLOW AND SOFTWARE IN USE .....	48
3.2 DATA PRE-PROCESSING AND WELL-CONFIGURATION .....	49
3.3 SIMULATION HYPOTHESIS .....	52
3.4 HEAT POWER SIMULATION AND LCOH .....	56
3.5 ELECTRIC POWER SIMULATION AND LCOE .....	57
<b>CHAPTER 4 RESULTS .....</b>	<b>60</b>
4.1 HEAT POWER POTENTIAL AND LCOH .....	61
4.2 ELECTRIC POWER POTENTIAL AND LCOE EXPECTED .....	67
4.3 ELECTRIC POWER POTENTIAL AND LCOE LAZARD .....	73
<b>CHAPTER 5 ORC OPTIMIZATION .....</b>	<b>77</b>
5.1 GEOTHERMAL ORC TYPICAL CONFIGURATIONS .....	78

---

5.2 RESERVOIR A: ORC SIMULATION HYPOTHESIS AND RESULTS .....	79
5.3 RESERVOIR A: COMPARISON WITH GEOPHIRES RESULTS .....	85
<b>CHAPTER 6 CONCLUSIONS .....</b>	<b>87</b>
<b>BIBLIOGRAPHY.....</b>	<b>89</b>
<b>APPENDIX PROGRAM SCRIPTS AND INPUT FILES .....</b>	<b>93</b>



---

## Table of Figures

<i>Figure 1. Worldwide geothermal power plants classification. On the left, the installed capacity in MWe (and %) for each plant typology (total 12.6 GWe). On the right, the number of units (and %) for each plant typology (total 613). Taken from (Stimac James et al., 2015).</i>	17
<i>Figure 2. Map of geothermal systems capable of power production related to lithospheric plate boundaries. Geothermal systems producing electricity are represented by green circles while geothermal prospects that are likely to produce power in the future are in black x's. Dashed black lines are subduction and collision zones, solid red lines are spreading centres and dashed red lines are continental rifts. Installed geothermal capacity is shown by country in MWe. Taken from (Edenhofer et al., 2012).</i>	17
<i>Figure 3. Scheme showing convective hydrothermal systems taken from (Edenhofer et al., 2012).</i>	18
<i>Figure 4. Doublet scheme adapted from (Stober &amp; Bucher, 2013).</i>	21
<i>Figure 5. Scheme of the ORC power plant taken from (International Renewable Energy Agency, 2017).</i>	22
<i>Figure 6. Temperature ranges and power output of ORC plants according to the energy source. Taken from (Macchi, 2016).</i>	23
<i>Figure 7. Well coverage and seismic data taken from (NLOG.nl, n.d.).</i>	34
<i>Figure 8. Dutch sedimentary reservoirs characteristics elaborated starting from the data available on ThermoGIS (ThermoGIS, n.d.). Each point is a reservoir.</i>	36
<i>Figure 9. Doublet system scheme and segments where the mass, pressure and energy balance is performed by the model DoubletCalc1D. Taken from (Vrijlandt et al., 2019).</i>	38
<i>Figure 10. GEOPHIRES built-in utilization correlation for power plants taken from Beckers (2016). In this study, the subcritical ORC is simulated so the violet line is used.</i>	45
<i>Figure 11. Correlation functions for the power plant cost taken from (Koenraad F. Beckers &amp; McCabe, 2019).</i>	46
<i>Figure 12. Correlation functions for the well cost taken from (Koenraad F. Beckers &amp; McCabe, 2019).</i>	46
<i>Figure 13. Scheme of the work done in this study.</i>	47
<i>Figure 14. Workflow and software in use.</i>	48
<i>Figure 15. Details of the data pre-processing in QGIS.</i>	50

---

<i>Figure 16. Spatial discretization and well pattern.</i>	51
<i>Figure 17. Optimization of the flow rate in the best reservoir. The red dotted line intersects the minimum LCOE while the black dashed line intersects the maximum net power.</i>	59
<i>Figure 18. Heat power comparison between TNO results and GEOPHIRES results. The actual regression line is in red, while the ideal regression line is in black and represent the ideal case where the results of the two models perfectly overlap.</i>	61
<i>Figure 19. Comparison of the water specific heat correlations used in the two models (blue line and green line) as a function of reservoir temperature. The red dashed line is the DoubletCalc1D correlation considering salinity equal to 0 gNaCleqkgwater.</i>	62
<i>Figure 20. Comparison of the heat power obtained considering also in GEOPHIRES the reservoir temperature in the middle of the thickness instead of the top depth.</i>	63
<i>Figure 21. Comparison between the TNO classification and the LCOH obtained with GEOPHIRES. Only reservoirs with heat power equal or greater than 0.1 MW<sub>th</sub> are considered. Green and orange areas represent the percentage of reservoirs where the economic classifications of GEOPHIRES and TNO are in accordance.</i>	64
<i>Figure 22. Advantages of the LCOH map configuration proposed with this work.</i>	65
<i>Figure 23. Geothermal economic potential map of the Netherlands. On the left, the map produced by TNO taken from (Vrijlandt et al., 2019). After the technical simulation with DoubletCalc1D, TNO has assigned an economic potential class to each reservoir. The legend shows the classes going from “good” to “unknown”. On the right, the map of LCOH values obtained after the GEOPHIRES simulation. The LCOH values are grouped manually to resemble the TNO classes, as the UTC values calculated by TNO for each reservoir are not available.</i>	66
<i>Figure 24. LCOE and correspondent net electric power for the reservoirs where this is greater than 1 [MW<sub>e</sub>].</i>	67
<i>Figure 25. LCOE and characteristics of the 238 reservoirs above 1 MW<sub>e</sub> capacity. The black dashed box highlights the best reservoirs that are the ones with the lowest LCOE values.</i>	68
<i>Figure 26. LCOE expected map of the Netherlands. On the left, the map of the whole Netherlands showing a few places where the LCOE is below 500 €/ (MW h). On the right, the zoom on the more promising area, 20 km north from Groningen. The reservoirs A, B and C have the lowest LCOE and their characteristic are summarized in the following table. They all belong to the Upper Rotliegend Group, the RO STACKED basin.</i>	70
<i>Figure 27. Transmissivity of the Rotliegend Group taken from Mijnlief (2020). TYH is the structural geological domain. The dashed line separates the Zechtein seal area from the rest of the basin.</i>	72
<i>Figure 28. Electricity cost projection for European countries in 2030, taken from (Energy prices and costs in Europe., 2019).</i>	73
<i>Figure 29. LCOE obtained with Lazard economic hypothesis and with TNO hypothesis as a function of the cumulative capacity.</i>	74

---

---

<i>Figure 30. Zoom of the previous figure.</i>	75
<i>Figure 31. LCOE Lazard for the Netherlands and comparison with other sources. Adapted from Lazard's (2019).</i>	75
<i>Figure 32. Scheme of the ORC cycle configuration optimized for the reservoir A. This is a subcritical ORC where the working fluid is condensed with air at ambient temperature. Adapted from (Astolfi et al., 2014)</i>	80
<i>Figure 33. Plot of the heat exchanged between the geothermal fluid and the working fluid.</i>	80
<i>Figure 34. Plot of the ORC power and re-injection temperature as functions of the evaporation temperature.</i>	82
<i>Figure 35. T-s diagram of the ORC cycle in reservoir A.</i>	84
<i>Figure 36. Reservoir A: simulation in GEOPHIRES of the ORC power, pumping power and net electric power varying the flow rate. On the right the simulation done in the regional assessment using a re-injection temperature of 30 [°C]. On the right reservoir A is simulated again using the new re-injection temperature of 68.15 [°C] found with the Excel optimization.</i>	85

---

## Abstract

This study proposes and tests a methodology to assess the economic geothermal potential of heat and electricity power production in the sedimentary basins of the Netherlands. The chosen representative indicators are respectively LCOH (Levelized Cost of Heat) and LCOE (Levelized Cost of Electricity) both expressed in  $\left[\frac{\text{€}}{\text{MWh}}\right]$ .

The calculation is performed using GEOPHIRES as techno-economic model customized to run over a spatial grid whose basic unit is called *reservoir* having surface dimensions of 1 km by 1 km and variable thickness. Input values for each reservoir are taken from ThermoGIS, the Dutch public geothermal database provided by TNO (The Netherlands Organisation for applied scientific research). For the heat power potential assessment, ThermoGIS values of pumped flow rates are used as input for GEOPHIRES and the results are compared with the ones provided by TNO. Whereas for the electricity, the optimal pumped flow rate is found minimizing the LCOE for an ORC plant in each reservoir.

The main outputs are two maps of the whole Netherlands presenting the lowest values of LCOH and LCOE for each reservoir. The LCOH values match satisfactorily with the ThermoGIS economic classification while giving better defined information about the cost. The LCOE map provides the first assessment tool of the economic potential for electricity generation from geothermal sources in the Netherlands. The LCOE is additionally evaluated under the financial hypothesis proposed by Lazard's report (2019). This allows comparing the LCOE range with the ones from other renewable energy and conventional power plants.

The LCOE expected results show a potential of 100  $[MW_e]$  power available under 200  $\left[\frac{\text{€}}{\text{MWh}}\right]$  and 600  $[MW_e]$  power available under 400  $\left[\frac{\text{€}}{\text{MWh}}\right]$ . The most promising reservoirs are located in the Upper Rotliegend Group, a basin in the north within 20 km distance to Groningen. The LCOE under Lazard's hypothesis goes from 228  $\left[\frac{\text{€}}{\text{MWh}}\right]$  to 320  $\left[\frac{\text{€}}{\text{MWh}}\right]$  when considering an available capacity of 100  $[MW_e]$ .

---

For the electric power simulation, a trade-off between the lowest achievable cost and the highest available net power is detected and addressed with an ORC net power optimization for one reservoir using an Excel spreadsheet coupled with FluidProp. Particularly, 2.84 [ $MW_e$ ] ORC power is obtained with GEOPHIRES and 2.78 [ $MW_e$ ] with the Excel. When simulating the reservoir back in GEOPHIRES under the newfound conditions, the net electric power goes from 2.28 [ $MW_e$ ] to 2.12 [ $MW_e$ ] and the LCOE increases from 149 [ $\frac{\text{€}}{\text{kWh}}$ ] to 159 [ $\frac{\text{€}}{\text{kWh}}$ ]. This further analysis shows technical results compatible with the ones already obtained, supporting the reliability of the regional assessment proposed.

---

## Extended abstract in Italian

In questo studio viene proposto e applicato un nuovo metodo per valutare il potenziale economico sia per le applicazioni dirette del calore sia per la produzione elettrica a partire dall'energia geotermica estratta dai bacini sedimentari dell'Olanda. Si tratta di una risorsa geotermica a bassa temperatura essendo il gradiente di circa  $31 \left[ \frac{^{\circ}\text{C}}{\text{km}} \right]$  (Vrijlandt et al., 2019). Nei bacini sedimentari olandesi sono presenti 29 acquiferi che garantiscono la presenza in loco dell'acqua necessaria per trasportare il calore in superficie. L'estrazione di calore avviene attraverso un pozzo di produzione abbinato a un pozzo di reiniezione del fluido geotermico (l'acqua di falda raffreddata), garantendo così stabilità al sistema. La coppia di pozzi è nota in letteratura come *doublet*. Per la produzione elettrica viene considerato come ciclo termodinamico l'Organic Rankine Cycle (ORC) subcritico. Questa tecnologia è la più adatta per generare elettricità anche da sorgenti a bassa temperatura. Impianti ORC geotermici sono attivi commercialmente dagli anni '80 e sono in continuo sviluppo (Macchi, 2016).

L'indicatore scelto per rappresentare il potenziale economico è il costo medio di produzione dell'energia, rispettivamente LCOH (Levelized Cost of Heat) per il calore e LCOE (Levelized Cost of Electricity) per l'elettricità, entrambi espressi in  $\left[ \frac{\text{€}}{\text{MWh}} \right]$ . Un valore inferiore di LCOH o LCOE rende una certa alternativa di progetto preferibile a un'altra.

Il metodo proposto si basa su strumenti di calcolo e di elaborazione di dati territoriali ampiamente in uso che qui vengono combinati per ottenere *hot-spots maps* utili sia per la pianificazione territoriale pubblica sia per investimenti privati. I vantaggi principali del metodo sono la possibilità di calcolare nella stessa simulazione la potenza termica o elettrica insieme al rispettivo indicatore economico e l'interoperabilità di questi risultati con i sistemi GIS.

I dati di input e di output sono elaborati con il software open source QGIS (QGIS, n.d.). Il simulatore tecno-economico scelto è GEOPHIRES (Koenraad F. Beckers & McCabe, 2019), un codice open-source per i sistemi geotermici scritto in Python. È stato necessario implementare GEOPHIRES per rendere automatica la simulazione su una griglia spaziale la cui unità fondamentale è un volume di

---

acquifero qui chiamato *reservoir*, avente una superficie di 1 [km<sup>2</sup>] e spessore variabile. L'obiettivo infatti è una valutazione del potenziale a scala regionale e devono essere simulati centinaia di migliaia di reservoirs, tutti quelli individuati dalla discretizzazione dei dati spaziali di input. Questi provengono da ThermoGIS (*ThermoGIS*, n.d.), una piattaforma web con tutti i dati geotermici del sottosuolo olandese presentati come mappe, costruita, gestita e aggiornata da TNO (The Netherlands Organisation for applied scientific research). ThermoGIS non fornisce solo dati di input, ma anche mappe del calore ottenibile per usi diretti e il corrispondente potenziale economico. I reservoirs sono classificati in quattro gruppi: potenziale economico buono, moderato, indicativo, sconosciuto. Questi dati vengono utilizzati come benchmark per confrontare i risultati ottenuti con GEOPHIRES per la simulazione della potenza termica e del relativo potenziale economico. La potenza elettrica ottenuta e il relativo LCOE costituiscono invece la prima valutazione di questo tipo fatta in Olanda.

Per la produzione termica, vengono utilizzati come input i valori di portata forniti da ThermoGIS così da poter confrontare per ogni reservoir la potenza termica ottenuta. I risultati di GEOPHIRES confermano quelli già trovati da TNO. Per la produzione elettrica viene invece implementato in Python uno script per trovare la portata ottima che minimizzi l'LCOE per ogni reservoir simulato da GEOPHIRES. In questa fase viene individuato un trade-off tra il minimo costo raggiungibile e la potenza elettrica massima ottenibile. In GEOPHIRES e quindi per la valutazione a scala regionale si è scelto di minimizzare il costo. Nel caso del miglior reservoir trovato viene poi condotta un'ulteriore analisi per uno specifico reservoir. Questa è focalizzata sul ciclo termodinamico ed è realizzata tramite un apposito foglio Excel avente le funzionalità di FluidProp (*FluidProp*, n.d.). L'ORC viene ottimizzato per ottenere il massimo della potenza elettrica per il ciclo ed il valore così ottenuto risulta compatibile con quello precedentemente trovato: il calcolo dell'ORC consente inoltre di valutare la temperatura di reiniezione reale, che è un dato di input di GEOPHIRES. Si conferma così da un lato la subottimalità della potenza elettrica calcolata da GEOPHIRES quando viene minimizzato il LCOE e dall'altro l'affidabilità della valutazione a scala regionale.

Gli output principali dell'indagine sono due mappe dell'intera Olanda che presentano per ogni km<sup>2</sup> il reservoir avente il valore più basso di LCOH in un caso, e di LCOE nell'altro. I valori di LCOH sono in accordo con la classificazione economica proposta in ThermoGIS. Allo stesso tempo viene fornito un indicatore economico univoco per ogni reservoir rendendo possibile distinguere i reservoir migliori o peggiori anche all'interno di ogni classe individuata da TNO. La mappa dei LCOE mostra l'esistenza di un potenziale economico per la produzione elettrica da fonte

---

geotermica in Olanda. Si dimostra come non sia sempre consigliabile escludere a priori la possibilità di produrre energia elettrica a costi ragionevoli da una sorgente geotermica solo perché a bassa temperatura. Meglio quindi condurre una verifica in termini quantitativi.

Il LCOE è valutato sia con le stesse ipotesi economiche utilizzate per il calcolo del LCOH (LCOE atteso) sia con le ipotesi proposte dal report di Lazard (Lazard's, 2019). Lazard è una banca d'affari attiva nel settore della consulenza e il suo report annuale sui costi medi dell'energia da diverse fonti è un riferimento molto utilizzato anche in letteratura. Utilizzare anche le ipotesi di Lazard consente di confrontare il range di LCOE ottenuto con GEOPHIRES con i valori di LCOE di altre fonti di energia sia rinnovabili che convenzionali.

I risultati del LCOE atteso mostrano una capacità cumulativa di 100 [ $MW_e$ ] disponibili sotto 200 [ $\frac{\text{€}}{MW\ h}$ ] e 600 [ $MW_e$ ] disponibili sotto 400 [ $\frac{\text{€}}{MW\ h}$ ]. I reservoirs più promettenti sono localizzati nel bacino sedimentario Upper Rotliegend Group, a nord dell'Olanda entro 20 km da Groningen. Considerando una capacità cumulata da 2 [ $MW_e$ ] (il minimo ottenibile) a 100 [ $MW_e$ ], il range di LCOE atteso va da 149 [ $\frac{\text{€}}{MW\ h}$ ] a 200 [ $\frac{\text{€}}{MW\ h}$ ]. Lo stesso range valutato con le ipotesi di Lazard va da 228 [ $\frac{\text{€}}{MW\ h}$ ] a 320 [ $\frac{\text{€}}{MW\ h}$ ]. Convertendo questo range in [ $\frac{\text{\$}}{MW\ h}$ ] e confrontandolo con i LCOE da altre fonti, installare ORC in Olanda da fonte geotermica appare una soluzione al momento più costosa rispetto all'impiego di altre fonti energetiche. Bisogna però ricordare che il LCOE così calcolato non include né incentivi né i costi ambientali da rilascio di  $CO_2$ , evitati nel caso del geotermico e da sostenere nel caso delle fonti fossili.

A prescindere dalle considerazioni sul potenziale tecnico ed economico trovato nel caso particolare dell'Olanda, il metodo presentato si dimostra robusto e affidabile sia a livello regionale (individuazione dei reservoir più promettenti) sia in vista di una successiva progettazione di un impianto (valori di potenza termica ed elettrica ottenibile). Questo tipo di indagine può essere pertanto esteso ad altri bacini sedimentari in cui vengano forniti o si possano adeguatamente ipotizzare i dati di input fondamentali: temperatura del reservoir, spessore, profondità e permeabilità. Non solo, adattando opportunamente i parametri di GEOPHIRES, si possono simulare anche reservoir con fratture, impianti di produzione elettrica diversi dall'ORC subcritico e ottenere indicatori economici diversi dal Levelized Cost Of Energy. Come illustrato è poi possibile esportare i risultati in ambiente GIS e averne anche una rappresentazione spaziale.



---

# CHAPTER 1

## INTRODUCTION

Geothermal energy is defined as energy in the form of heat below the Earth's solid surface. Geothermal resources consist of thermal energy from the Earth's interior stored in both rock and trapped steam or liquid water.

Geothermal resources can vary significantly worldwide. Different classifications exist based either on the resource temperature, heat transfer mechanism or geological structure. Depending on rock and fluid properties and on the available technology, the subsurface heat can be exploited more or less successfully. The ultimate objective of the resource assessment is to estimate the power output of a target geothermal system. The correspondent cost represents the economic potential. There is not a standard procedure for the resource assessment and its accuracy depends on geophysical, geological and geochemical data availability and uncertainty.

In

*Table 1*, geothermal resources are classified according to their heat transfer mechanism (type), geological structure (subtype), resource temperature (temperature range) and correspondent utilization (Edenhofer et al., 2012). Hydrothermal resources are characterized by hot fluid in permeable hot rock and they can be economically exploited by drilling to bring hot fluid to the surface. They are convective systems because the heat moves with the hot fluid rising. Deep aquifers benefit from the high temperatures that can be found at depth even when the gradient is not very high. Hot-dry rocks occur in impermeable rocks that need to be artificially fracked and supplied with water. The heat flows within the rocks from a hot temperature to cold temperature with no fluid to carrying it, thus through a conductive mechanism.

According to the resource characteristics, either heat or electricity can be produced. Direct heat utilization is usually applied to systems with a temperature lower than 100-120 [°C] because even a small amount of heat can be efficiently exploited. Common uses are district heating and cooling, horticulture, industrial processes, bathing (Gudmundsson, 1988).

Higher temperatures make electric power production more advantageous.

Type	In-situ fluids	Subtype	Temperature range	Utilization	
				Current	Future
Convective (hydrothermal)	Yes	Continental	H, I, L	Direct use, power	
		Submarine	H	None	Power
Conductive (petrothermal)	No	Shallow (< 400 m)	L	Direct use (GHP)	
		Hot rock (EGS)	H, I	Prototypes	Direct use, power
		Magma bodies	H	None	Direct use, power
Deep aquifer	Yes	Hydrostatic	H, I, L	Direct use, power	
		Geo-pressured		Direct use, power	

Table 1. Classification of geothermal resources. Temperature range: H: High (>180 °C), I: Intermediate (100-180 °C), L: Low (ambient to 100°C). EGS: Enhanced (or engineered) geothermal systems. GHP: Geothermal heat pumps. Adapted from (Edenhofer et al., 2012).

Geothermal electricity generation relies mainly on technologies that exploit conventional geothermal resources, such as dry steam plants, flash plants (single, double and triple), binary plants, and combined-cycle or hybrid plants (Bertani, 2016). The first two plants are used for sources ranging from 200-350 [°C], where the subsurface fluid can be steam or a mixture of steam and water. The steam extracted is directly used in the turbogenerator as working fluid to produce electricity. These plants have the highest installed capacity worldwide *Figure 1* accounting together for the 86% of the total installed capacity which is 12.6 [GW<sub>e</sub>] (Bertani, 2016).

Dry steam and flash plants are built to exploit hydrothermal convective systems resulting from volcanic and tectonic activities. As shown in *Figure 2*, they are mainly located in correspondence to plate boundaries. The heat source is usually solidifying magma which easily replenishes the extracted heat. At the same time, the meteoric water recharges the fluid supply to the system. The same mechanism holds for geothermal systems found in aquifers relying on natural gradients which are way lower compared to the ones of the volcanic area. The average crust gradient is

around  $25 \left[ \frac{^{\circ}\text{C}}{\text{km}} \right]$  but in volcanic related geothermal systems it can go up to  $120 \left[ \frac{^{\circ}\text{C}}{\text{km}} \right]$  (Arnórsson et al., 2015).

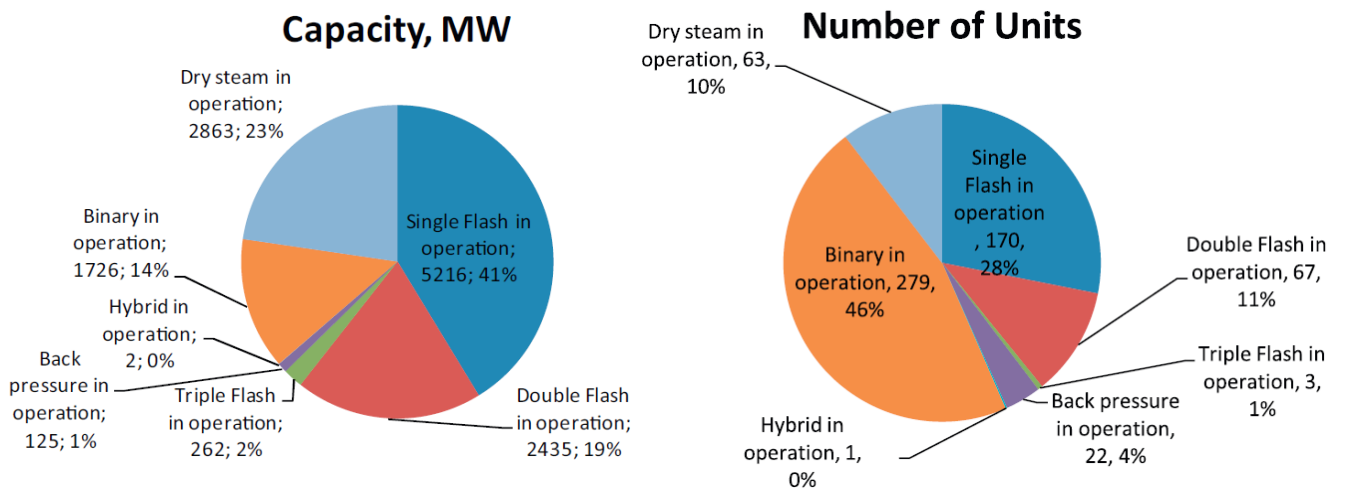


Figure 1. Worldwide geothermal power plants classification. On the left, the installed capacity in  $[MW_e]$  (and %) for each plant typology (total  $12.6 [GW_e]$ ). On the right, the number of units (and %) for each plant typology (total 613). Taken from (Stimac James et al., 2015).

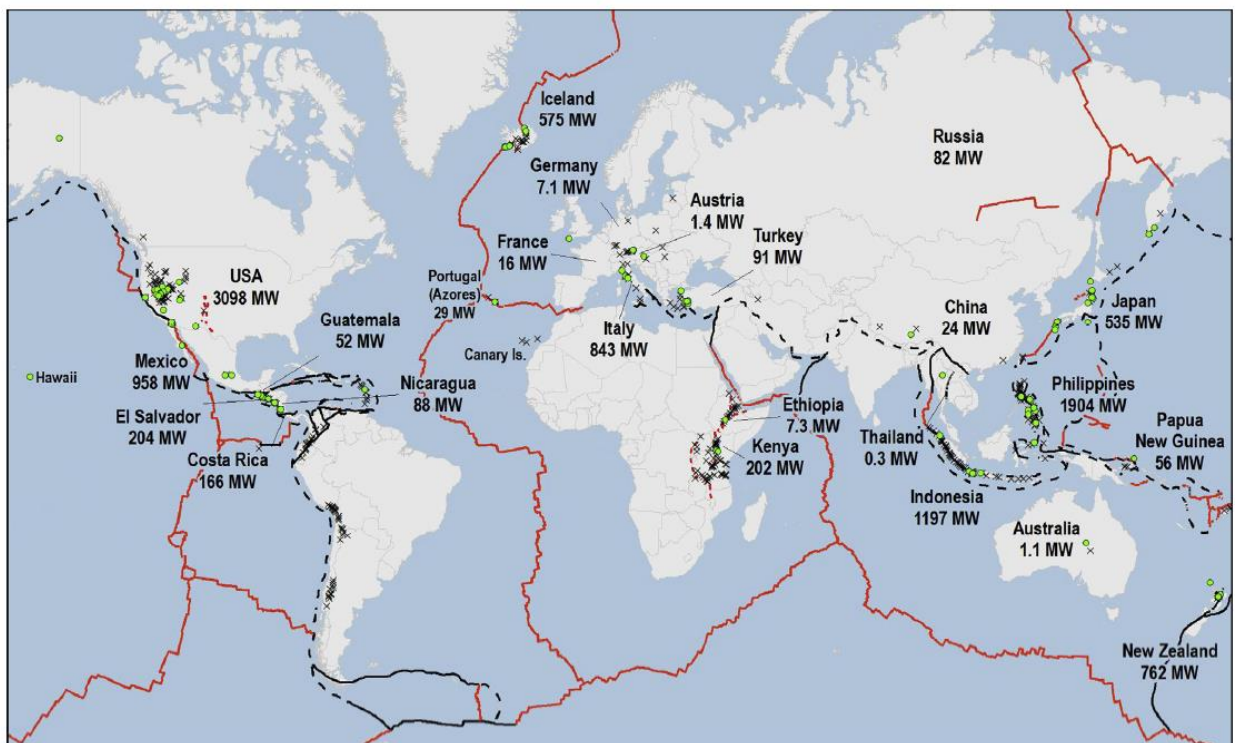
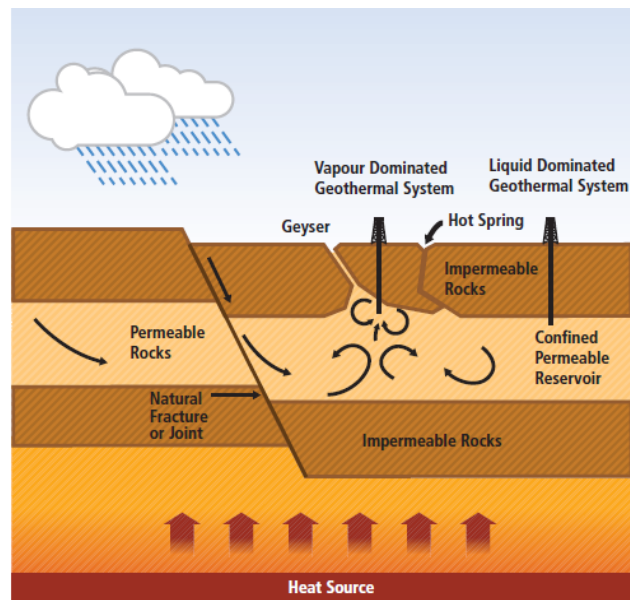


Figure 2. Map of geothermal systems capable of power production related to lithospheric plate boundaries. Geothermal systems producing electricity are represented by green circles while geothermal prospects that are likely to produce power in the future are in black x's. Dashed black lines are subduction and collision zones, solid red lines are spreading centres and dashed red lines are continental rifts. Installed geothermal capacity is shown by country in  $MW_e$ . Taken from (Edenhofer et al., 2012).

*Figure 3* shows the processes taking place in convective hydrothermal systems where water recharge is provided by precipitations and heat is continuously supplied by the source at the bottom. Layers of impermeable rocks are natural boundaries for a permeable rock layer hosting the geofluid and called *reservoir*. The heat flows up with a convection mechanism, carried by steam in vapour dominated geothermal systems and by water in liquid dominated geothermal systems. In both cases, drilling wells down to the permeable reservoir is the essential condition to exploit the subsurface heat. Secondary geothermal manifestations are geysers, fumaroles and hot springs.



*Figure 3. Scheme showing convective hydrothermal systems taken from (Edenhofer et al., 2012).*

The natural renewal of heat and fluid in hydrothermal systems qualifies for being a renewable energy source. This definition can't include Enhanced Geothermal Systems (EGS) as they refer to hot dry rocks where the permeability is enhanced by fracking and the circulating water is carried and injected to the site (Arnórrsson et al., 2015).

It is worth pointing out that the subsurface fluid is not pure water because the meteoric water penetrating in the subsurface interacts with minerals, rocks altered by high temperatures and magmatic constituents. This results in aqueous solutions with altered acidity and variable chemical compositions. For example, NaCl-fluids have a pH largely buffered by CO<sub>2</sub>, acid sulfate fluids contain H<sub>2</sub>SO<sub>4</sub> which controls the pH and sometimes HCl often from a magmatic origin (Stefánsson & Kleine, 2017). Saline fluids, usually called brine, derived from seawater intrusions can be found as

---

well. Evaluating the chemical compositions of the subsurface fluids is very important for the sake of the pipes and surface equipment. One of the major problems related to chemically altered geofluids is the scaling. This refers to the deposition of minerals - mostly amorphous silica and calcium carbonate – within the wells, pipes and turbine blades. This dramatically reduces the efficiency and the lifetime of the power plants components (DiPippo, 2016). Also, geofluids can contain non-condensable gases (NCG) such as carbon dioxide (CO<sub>2</sub>), hydrogen sulphide (H<sub>2</sub>S) and hydrogen (H<sub>2</sub>) (Schütz F., Huenges E., Spalek A., Paloma Pérez D. B., 2013). This means that they need to be treated to prevent discharge in the atmosphere.

On the other side, binary plants technology involves the reinjection of the whole geothermal fluid as it is used to heat another fluid which does the work in the power cycle. The working fluid of the power cycle, chosen for its appropriate thermodynamic properties, receives heat from the geofluid, evaporates, expands through a prime mover, condenses, and is returned to the evaporator by means of a feed pump (DiPippo, 2016). Organic fluids like hydrocarbons are used for this purpose and the power cycle is called Organic Rankine Cycle. This has two main advantages: no discharge of greenhouse gases in the environment and the possibility of exploiting even low-temperature sources for power production. Binary plants are already well developed worldwide accounting for 46% of power units installed (*Figure 1*) but have a smaller capacity reflecting the fact they are applied to low-temperature sources.

The development of geothermal energy for electricity production, particularly the low-impacting binary cycle plants, are promising options to increase the share of renewable and carbon-neutral energies (Holm et al., 2012). However, it has to be noted that anthropogenic CO<sub>2</sub> release occurs in the drilling phase and natural emissions can be related to volcanic sites. Quantifying geothermal natural and power plant emissions is a complicated task, greatly impacted by the variability between geothermal sites. On the other hand, replacing fossil fuel electrical generation with geothermal energy will result in a significant net reduction of greenhouse gas emissions and all their associated effects (Renewable Energy Agency, 2019).

There is almost a worldwide urge – at least in principle - for the transformation of the global energy system to meet the objectives towards carbon neutrality of the Paris Agreement signed in 2015 (*Paris Agreement*, n.d.). No net emissions of greenhouse gases within 2050 are one of the goals stated by the recently – 11<sup>th</sup> December 2019 – European Green Deal presented by the European Commission and supported by the Parliament (*The European Green Deal*, 2019). Decarbonising the

---

energy sector is among the proposed actions. In this context, geothermal energy provides a renewable energy source that has the potential to supply reasonable amounts of electricity, heating, and cooling (Anderson & Rezaie, 2019). Moreover, differently from wind and solar, it provides a baseload energy supply.

Thus being a low-carbon and non-intermittent technology the use of geothermal energy is expected to grow rapidly over the next several decades at many places in the world. By 2050 geothermal energy plants, partly in competition with renewables like solar and wind power, as well as with incumbent fossil fuel-based power production, could contribute approximately 2–3% to global electricity generation (van der Zwaan & Dalla Longa, 2019). In (Bertani, 2016) the expected geothermal targets for the year 2050 are 70 [ $GW_e$ ] from hydrothermal resources and 140 [ $GW_e$ ] in total, in this case being up 8.3% of total world electricity production.

The direct use of geothermal energy is increasing as well. An estimation of the installed thermal power for direct utilization at the end of 2014 equals 70'885 [ $MW_{th}$ ], 46.2% increase over the 2010 data, growing at a compound rate of 7.9% annually. Energy savings amount to 52.8 million tonnes of equivalent oil annually, preventing 149.1 million tonnes of  $CO_2$  being released to the atmosphere (Lund & Boyd, 2016).

Given the advantages of geothermal plants in low-temperature areas as well, it is worth assessing their viability in sedimentary basins.

## 1.1 Geothermal energy in sedimentary basins

Sedimentary basins are formed over hundreds of millions of years by the combined action of deposition of eroded material and precipitation of chemicals and organic debris within water environment. Over time continuing sedimentation occurs in the water environment and the additional weight caused subsidence (Onajite, 2014). Within sedimentary basins, aquifers can be defined as geologic units that are highly permeable and can store and transmit a significant amount of groundwater (Ge & Gorelick, 2015). According to the gradient, the aquifers can have favourable thermal properties like high temperature, high heat capacity of the water and thermal conductivity. This implies respectively an initial high heat content of the reservoir, a nice capacity of the water to carry the heat and an easy flow of the heat through the reservoir (Stober & Bucher, 2013). The described system is of the hydrothermal type and the way to exploit the heat is by drilling a well up to the target depth. The hot groundwater is pumped out from a production well, the heat is extracted and the colder water is injected back to the aquifer through the reinjection well. The couple formed by the production well and the injection well is called

doublet. *Figure 4* gives a visual representation of the scheme. The blue line is the undisturbed groundwater table while the red line follows the groundwater table boundary during operation that is while the water is pumped by the submersible pump. In the production well the depression cone can be noted and it is mirrored by the injection cone.

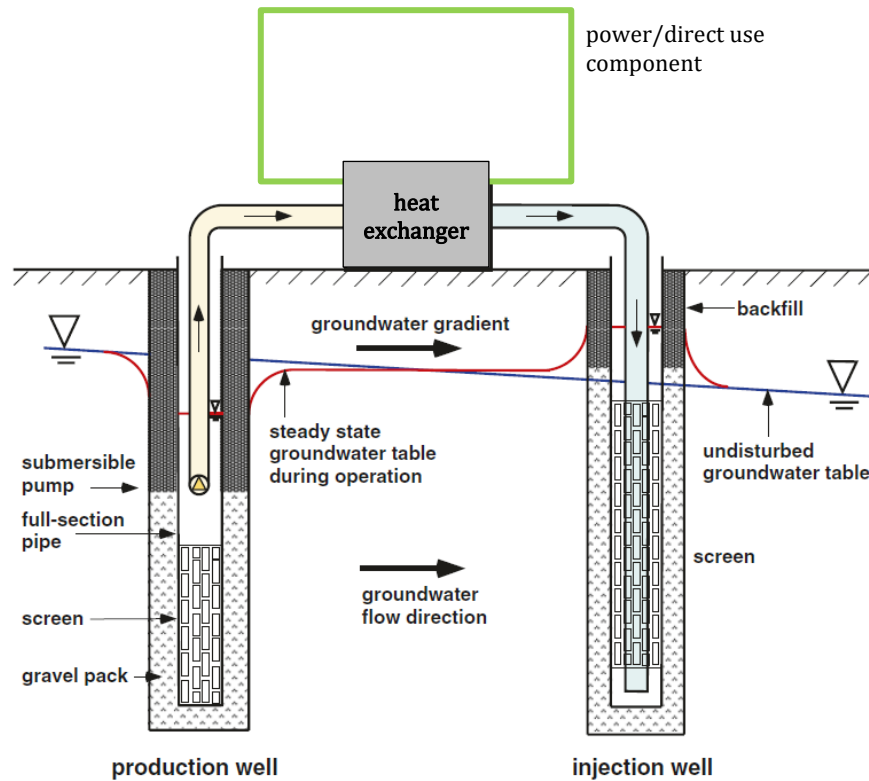


*Figure 4. Doublet scheme adapted from (Stober & Bucher, 2013).*

The two wells must not interfere thermally with each other. The re-injection of the cooled water should not be upstream of the production well. The injection well is placed normal to the hydraulic gradient (normal to the groundwater flow direction) or, second-best geometry, downstream from the production well (Stober & Bucher, 2013). It becomes clear that hydraulic and thermodynamic processes are intertwined.

## 1.2 Direct use of low-temperature geothermal sources

Direct applications of geothermal heat present good opportunities for increasing the revenue of a geothermal project (Moya et al., 2018). They are particularly interesting for low-temperature sources because they have heat exchange losses but not conversion losses.

Direct uses include a variety of applications. Lund and Boyd (Lund & Boyd, 2016) list the worldwide distribution of thermal energy used by category which is

---

approximately 55.2% for ground-source heat pumps, 20.2% for bathing and swimming (including balneology), 15.0% for space heating (of which 89% is for district heating), 4.9% for greenhouses and open ground heating, 2.0% for aquaculture pond and raceway heating, 1.8% for industrial process heating, 0.4% for snow melting and cooling, 0.3% for agricultural drying, and 0.2% for other uses.

Norden (Norden, 2011) described the typical district heating networks. They are fed by a small number of heating stations, which are located preferably close to the heat customers to avoid large energy losses when transporting the heat. The supply of district heat is characterised by supply temperatures between 50 [°C] and 90 [°C] and return temperatures between 30 [°C] and 70 [°C], sometimes even lower. In contrast to an annually constant heat demand for many industrial processes, the demand for space heating is characterised by a variable heat demand during the year.

### 1.3 Electricity generation from low-temperature geothermal sources

When the temperature and/or the thermal power available from the geothermal source is higher than in the previous case of direct heat use, but still limited, it becomes attractive to adopt a binary cycle known as ORC (Organic Rankine Cycle). *Figure 5* presents the scheme of this cycle. It is the characterization of the green squared line of *Figure 4* in the case of power production.

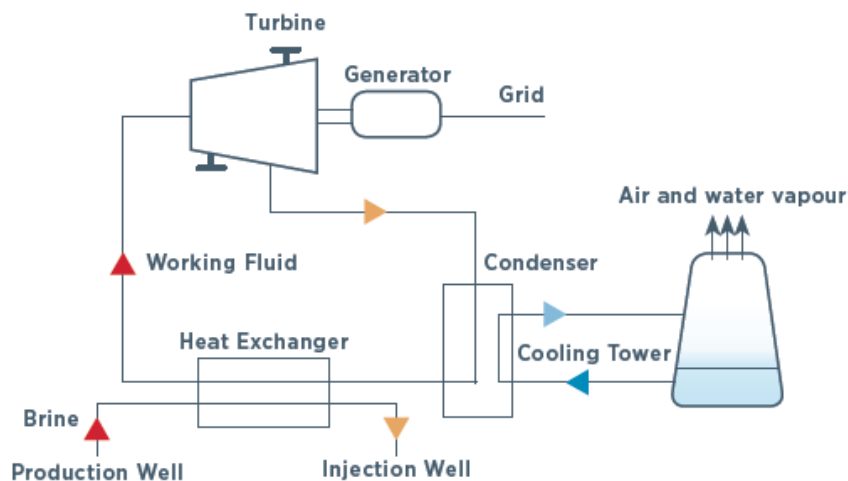


*Figure 5. Scheme of the ORC power plant taken from (International Renewable Energy Agency, 2017).*

The water coming from the subsurface is here called brine to stress that it is not pure water but there are other chemicals as well. The hot brine from the production well goes into the heat exchanger and releases heat to the working fluid. It becomes



colder and is reinjected back to the ground. The exploitation of a geothermal resource using binary technology is based on the utilization of a secondary fluid in the power cycle, which vaporizes in heat exchangers by receiving heat from the geothermal fluid. Working fluids for geothermal applications generally are low boiling, meaning that the evaporation takes place at a higher pressure than water saturation pressure at the same temperature (Macchi, 2016). The vaporized working fluid moves the turbine coupled with the electricity generator which transfers the power to the grid. The fluid is then condensed back to the liquid state. So it can enter again in the heat exchanger to receive heat from the geothermal brine and another cycle begins. Due to the low heat source temperatures, low condenser temperature and small temperature differences in the heat exchanger are very important (Walraven et al., 2013).

The cycle takes advantages of the thermodynamics properties of a changing phase working fluid to get power thus being a Rankine cycle. The adjective Organic refers to the working fluid which is usually an organic fluid differently from the original Rankine cycle which uses water.

The ORC technology is mature and worldwide present. *Figure 6* presents the different energy sources to which an ORC can be applied.

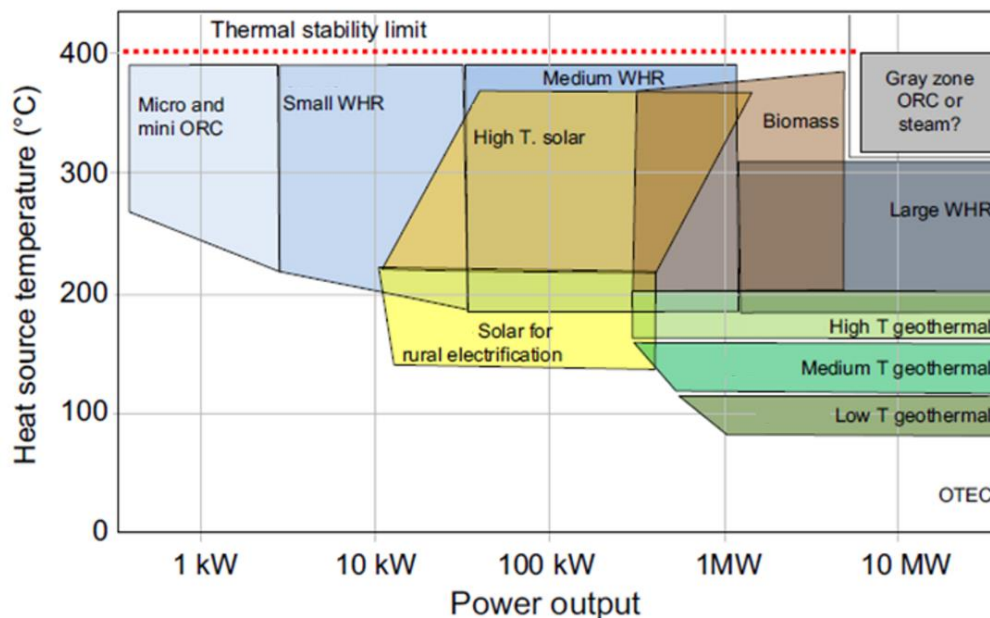


*Figure 6. Temperature ranges and power output of ORC plants according to the energy source. Taken from (Macchi, 2016).*

For each source, a range of input temperature and correspondent power output is identified. Low-temperature geothermal sources have a power output ranging from around 1 [ $MW_e$ ] up to more than 10 [ $MW_e$ ] given a source temperature around 100

---

[°C]. As of 2015, one of the first ORC manufactures, Ormat (*Ormat*, n.d.), has built approximately 500 modules in the power range of 1 to 25 [ $MW_e$ ] (Macchi, 2016).

## 1.4 Levelized Cost of Energy as an economic metric

When evaluating the opportunity of initiating a power production project, one of the main criteria influencing the choice is the economic one. The most used indicator is the levelized cost of energy (LCOE). In the work of Aldersey-Williams and Rubert (Aldersey-Williams & Rubert, 2019), this metric is compared with other indicators to highlight its strengths and weaknesses. Although widely accepted as a measure of the comparative lifetime costs of generation alternatives, the LCOE lacks a theoretical foundation in the academic literature. The authors aim to bridge this gap.

Among the analyzed indicators, the LCOE defined by the Department for Business, Energy & Industrial Strategy (BEIS) in the UK has proven to be widely used to compare energy alternatives both by national energy departments and commentators. This LCOE is defined as discounted total costs (excluding finance costs) divided by discounted total energy. It gives as output the constant real price required to generate Investment Return Rate equal to the discount rate. So it returns a meaningful metric equivalent to the minimum economic price.

The principal strengths of this metric are simplicity, sophistication, interpretation, and adoption. The study highlights the major drawbacks in the sensitivity to the discount rates, the treatment of inflation, and dealing with uncertainty in future costs. These rates reflect the weighted average cost of capital (WACC). This has the effect of raising the LCOE for technologies considered to be riskier, and potentially skews the metric in favour of apparently less risky technologies. As the discount rate reflects the project risk, it is also important to recognise that the appropriate discount rate to be applied can change through a project's life. As for the inflation and changes in future costs, they have a greater impact when comparing renewable generation alternatives with thermal ones.

Aldersey-Williams and Rubert point out that over a full life cycle, the costs of thermal plants are dominated by operating and fuel costs which has proven to be highly variable timewise. Renewables are dominated by the capital costs, which are less susceptible to the effects of inflation, as they take place over a limited period (and can potentially be limited by contractual arrangements).

When using this metric, as in this work, it is good being aware of the pros and cons this choice implies.

---

## 1.5 Resource assessment and economic potential methods

As previously mentioned, the main objective of the resource assessment is to quantify how much power can be obtained from a target geothermal area. Usually, the scale of the analysis is a regional or country level. When coupled to economic potential assessment, the quantification of the project cost is included. The output is usually a hot-spot map identifying the most promising places for a geothermal power plant development.

When approaching a resource assessment, the first problem to arise is the lack of a standard procedure. This results in a wide variety of tools which changes across the countries. Geothermal databases have different design and purposes worldwide. For example, the Canadian one is not fully accessible but it is possible to buy the shapefiles with the most interesting information about the subsurface and the heat potential (*CanGEA*, n.d.). The availability of subsurface data is crucial for any resource estimate. In Alaska, for example, all the geothermal data are from one campaign of the early 80s mostly based on the thermal and chemical analysis of the surface geothermal manifestations that are hot springs (*Data.gov*, n.d.). The available maps don't extrapolate these data for the surroundings of the hot-spring data points and are not coupled with the geological formations. So there is no indication of source depth, target rock thickness or temperature at depth. Data about the rock porosity from which the permeability can be derived are of key importance as well. Depth influences the well drilling feasibility and cost. The temperature at depth and thickness are used to estimate the amount of available heat. However, the permeability determines whether and how easily the heat can be extracted. For example, in southern Italy, the Vigor project collects the subsurface data with power and economic potential estimate presented as maps. The products can be downloaded for free (*vigor-geothermia.it*, n.d.). Unfortunately, the permeability maps are not available making it difficult to simulate the heat extraction from a doublet over time.

The lack of a standard procedure gives freedom to the analysts in terms of methodology. To date, the volumetric method and reservoir simulation remain the most appropriate tools to use for geothermal resource assessment. The former method is the recommended approach for projects that are still at the early stage of development, while the latter technique is for predicting sustainable production capacity after exploration drilling (Ciriaco et al., 2020). The volumetric method consists of identifying a volume of rock defined by the spatial resolution of the available data. The heat content of this volume is calculated and then a theoretical percentage for the recoverable heat is used. The volumetric method is also known as

---

*heat in-place method*, originally outlined by USGS (Muffler & Cataldi, 1978). A more refined estimate can be done including a probabilistic approach (Garg & Combs, 2015). When data about groundwater flow and/or permeability are available, the rock volume can be modelled as a reservoir with water circulating through the doublet (see again 1.1). This allows having a better estimate of the heat, power and eventually cost compared to the volumetric method.

The sedimentary basins can represent a very fortunate case study to apply a preliminary reservoir simulation even before the test drilling by using subsurface data already available from oil and gas exploration wells. In sedimentary basins, hydrocarbons are formed by organic evolution. Oil and gas are generated when large quantities of organic (plants and animals) debris are continuously buried in deltaic, lake and ocean environment (Onajite, 2014). The sedimentary basins of Europe have been exploited since the 1850s. There is a long history of exploration, production and consumption of oil and gas in many parts of Europe, as well as of oil- and gas-related science and technology, much of which had a profound influence on the oil and gas industry worldwide. Several European countries, among them France, Germany and Italy, have an important oil heritage, rich in invention and technology, even though they never achieved globally significant levels of conventional oil production. Britain, Norway, Denmark and The Netherlands were largely self-sufficient in oil and gas from the late 1970s and early 1980s, following the discovery of oil and gas under the North Sea (Craig et al., 2018). This means there is a lot of log-data from oil and gas wells to characterize the subsurface. However, they might not publicly available everywhere since they might belong to the oil and gas companies which can be either private or governmental.

The Netherlands represents a unique example of punctual and almost complete subsurface characterization. The good data coverage of The Netherlands is due to almost 6000 wells both onshore and offshore historically used to search for oil and gas (Vrijlandt et al., 2019). These data are accessible free thanks to the Dutch mining law from 1831 which states that all acquired subsurface data becomes publicly available after five years (*Dutch Mining Act*, n.d.). Data must be supplied to TNO, the Netherlands Organisation for applied scientific research (*TNO.nl*, n.d.) which is an independent organisation regulated by public law. TNO fields of work are very wide, including AI, defence, circular economy, building and infrastructure, energy transition and environment. At the request of the Dutch Ministry of Economic Affairs, the TNO's Geological Survey of the Netherlands has developed a web GIS database NLOG (*NLOG.nl*, n.d.) which collects all the available information about the Dutch subsurface. They provide not only a 3D model of the geological

---

formations and aquifers but also a dedicated GIS platform for the geothermal assessment, ThermoGIS (*ThermoGIS*, n.d.). It provides depth, thickness, porosity and permeability maps of many potential aquifers in the Netherlands at a spatial resolution of 1 km<sup>2</sup>. Moreover, geothermal performance maps are calculated with the use of an integrated, stochastic, techno-economic performance module. In this framework, the technical simulation of the doublet system is performed by the model DoubletCalc1D (H F Mijnlief et al., 2014) built by TNO. The most important outputs of ThermoGIS are geothermal potential maps of the Netherlands. The power potential is measured in [ $MW_{th}$ ] and four classes of economic potential are defined: good, moderate, indication, unknown. The different Dutch areas are classified accordingly in the correspondent maps. The maps can be explored online and downloaded as raster files. TNO's analysis brings great improvement to the generic volumetric assessment. The methodology designed ad-hoc in this work represents a further improvement as shown in *Table 2*.

As previously mentioned, the first step is the identification of the basic unit which is the reservoir. ThermoGIS provides all the necessary characteristics (depth, thickness, temperature at depth and permeability) at a spatial resolution of 1 [ $km^2$ ]. The resulting volumes of 1 [ $km^2$ ] surface and variable thickness are defined as reservoirs. When using the volumetric method, the simple equations in *Table 2* are used. The reservoir energy is a function of the listed reservoir characteristics while the recovery factor and conversion efficiency are percentages taken from literature. The cost estimate is mainly influenced by the depth and power output and usually based on literature as well. The main drawback of the volumetric method is that the power estimate is not data-driven.

TNO has overcome this disadvantage by using a doublet simulator. The newly introduced variable is the pumped water mass-flow rate which is not to be confused with the natural groundwater flow. Thanks to the flow rate, the heat and pressure losses can be modelled as well as the heat transport mechanism, refining the quantification of the heat recoverable over time. Instead of applying theoretical percentages, the process is modelled based on the physics of the system using DoubletCalc1D. However, electricity production is not considered because the geothermal source is low-temperature, the gradient being around 31 [ $\frac{^{\circ}C}{km}$ ] (Vrijlandt et al., 2019) and DoubletCalc1D is not designed to evaluate electric power. The cost is estimated starting from the depth data following a procedure which is not described in ThermoGIS reference study (Vrijlandt et al., 2019). Instead, the output map is available showing the economic potential represented by qualitative classes.

**GEOHERMAL RESOURCE ASSESSMENT IN THE NETHERLANDS**

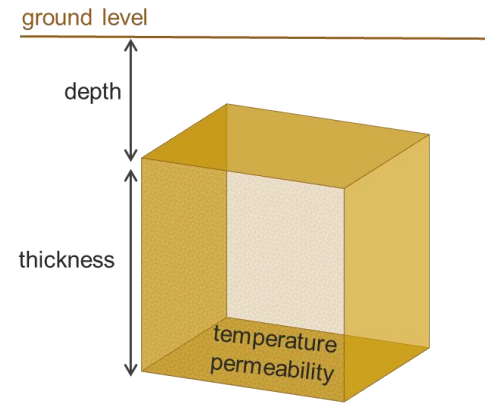
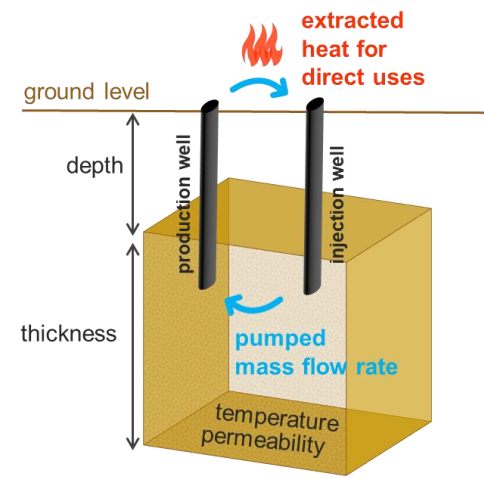
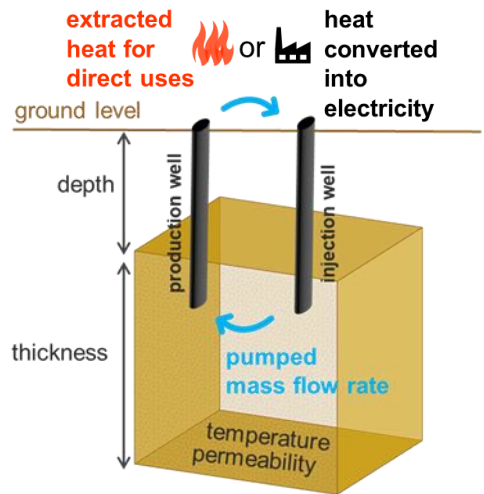
	<b>Volumetric Method</b>	<b>ThermoGIS improvement</b>	<b>This work improvement</b>
<b>Reservoir characteristics</b>			
<b>Power Estimate</b>	<p><b>Heat</b></p> $P_{th} = \frac{\text{Reservoir Energy} \times \text{Recovery factor}}{\text{Utilization Time}}$ <p><b>Electricity</b></p> $P_e = P_{th} \times \text{Conversion efficiency}$	<p><b>Heat</b></p> simulated with the technical model DoubletCalc1D <p><b>Electricity</b></p> not considered because it is a low-temperature source	<p><b>Heat</b></p> simulated using the same mass flow rate as DoubletCalc1D <p><b>Electricity</b></p> simulated using an (economically) optimized mass flow rate for an ORC (Organic Rankine Cycle)
<b>Cost Estimate</b>	It is usually a function of <b>depth</b> and <b>power</b> .	Evaluated with another model (procedure not available). It is mainly a function of <b>depth</b> . The reservoirs are finally sorted in 4 classes: Good – Moderate – Indication (Poor) – Unknown	Function of <b>depth, power, well diameter</b> . Expressed with a numerical indicator in <b>[€/ (MW h)]</b> : <b>LCOH</b> (Levelized Cost of Heat) or <b>LCOE</b> (Levelized Cost of Electricity). Simulated all at once by adapting the techno-economic model GEOPHIRES.

Table 2. Comparison of the geothermal resource assessment methods and outcome done in the Netherlands. The first column presents a generic volumetric method, the second one shows the improvements made by the TNO when producing the ThermoGIS maps. The third one highlights the improvement achieved thanks to the methodology developed with this study.

---

The resource assessment methodology designed for this work allows evaluating both heat and electric power with their correspondent economic numerical indicators all at once. This is possible thanks to the techno-economic model GEOPHIRES developed by Beckers and McCabe (Koenraad F. Beckers & McCabe, 2019). This is an open-source code written in Python that simulates one reservoir at a time. It can be chosen among six different types of geothermal reservoirs ranging from fractured to sedimentary. The results of TOUGH (the suite of Simulators for Nonisothermal Multiphase Flow and Transport in Fractured Porous Media) can be coupled as well (*TOUGH*, n.d.). Any configuration of the wells can be set, not only a doublet. Five different power plants can be simulated: direct heat, single- or double- flash, subcritical or supercritical ORC. There are three different options for the economic metrics: the Net Present Value (NPV), the standard (see definition in 1.4) Levelised Cost of Energy (LCOE or LCOH in the case of direct heat uses) and the Bicycle LCOE which includes additional and detailed financial hypothesis. Depending on the study area, the user has to write a customized input file and manually set the correspondent simulation parameters. In this case study, the chosen reservoir is the closest one to the sedimentary basin. The doublet configuration allows the use of the ThermoGIS results as a benchmark for the heat power simulation. As the geothermal source is low-temperature, the ORC technology is tested considering the widely used subcritical case (Astolfi et al., 2014). The standard LCOH and LCOE are chosen because they are the most used metric for energy comparisons as already discussed in 1.4.

The computational novelties of the designed method are both making GEOPHIRES running automatically over more than a hundred thousands of reservoirs and at the same time performing an optimization of the pumped flow-rate to get the lowest LCOE in the case of electric production. The optimization is not present in the available open-source code and a new script was written for this purpose.

The great advantage of the proposed methodology is the evaluation of the economic potential with a numeric metric univocally attached to each reservoir instead of a qualitative class as in the case of ThermoGIS. Not only all the reservoirs can be ranked accordingly, but also under the appropriate hypothesis, the cost of producing a unit of energy from geothermal source can be compared to the levelized costs of other sources. In this perspective, the maps of LCOH and LCOE for the Dutch subsurface become very powerful tools both for public and private development. Moreover, the technical and economic potential of electric production from geothermal source is evaluated for the first time in the Netherlands.

---

The methodology is discussed in details in the following chapters. In particular, in chapter 2 the sedimentary basins of the Netherlands and ThermoGIS dataset are described together with the Dutch energy policy. DoubletCalc1D, the simulator used in TNO's method is compared to GEOPHIRES considering its setting suitable for this case study. Chapter 3 presents the workflow set-up for this analysis. It includes ThermoGIS maps pre-processing to get the reservoir input data, the Python coding to run both the direct heat simulation and the optimization of the electric production cost and the post-processing of the results to obtain the final maps. The results are discussed in chapter 4. Chapter 5 gives an insight into the optimization of the ORC cycle in one target reservoir. The most promising reservoir is chosen then the working fluid evaporation temperature and the geothermal reinjection temperature are optimized using an excel spreadsheet. This further analysis at a local scale shows technical results compatible with the ones already obtained, supporting the reliability of GEOPHIRES as a tool for the regional assessment. The trade-off between the lowest achievable cost and the highest available net power is addressed here. In chapter 6 the conclusions are presented both about the methodology used and the specific results obtained for the Netherlands.



---

## CHAPTER 2

# CASE STUDY AND MODELLING TOOLS

Temperature-wise the Dutch geothermal source is classified in the low-temperature class. The average geothermal gradient in the Netherlands is  $31 \left[ \frac{^{\circ}\text{C}}{\text{km}} \right]$  with an average surface temperature of  $10 [^{\circ}\text{C}]$  (Harmen F. Mijnlief, 2020). From a hydrogeological viewpoint, the subsurface of the Netherlands is dominated by a regional aquifer, consisting of medium-grained Plio-Pleistocene fluvial sand with a thickness ranging from 25 to 250 [m]. The aquifer is at the surface in the eastern half of the country and dips below semi-confining layers of lagoonal clay and peat in the western coastal area (de Vries, 2007). The web geothermal database ThermoGIS presents a refined subclassification of the regional aquifer depending on the sedimentary geological host formation (*ThermoGIS*, n.d.). This allows including the information about the permeability differences in the subsurface which is a key element in the geothermal assessment. The Netherlands has been interested in geothermal development for some decades (Harmen F. Mijnlief, 2020). Paragraph 2.1 discusses the role of geothermal in the Dutch energy policy framework. An insight into the ThermoGIS database is given in paragraph 2.1. This represents the state of the art of the geothermal resource assessment in the Netherlands. ThermoGIS heat power results are calculated with the TNO's technical simulator, DoubletCalc1D, described in paragraph 2.3. To understand differences and similarities with the simulator used in this work, GEOPHIRES is described in paragraph 2.4 and compared to DoubletCalc1D.

---

## 2.1 The Netherlands energy framework

The electricity production in the Netherlands in 2017 came for 45% from natural gas, 32% from coal, 13% from renewable energy, 4% from oil, 3% from nuclear energy and 3% from other sources (*ebn.nl*, 2019). Wind turbines generated the largest share of this total, with 58%, followed by biomass with 29%. Almost 13% was generated by solar panels, while the share of hydropower was limited to 0.5%. However, being the total consumption of 3157 PJ (both heat and electricity) in 2017, 41% consumption relied on natural gas, 39% on petroleum and 12% on coal. Slightly more than 8% came from renewable sources, nuclear energy and waste (*cbs.nl*, 2018). So far the Netherlands has had a CO<sub>2</sub>-intensive economy. Due to the continuing large shares of fossil fuels in industry and power generation sectors, the energy sector is significantly responsible for it (Musch, 2018). Approximately half of the energy for industrial consumption is generated using petroleum raw materials and products. Coal is used for the production of electricity, iron and steel (*cbs.nl*, 2018). However, the government's decision in March 2018 to terminate gas extraction by 2030 will lead to changes in the energy system (Musch, 2018).

The Netherlands has chosen to actively embrace the transition to low-carbon energy supply, implementing a strategy with short and long terms goals. The objective for 2030 is a 49% reduction of greenhouse gas emissions, and then keeping with a gradual transition towards 80% to 95% CO<sub>2</sub> reduction in 2050 (*Energy Agenda Towards a low-carbon energy supply*, 2017). Energy savings, biomass, clean electricity production and the capture and storage of CO<sub>2</sub> (CCS) are likely to be robust elements in the energy mix on the road to 2050. The electricity market is transitioning toward renewable energy sources. In eight years, offshore wind farms will generate enough electricity for five million households. There will be no place for new coal-fired power plants in this transition and the electricity market needs to intensify the focus on the least polluting technologies. The innovation tasks will form an integral part of these transition paths. Along with compliance with the European climate agreements, the implementation of this policy (*Energy Agenda Towards a low-carbon energy supply*, 2017) aims to exploit economic opportunities.

The subsidy scheme (SDE+) is a governmental tool for pursuing climate goals. Geothermal development projects are eligible under certain criteria, but only direct use is considered. ThermoGIS economic classification is based on compliance with the SDE+ scheme. TNO evaluated under which percentage they are eligible for being subsidized meaning that the development is economically viable. Also, the technical lifetime is simulated according to the duration of public financing (*rvo.nl*, 2019). Using geothermal energy source for district heating and supporting part of the

---

heat supply to the industrial sector is a precise action of the overall strategy as around 40% of Dutch emissions are due to heat consumption. At the same time, the dependence of natural gas is reduced, especially after the decision to gradually phasing out the Groningen gas field taken in March 2018 due to social security reasons linked to the seismic sensitivity of the area (*govenment.nl*, 2018). It is useful to note that the geothermal sources are located in the same reservoirs/aquifers in which the oil and gas accumulations are hosted.

By January 2019, part of the Dutch geothermal strategy has successfully been implemented. 24 geothermal systems are in operation or under construction. 22 devoted to greenhouse heating, 1 for district heating and 1 for greenhouse and district heating. Total geothermal heat production in 2018 was 3.7 [PJ] from 18 geothermal systems (Harmen F. Mijnlief, 2020).

## 2.2 ThermoGIS dataset

ThermoGIS is a public, web-based geographical information system with the main goal of supporting companies and the government to develop geothermal energy in the Netherlands. ThermoGIS provides depth, thickness, porosity and permeability maps of many potential aquifers in the Netherlands. Geothermal performance maps for direct-use are calculated with the use of an integrated, stochastic, techno-economic performance module called DoubletCalc1D. The most important outputs of ThermoGIS are geothermal heat power potential maps of the Netherland (*ThermoGIS*, n.d.).

The geological characteristics of the Dutch subsurface are assigned to each point by elaborating well log-data. There is a good data coverage of the Netherlands thanks to almost 6000 wells (*Figure 7*) both onshore and offshore historically used to search for oil and gas. These data are accessible free thanks to the Dutch mining law from 1831 (*Dutch Mining Act*, n.d.) which states that all acquired subsurface data becomes publicly available after five years.

TNO has elaborated the log-data and organized them into ThermoGIS dataset. 29 basins are identified plus the stacked layers which cluster some of the basins in 5 groups.

*Table 3* presents their names and geological classification. These basins are selected as they are aquifers known to have sufficiently high flow properties from available subsurface data (Vrijlandt et al., 2019). When a stacked layer is identified, all the correspondent formations are piled up (where they are present) and considered to act as a single aquifer. That is possible because there are no sealing layers within the stacked formation belonging to the same group.

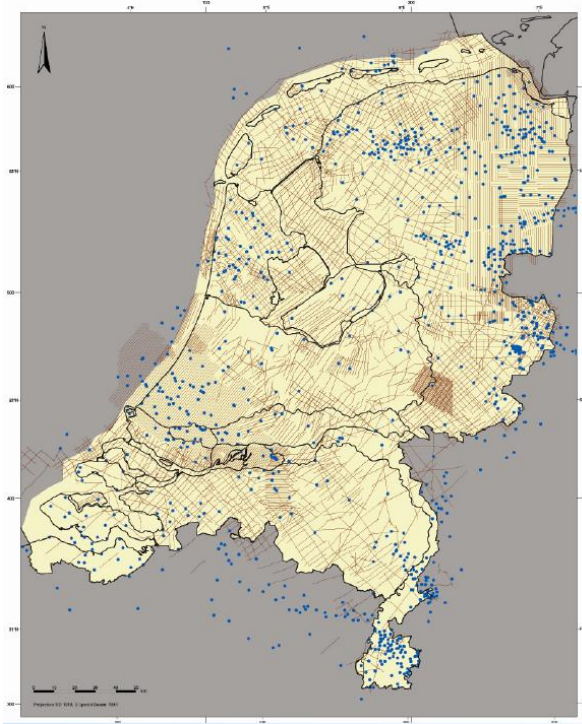


Figure 7. Well coverage and seismic data taken from (NLOG.nl, n.d.).

TNO has elaborated for each basin a map for:

- the thickness [m]
- the depth of the aquifer top [m]
- the temperature [°C]
- the permeability [mD]

For each basin map, there is a data value every squared kilometre. It has to be noted that these subsurface parameters are the results of a previous stochastic elaboration of the borehole data done by TNO. Each available datum is the median of the triangular distribution that describes a subsurface parameter in each squared kilometre. These median values are taken as input for the study of this work.

Figure 8 summarizes the characteristics of the Netherlands basin: each point is a reservoir of 1 [km<sup>2</sup>]. On the x-axis, there is the transmissivity which is the product between thickness and permeability. This quantity is more representative than the two characteristics taken singularly. On the y-axis, there is the depth of the reservoir. The colours give the third dimension of the analysis which is the temperature. The geothermal source has already been classified as low-temperature, the subsurface gradient being on average 31  $\left[\frac{^{\circ}\text{C}}{\text{km}}\right]$  (Vrijlandt et al., 2019).

Formation/ Member code	Formation / Member	Stacked layers
NMVFS	Someren Member	Middle & Lower North Sea Groups: N_STACKED
NMVFV	Voort Member	
NMRFT	Steensel Member	
NMRFV	Vessem Member	
NLFFS	Brussel Sand Member	
NLFFD	Basal Dongen Sand Member	
NLLFR	Reusel Member	
NLLFS	Heers Member	
KNGLG & KNGLS	Holland Greensand & Spijkenisse Greensand members	Rijnland Groups: KN_STACKED
KNNSG	Gildehaus Sandstone Member	
KNNSL	De Lier Member	
KNNSY	IJsselmonde Zandsteen Member	
KNNSB	Berkel Sandstone Member	
KNNSR	Rijswijk Member	
KNNSF & KNNSP	Friesland & Bentheim Sandstone members	
SLDN (SLDNA & SLDND)	Alblasserdam & Delft Sandstone members	Jurassic Groups
RNROF	Röt Fringe Sandstone Member	Upper- & Lower Germanic Triassic Groups: R STACKED
RNSOB	Basal Solling Sandstone Member	
RBMH	Hardegsen Formation	
RBMDU	Upper Detfurth Sandstone Member	
RBMDL	Lower Detfurth Sandstone Member	
RBMVU	Upper Volpriehausen Sandstone Member	
RBMVL	Lower Volpriehausen Sandstone Member	
RBSHN	Nederweert Sandstone Member	
ROSL & ROSLU	Slochteren Formation & Upper Slochteren Member	Upper Rotliegend Group: RO STACKED
ROSL	Lower Slochteren Member	
DCH (DCHS & DCHL)	Hunze Subgroup (Strijen & De Lutte formations)	Limburg Group: DC_STACKED
DCD (DCDH & DCDT)	Dinkel Subgroup (Hellevoetsluis & Tubbergen formations)	
CLZL	Zeeland Formation	Carboniferous Limestone Group

Table 3. Dutch sedimentary basins adapted from (Vrijlandt et al., 2019).

The gradient is homogeneous as the figure shows: the temperature classes draw a clear horizontal pattern with regards to the depth. This means that reservoirs at the same depth have also the same temperature. It can be further noticed that the shallow reservoirs in red in the range of 22-40 [°C] still have high transmissivity, in principle allowing for the exploitation of even cold reservoirs close to the surface.

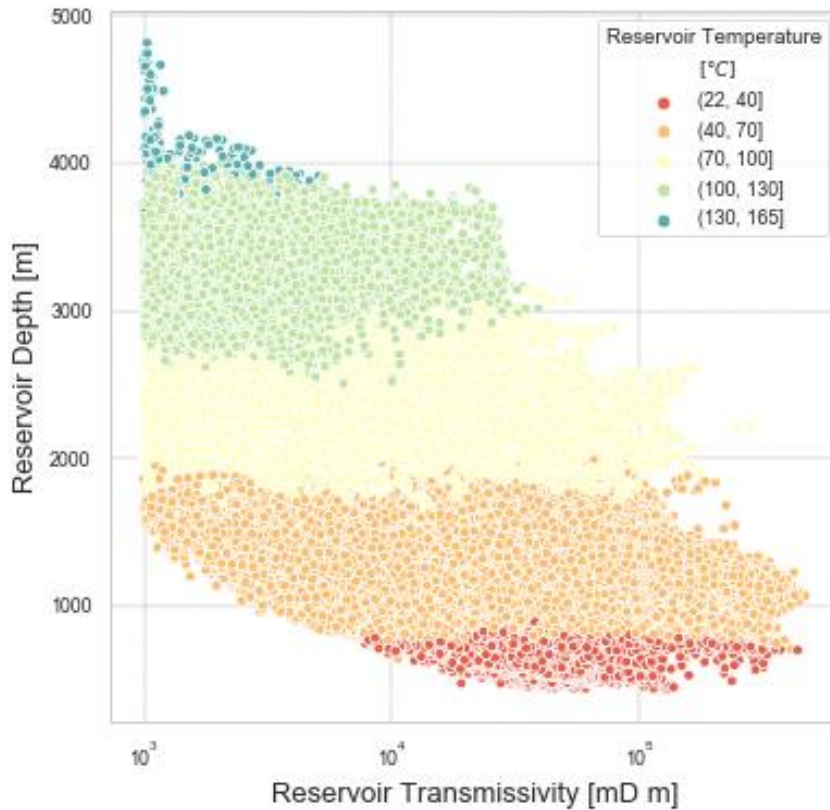


Figure 8. Dutch sedimentary reservoirs characteristics elaborated starting from the data available on ThermoGIS (ThermoGIS, n.d.). Each point is a reservoir.

Applying the DoubletCalc1D technical model, TNO has produced for each basin a map of:

- flow rate  $\left[\frac{m^3}{h}\right]$
- heat power  $[MW_{th}]$

The flow rate is used as input while the heat power is taken as a benchmark for this study.

As already introduced in paragraph 1.5, TNO has done an economic assessment as well. The procedure is not explained in details but briefly described in (Vrijlandt et al., 2019). After the economic evaluation, TNO has given the reservoirs a UTC (Unit Technical Cost) in  $\left[\frac{\text{€ct}}{kW h}\right]$ . This UTC are probabilistic values as a result of the stochastic approach used, that is the Monte-Carlo simulation starting from the triangular distribution of the subsurface parameter. Even if the UTC has the same dimensions as the LCOH used in this work, it is not possible to do a comparison between these two values as the UTC are not published. Actually, each reservoir is classified comparing the probability distribution of the UTC output with a threshold value. The only available output is the final map of the economic potential showing the classified reservoirs.

---

The classes and the classification rules are:

- Unknown: UTC P10 > reference price → class 1
- Indication: UTC P10 < reference price → class 2
- Moderate: UTC P30 < reference price → class 3
- Good: UTC P50 < reference price → class 4

The reference price is  $5.1 \left[ \frac{\text{€ct}}{\text{kWh}} \right]$  equivalent to  $51 \left[ \frac{\text{€}}{\text{MWh}} \right]$ , which corresponds to the threshold set by the SDE+ (Dutch subsidy scheme presented in paragraph 2.1) for geothermal energy. P10 is the 10% probability given to the occurrence of that UTC, P30 is the 30% probability, P50 is the 50% probability and reflect the stochasticity of the input used by TNO.

The economic cost functions are not available either the UTC values as TNO has produced a map only for:

- economic classes [–]

The comparison between these economic classes and the LCOH output of this work analysis can't be a straightforward operation. The procedure is discussed in the result paragraph 4.1.

The ThermoGIS dataset includes other maps with the same kind of output (flow rate, heat power, economic potential) but evaluated for other three scenarios: heat pump, well stimulation and the combination of heat pump and well simulation. This study considers only the base case scenario presented above.

## 2.3 DoubletCalc1D

The DoubletCalc1D is the model used by TNO to evaluate the geothermal heat power and correspondent flow-rate in the sedimentary basin of the Netherlands. It does not simulate electric power either the costs.

It is based on a geothermal doublet and takes into account the geological aquifer uncertainty. The uncertainty is expressed by setting a mean, a median and a maximum value as input for each reservoir parameters. This is the triangular probability distribution used for the Monte-Carlo simulation already mentioned in paragraph 2.2.

The reservoir geological inputs are:

- the permeability [ $mD$ ]
- the gross thickness [ $mD$ ]
- net-to-gross fraction [–] of useful thickness
- groundwater salinity [ $ppm$ ]
- depth of the top aquifer [ $m$ ]

The aquifer is modelled as homogeneous, with a uniform thickness, net-to-gross

ratio, permeability, salinity. Correlations have been used to determine the relevant water properties that are density, viscosity and heat capacity. Density is a function of pressure, temperature and salinity. Viscosity and heat capacity are functions of temperature and salinity (H F Mijnlief et al., 2014).

The model performs a mass, pressure and energy balance in each segment of the system, labelled from 1 to 11 in *Figure 9*:

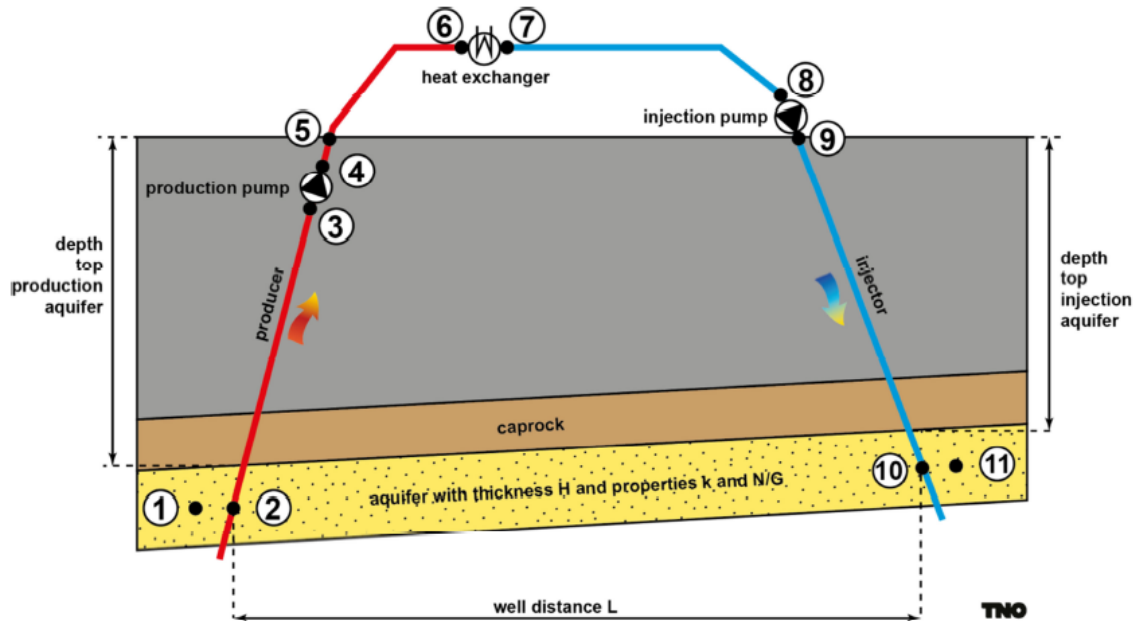


*Figure 9. Doublet system scheme and segments where the mass, pressure and energy balance is performed by the model DoubletCalc1D. Taken from (Vrijlandt et al., 2019).*

The mass flow  $\left[\frac{kg}{s}\right]$  is constant in the doublet system from the intake in the production well until the injection in the aquifer, because it is a closed system.

The sum of the pressure differences over all elements in the system is zero. The pressure balance determines the mass flow at a given pump pressure. The losses considered are (H F Mijnlief et al., 2014):

- pressure loss caused by flow in the aquifer to the production well and from the injection well;
- pressure loss in the production and injection wells as a result of friction by flow;
- pressure difference caused by gravity;
- pressure difference caused by the pump in the production well.

In the energy balance, the release of heat to the immediate surroundings of the well and temperature drop in the heat exchanger are taken into account.

The salinity is constant and equal to the salinity of the aquifer water. For the calculation of the hydrostatic pressure, it is assumed that the salinity increases



linearly with depth from zero at surface level to the specified median value at the target reservoir level (H F Mijnlief et al., 2014).

It is implicitly assumed that the entire aquifer has been drilled and completed. The model also assumes, in principle, that the aquifer is drilled vertically.

The model calculates the output listed below.

Geothermal power:

$$P_{th} = \dot{m} c_{p_{water}} \Delta T_{he} \quad [MW_{th}] \quad (1)$$

$\dot{m}$  is the mass flow which is constant in the system  $\left[\frac{kg}{s}\right]$

$c_{p_{water}}$  is the water heat capacity at the inlet of the heat exchanger (point 6 in Figure 9)  $\left[\frac{kJ}{kg}\right]$

$\Delta T_{he}$  is the temperature difference between the fluid inlet and outlet of the heat exchanger  $[^{\circ}C]$

Required pump power:

$$P_{pump,net} = \frac{\dot{m}}{\rho} \Delta p_{pump} \quad [MW_e] \quad (2)$$

$\dot{m}$  is the mass flow which is constant in the system  $\left[\frac{kg}{s}\right]$

$\rho$  is the water density  $\left[\frac{kg}{m^3}\right]$

$\Delta p_{pump}$  is the pressure development in the pump which is a constant specified by the user  $[Pa]$

Currently, the software ignores a possible relationship between  $\Delta p_{pump}$  and  $\frac{\dot{m}}{\rho}$ . The pump efficiency is not considered.

DoubletCalc1D does not include equations to evaluate the electric power production either the costs.

## 2.4 GEOPHIRES

GEOPHIRES is a Python code to perform techno-economic simulations of geothermal energy systems. It is open-source and available on GitHub (Beckers, 2020). The simulated output includes the reservoir production temperature and instantaneous and lifetime surface plant heat and/or electricity production. Combined with capital and operation and maintenance (O&M) cost correlations, GEOPHIRES applies leveled cost models to estimate the overall required investment and leveled cost of electricity and/or heat (LCOE and LCOH). Possible end-use configurations are direct-use heat (e.g., for district heating or an industrial

---

process), electricity, and cogeneration or combined heat and power (CHP). Ground-source heat pumps are not considered (Koenraad F. Beckers & McCabe, 2019).

According to the type of study, different combinations of parameters and equations can be set. Here all the options are listed then the equations used in the study are discussed and compared to DoubletCalc1D if possible.

Differently from DoubletCalc1D, GEOPHIRES does not perform a Monte-Carlo simulation. The considered geofluid is pure water and for density, viscosity, heat capacity and vapour pressure correlations are provided as functions only of the temperature. Salinity is not considered while it is used in DoubletCalc1D. In GEOPHIRES the mass flow rate is an input influencing the pumping power needed. On the other hand, in DoubletCalc1D the needed pumping power is set as an input while the mass flow rate is an output but not related to the  $\Delta p_{pump}$ .

Whereas DoubletCalc1D is specifically designed for a geothermal doublet into a hydrothermal aquifer, GEOPHIRES can simulate also hot rock environments suitable for EGS. There are six available reservoir models (Koenraad F. Beckers & McCabe, 2019):

- multiple parallel fracture models;
- monodimensional heat sweep model, suitable for fractured geothermal reservoirs;
- mass loading (m/A) thermal drawdown parameter suitable for single-fractured geothermal reservoirs;
- percentage temperature drawdown model;
- generic user-provided temperature profile;
- coupling with *TOUGH2 Geothermal Reservoir Simulator (TOUGH, n.d.)* for non-isothermal multiphase flow in fractured porous media.

Each of these options come with a specific set of parameters. The choice depends on the heat and flow mechanism to be represented. According to the available input data from ThermoGIS, the percentage temperature drawdown model is chosen. This allows representing the reservoir in the simplest way possible.

Independently on the reservoir model chosen, the heat losses in the production wells can be set to a constant value or the built-in Ramey's model can be used. In this work, Ramey's model is enabled which is valid for vertical wells only. It gives an approximate solution to the wellbore heat-transmission problem. The solution assumes that heat transfer in the wellbore is steady-state, while heat transfer to the earth will be unsteady radial conduction (Ramey, 1962). The geofluid temperature drop in the production wells, due to the heat losses towards the earth is expressed as  $\Delta T_{prod}$ :

---


$$\Delta T_{prod} = (T_{r,0} - T_w) - \omega(L - \Gamma) + (T_w - \omega\Gamma - T_{r,0}) \exp\left(\frac{L}{\Gamma}\right) \text{ [}^\circ\text{C]} \quad (3)$$

$T_{r,0}$  is the initial rock temperature at the bottom of the well [°C]

$T_w$  is the geofluid temperature at the bottom of the well [°C]

$\omega$  is the average geothermal gradient  $\left[\frac{^\circ\text{C}}{\text{m}}\right]$

$L$  is the reservoir depth [m] which is equal to the length of the well, assuming vertical wells

$\Gamma$  is calculated assuming that the thermal resistances of the casing and the cement are negligible.

$$\Gamma = \frac{\dot{m} c_{p_{water}} f(t)}{2\pi r_{res}} \text{ [m]} \quad (4)$$

$\dot{m}$  is the production wellbore flow-rate  $\left[\frac{\text{kg}}{\text{s}}\right]$

$c_{p_{water}}$  is the specific heat capacity of the water  $\left[\frac{\text{kJ}}{\text{kg K}}\right]$

$r_{res}$  is the reservoir thermal conductivity  $\left[\frac{\text{W}}{\text{m K}}\right]$

$$f(t) = -\ln\left(\frac{D}{4\sqrt{\alpha t}}\right) - 0.29 \quad (5)$$

$D$  is the well diameter [m]

$t$  is the time step [year]

$\alpha$  is the reservoir diffusivity  $\left[\frac{\text{m}^2}{\text{s}}\right]$

The temperature drop is obtained by Ramey (Ramey, 1962) starting from the equation of the heat transferred from the fluid to the formation along the infinitesimal depth  $dz$ :

$$\frac{dq}{dz} = \frac{2\pi r_{res} \Delta T_{prod}}{f(t)} \left[\frac{\text{W}}{\text{m}}\right] \quad (6)$$

In DoubletCalc1D the heat loss per unit length follows from (Garcia-Gutierrez et al., 2002):

$$\frac{dq}{dz} = \frac{4\pi r_{res} \Delta T_{prod}}{\ln\left(\frac{16\alpha t}{1.78D^2}\right)} \left[\frac{\text{W}}{\text{m}}\right] \quad (7)$$

Equation (7) is rearranged from the DoubletCalc1D manual (H F Mijnlief et al., 2014) so that it is clear it has the same structure as equation (6).

It can be proved they are actually the same one.

a. Equation (5) is re-written in a compact form:

$$\begin{aligned}
f(t) &= -\ln\left(\frac{D}{4\sqrt{\alpha t}}\right) - 0.29 = \ln\left(\frac{4\sqrt{\alpha t}}{D}\right) - \ln(1.3364) \\
&= \ln\left(\frac{4\sqrt{\alpha t}}{1.3364D}\right)
\end{aligned} \tag{8}$$

b. The denominator of equation (7) is rearranged and compared it to (8):

$$\ln\left(\frac{16\alpha t}{1.78D^2}\right) = \ln\left(\frac{4\sqrt{\alpha t}}{1.3364D}\right)^2 = 2 \ln\left(\frac{4\sqrt{\alpha t}}{1.3364D}\right) = 2 f(t) \tag{9}$$

c. By substituting (9) in (7), (6) is obtained:

$$\frac{dq}{dz} = \frac{4\pi r_{res} \Delta T_{prod}}{\ln\left(\frac{16\alpha t}{1.78D^2}\right)} = \frac{4\pi r_{res} \Delta T_{prod}}{2 f(t)} = \frac{2\pi r_{res} \Delta T_{prod}}{f(t)} \tag{10}$$

The mass flow-rate is constant as the doublet is a closed system and it is set as an input. The pressure balance determines the required total pumping power given the mass flow-rate. While DoubletCalc1D set the pressure increase in the pump as an input and the mass flow-rate is an output.

The injection and production well pumping power is estimated in GEOPHIRES by calculating the frictional and hydrostatic pressure drop in the well and the reservoir pressure drop (Koenraad F. Beckers & McCabe, 2019).

For the injection and production wells pressure drop  $\Delta p_{prod, inj}$  the Darcy-Weisbach equation is used:

$$\Delta p_{prod, inj} = f \rho_{water, well} \frac{v^2 L}{2 D} [Pa] \tag{11}$$

$\rho_{water, well}$  is the temperature-averaged density of the water in each well  $\left[\frac{kg}{m^3}\right]$

$v$  is the average water velocity in the well  $\left[\frac{m}{s}\right]$

$f$  is the Darcy friction factor [-]

The Darcy friction factor is calculated differently whether the flow in the wells is laminar or turbulent. The flow is considered laminar when the Reynolds Number  $Re < 2300$ , turbulent when  $Re > 2300$  and it is a function of the well flow-rate.

For the laminar flow, the Darcy friction factor is:

$$f = \frac{64}{Re} [-] \tag{12}$$

For the turbulent flow, the Darcy friction is calculated iteratively until convergence of the Colebrook-White equation:

$$\frac{1}{\sqrt{f}} = -2 \log\left(\frac{\varepsilon}{3.7 D} + \frac{2.51}{Re \sqrt{f}}\right) [-] \tag{13}$$

$\varepsilon$  is the wellbore pipe surface roughness set to 0.0001 [m]

---

The hydrostatic pressure drop  $\Delta p_{well,hydro}$  is calculated as:

$$\Delta p_{well,hydro} = \Delta \rho_{water,well} g L \text{ [Pa]} \quad (14)$$

$\Delta \rho_{water,well}$  is the water density difference between

the production and the injection wells  $\left[\frac{kg}{m^3}\right]$

$g$  is the gravitational acceleration  $9.81 \left[\frac{m}{s^2}\right]$

The reservoir pressure drop  $\Delta p_{res}$  is calculated as:

$$\rho_{water,res} = \rho_{water,well}(0.1T_{inj} + 0.9T_{res,out}) \text{ [Pa]} \quad (15)$$

$T_{inj}$  is the temperature of the injected water  $[^{\circ}C]$

$T_{res,out}$  is the temperature of the extracted water  $[^{\circ}C]$

$$\Delta p_{res} = \frac{I N \dot{m}}{\rho_{water,res}} \text{ [Pa]} \quad (16)$$

$I$  is the impedance  $\left[\frac{Pa s}{kg}\right]$

$N$  is the number of production wells

The overall pressure drop is the sum of all the components:

$$\Delta p = \Delta p_{prod,inj} + \Delta p_{well,hydro} + \Delta p_{res} \text{ [Pa]} \quad (17)$$

So the required pump power is:

$$P_{pump,net} = \frac{\Delta p N \dot{m}(1 + w_{loss})}{\rho_{water,inj} \eta_{pump}} \text{ [MW}_e\text{]} \quad (18)$$

$w_{loss}$  is the fraction of water loss [-]

$\rho_{water,inj}$  is the water density at the injection well  $\left[\frac{kg}{m^3}\right]$

$\eta_{pump}$  is the pump efficiency [-]

$P_{pump,net}$  is the total pump power required to make the system work. This can be covered by a suitable amount of pumps. The number of pumps and their location is not a problem addressed by GEOPHIRES but is left to a subsequent design phase which is beyond the purpose of this study. Compared to equation (18), the equation (2) for pumping power in DoubletCalc1D does not include the pump efficiency. In this work, no water loss is considered.

The geothermal heat power is calculated the same way as DoubletCalc1D (equation 1) where:

$$P_{th} = \dot{m} c_{p,water} \Delta T_{he} \text{ [MW}_{th}\text{]} \quad (19)$$

---

If the electricity is the end-use option, the power production is calculated by multiplying the utilization efficiency of the power plant  $\eta_u$  with the exergy of the produced geothermal fluid  $B$  (Koenraad F. Beckers & McCabe, 2019):

$$P_e = \eta_u B [MW_e] \quad (20)$$

$$B = \dot{m} \left( h_{prod} - h_0 - T_0 (s_{prod} - s_0) \right) [MW] \quad (21)$$

$T_0$  is the ambient temperature which in this study is 283.65 [K]

$h_{prod,0}$  is the water enthalpy in the production well and at the ambient temperature  $\left[ \frac{kJ}{kg} \right]$

$s_{prod,0}$  is the water entropy in the production well and at the ambient temperature  $\left[ \frac{kJ}{kg K} \right]$

In GEOPHIRES code, the exergy is calculated with a direct correlation of the production well water temperature that already accounts for the heat losses calculate with equation 3:  $B = f(T_{res} - \Delta T_{prod})$ .

GEOPHIRES calculates the power production under the hypothesis of a heat source at a constant temperature. The utilization efficiency  $\eta_u$  is equivalent to the second law efficiency:

$$\eta_{II} = \frac{P_{useful}}{W_{rev}} = \frac{P_e}{B} = \eta_u [-] \quad (22)$$

The second law efficiency is the ratio between the useful work  $P_{useful}$  and the reversible work  $W_{rev}$ . The useful work  $P_{useful}$  is the obtained electric power (equation 20) and the reversible work  $W_{rev}$  is calculated using the exergy of the geofluid which is water circulating in the wells. Exergy is the theoretical limit for the work potential that can be obtained from a source or a system at a given state when interacting with a reference state (environment) at a constant condition. When the final state is the dead state, the reversible work equals exergy. In this study, the dead state is the set to the Netherlands ambient conditions of 1 atm and 10.5 [°C] so that the reversible work can be calculated as exergy. As the chosen technology is the ORC, in this work  $P_e$  is called  $P_{ORC}$ .

GEOPHIRES provides built-in correlation of the utilization efficiency and geofluid production temperature for sub- and supercritical ORC and single- and double-flash power plants (K. F. Beckers, 2016). The utilization efficiency of ORC and flash power plants has been validated by the author using  $\eta_u$  of existing geothermal power plants (DiPippo, 2004), shown in *Figure 10* with square markers. For each resource temperature, a working fluid maximizing the utilization efficiency is chosen from 25 organic fluids. However, the fluid choice is embedded in the correlation itself. The available outputs are the utilization efficiency and the ORC power  $P_e = P_{ORC}$ .

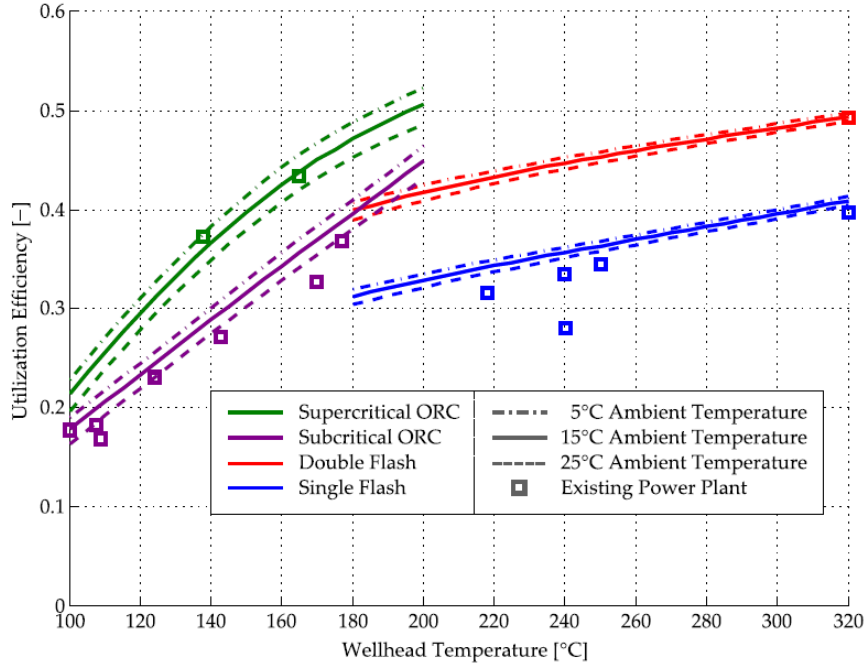


Figure 10. GEOPHIRES built-in utilization correlation for power plants taken from Beckers (2016). In this study, the subcritical ORC is simulated so the violet line is used.

The net electric power  $P_{el,net}$  (23) is then obtained by subtracting the pumping power  $P_{pump,net}$  (18) to the electric power  $P_e$  (20):

$$P_{el,net} = P_e - P_{pump,net} [MW_e] \quad (23)$$

Differently from DoubletCalc1D, GEOPHIRES has a component for the economic assessment as well. This is made of built-in cost correlation functions for capital and operational and management costs. They are again based on the analysis of existing power plants (K. F. Beckers, 2016). These correlations are functions of depth, power capacity and well diameter. The considered costs are listed in Table 4.

Examples of these correlation functions are given in Figure 11 and in Figure 12.

From the costs, the LCOH and LCOE indicators are evaluated using the equations shown in paragraph 3.4.

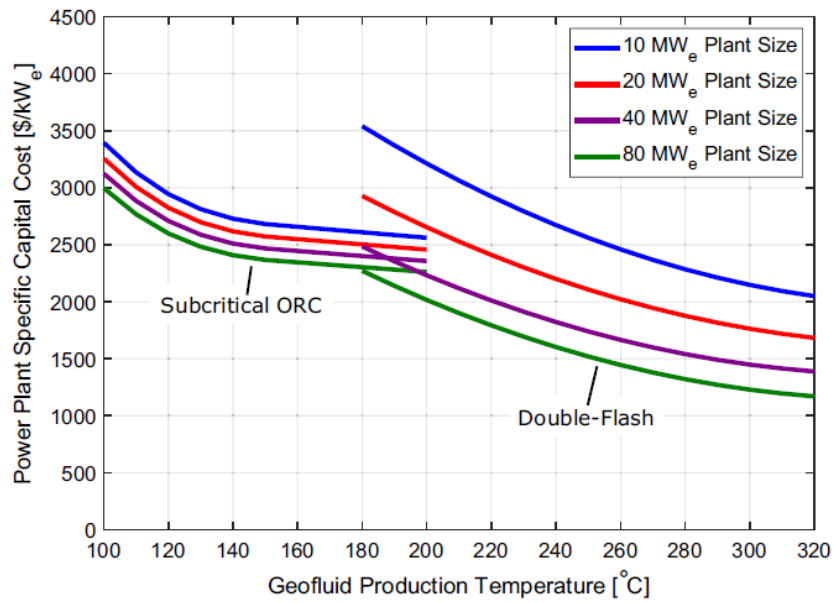


Figure 11. Correlation functions for the power plant cost taken from (Koenraad F. Beckers & McCabe, 2019).

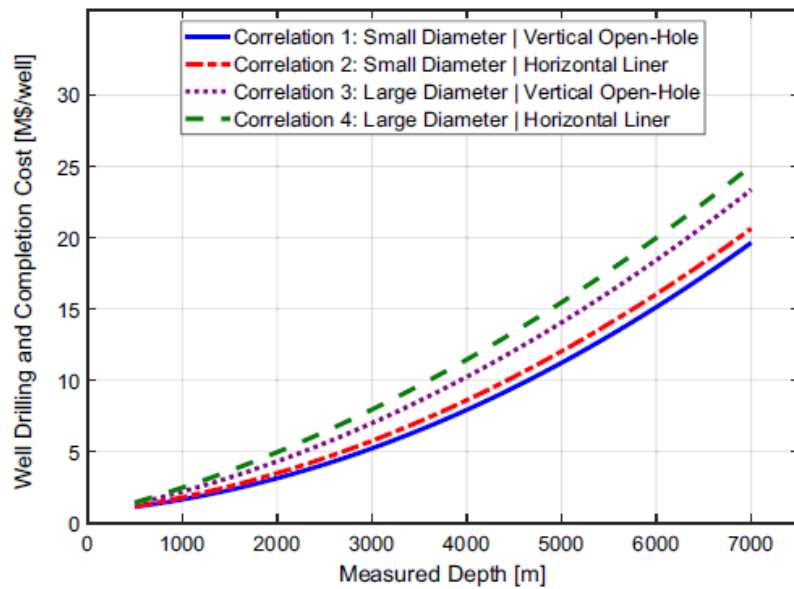


Figure 12. Correlation functions for the well cost taken from (Koenraad F. Beckers & McCabe, 2019).



---

## CHAPTER 3

# METHODOLOGY

This chapter gives a detailed description of the methodology used. The steps are summarized in the scheme of *Figure 13*. Computational workflow is described in paragraph 3.1. The input data are taken from the maps in ThermoGIS described in paragraph 2.1. Data need a pre-processing to be used in the simulator. In this phase, reservoirs are identified and configuration of the wells is set. The simulation hypotheses are listed and commented in paragraph 3.3. An insight into the heat simulation hypothesis is given in paragraph 3.4 while the electric power simulation settings and the correspondent optimization is discussed in paragraph 3.5. The output boxes of *Figure 13* are described in chapter 4.

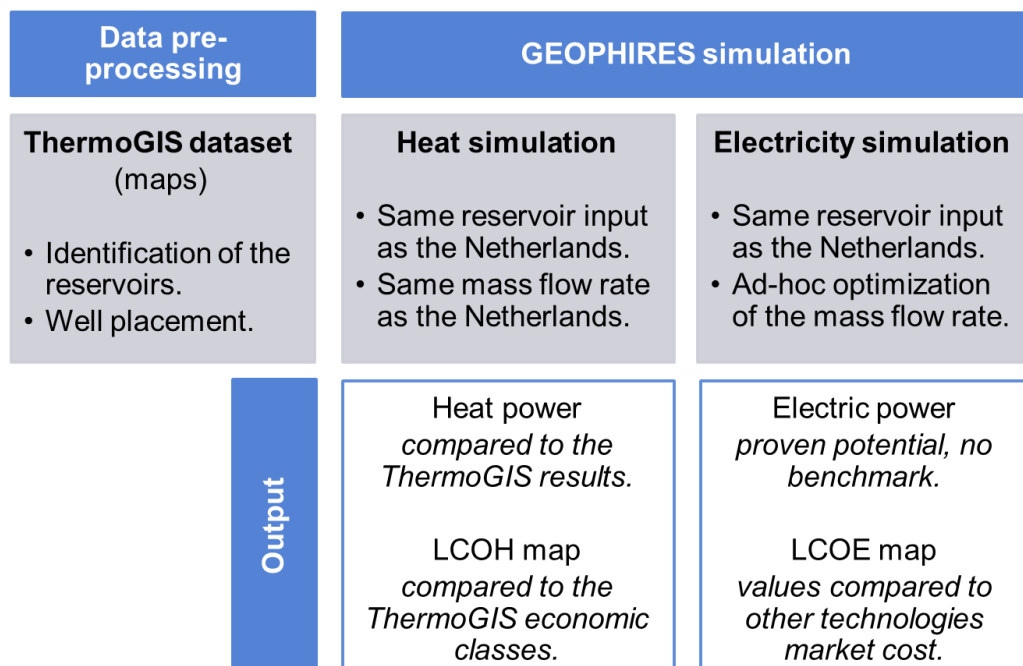


*Figure 13. Scheme of the work done in this study.*

### 3.1 Workflow and software in use

Going from the ThermoGIS input maps to the LCOH and LCOE output maps can't be a straightforward operation due to the different data types involved and the high amount of reservoirs to be simulated. Ad hoc workflow is set up and presented in *Figure 14*.

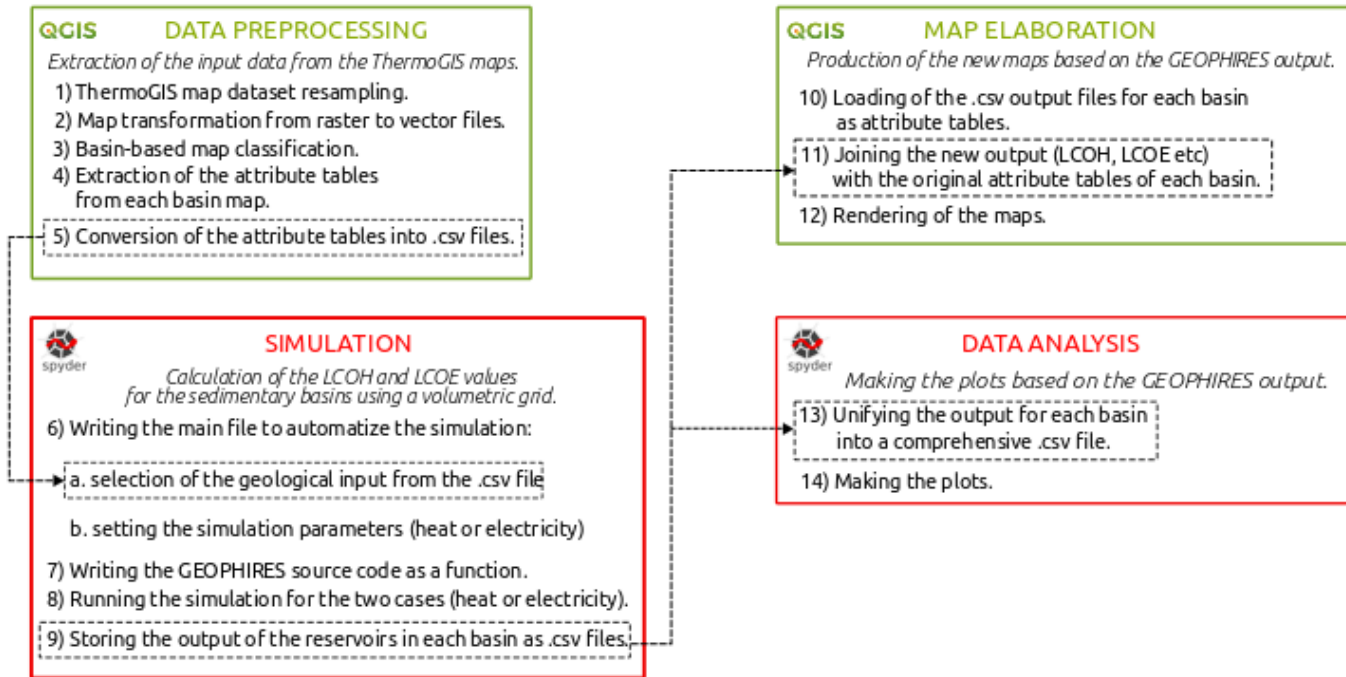


Figure 14. Workflow and software in use.

On one side, the maps are pre-processed by a Geographical Information System software, in this case, the open-source QGIS (QGIS, n.d.) is chosen. From the ThermoGIS dataset 28 basins are selected plus the stacked layers which cluster some of the basins in 5 groups. The CLZL basin is not considered as it does not provide all the input needed. Only the base case maps are picked. For each basin there is a map containing a value per pixel for each reservoir characteristics of interest: thickness, depth, temperature, permeability, produced mass flow rate (for heat production), heat power and class of economic potential. Each map is transformed into a vector map which makes the values accessible. Then the maps are grouped to have a map for each basin containing all the parameters of interest. During this process, empty rows are deleted.

On the other side, GEOPHIRES is a source code written in Python which is designed neither to deal with shapefiles nor to operate over thousands of reservoirs. Moreover, it does not provide an input file as each user is supposed to select the variables of interest and organize them into a text file according to the purpose of

---

the study. Along with the general GEOPHIRES input text file, it is written an additional interface program to take the reservoir parameters from each square of 1 [ $km^2$ ] in the maps and arrange them into a temporary input file suitable for the application of GEOPHIRES. Then the program repeats the simulation automatically for all the reservoirs, an operation that would not be possible when using GEOPHIRES alone.

In the case of the LCOE calculation, an additional optimization program was written to find the best-produced water mass flow rate. The Python scripts and the general GEOPHIRES input text file are reported and commented in Appendix A. The simulation and data analysis must be run outside the GIS platform to smooth and expedite the calculation process as well. The software used is Spyder (*spyder-IDE*, n.d.), an open-source cross-platform integrated development environment (IDE). Finally, the output needs to be imported back to QGIS to produce the LCOH and LCOE map rendering.

CSV is the key file format that allows exporting and importing the data from QGIS to Spyder and vice versa as shown by the dashed line path in *Figure 14*.

### **3.2 Data pre-processing and well-configuration**

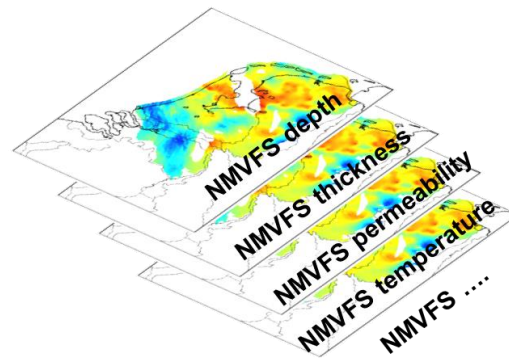
*Figure 15* represents a conceptual scheme of the map pre-processing in QGIS necessary to be able to extract the CSV file with all the information of interest. At first all the 7 maps (one for each parameter of interest) for each aquifer have to be grouped together in one final aquifer map. Each aquifer map is then discretized into a spatial grid which base unit is a reservoir of 1 km by 1 km. The discretization is done automatically during the pre-processing step in QGIS when transforming each map from raster file into a vector file. The discretization is pixel-based: the pixel in the raster file is converted into a square polygon in the vector file. The ThermoGIS dataset has a fixed scale so that each pixel on the map corresponds to a 1 [ $km^2$ ] square of the field. This assures that the same dimensions are transferred to the square polygon in the vector file. In the raster file, the information about the parameter values of each reservoir is not directly accessible, while in the vector file this information is univocally attached to the polygon and accessible through the attribute table. This table organizes the information displayed on the map: each row corresponds to a square polygon, that is a reservoir identified by an ID code, and each column displays the parameter values attached to it (thickness, depth, permeability, etc). The advantage of this operation is that the attribute table can be exported as a CSV file and used by a Python script.

## ThermoGIS dataset

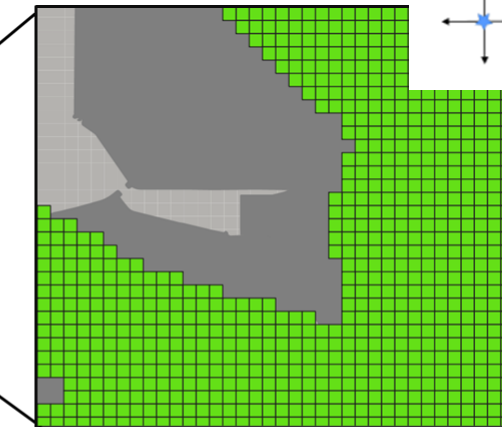
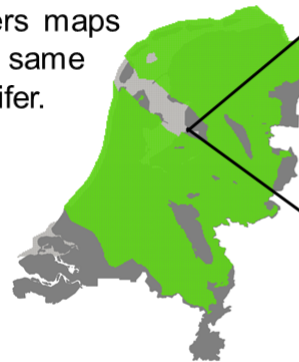
Stacked layers	Formation / Member	Formation / Member
	NMVFS	Someren Member
	NMVFV	Voorst Member
	NMRFT	Steensel Member
	NMRFV	Vessem Member
Middle & Lower North Sea Groups: N_STACKED	NLFFS	Brussel Sand Member
	NLFFD	Basal Dongen Sand Member
	NLLFR	Reusel Member
	NLLFS	Heers Member
	KNGLG & KNGLS	Holland Greensand & Spijkenisse Greensand members
	KNSNG	Gildehaus Sandstone Member
	KNSNL	De Lier Member
	KNSYS	IJsselmonde Zandsteen Member
	KNSNB	Berkel Sandstone Member
	KNSNR	Rijswijk Member
	KNSNF & KNSNP	Friesland & Beuntheim Sandstone members
Jurassic Groups	SLDN (SLDNA & SLDND)	Alblasserdam & Delft Sandstone members
	RNR0F	Röt Fringe Sandstone Member
	RNSOB	Basal Solling Sandstone Member
	RBMH	Hardegeen Formation
	RBMDU	Upper Detfurth Sandstone Member
	RBMDL	Lower Detfurth Sandstone Member
	RBMVU	Upper Volpriehausen Sandstone Member
	RBMLV	Lower Volpriehausen Sandstone Member
	RBSHN	Nederweert Sandstone Member
Upper Rotliegend Group: RO_STACKED	ROSL & ROSLU	Slochteren Formation & Upper Slochteren Member
	ROSL	Lower Slochteren Member
Limburg Group: DC_STACKED	DCH (DCHS & DCHL)	Hunze Subgroup (Strijen & De Lutte formations)
	DCD (DCDH & DCDT)	Dinkel Subgroup (Hellevootsluis & Tubbergen formations)
Carboniferous Limestone Group	GLZL	Zeeland Formation

1 aquifer → 7 maps, one for each parameter (depth, thickness, permeability, temperature, flow rate, heat power, economic class)

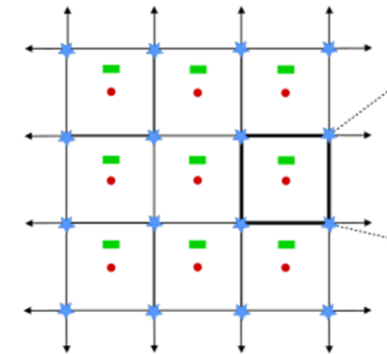
### Data pre-processing



1. Stacking all the parameters maps for the same aquifer.



2. Discretizing the aquifer in reservoirs of 1 km<sup>2</sup>.



3. Superimposition of the well pattern.

Figure 15. Details of the data pre-processing in QGIS.

As this study is carried at a regional level, each reservoir is simulated as a part of an overall system of geothermal reservoirs. The well pattern is chosen accordingly. The five-spots basic configuration is naturally suitable to this spatial discretization and it is also employed in several early-stage geothermal investigations. Moreover, a multiwell design allows enlarging the effective heat transfer area (Randolph & Saar, 2011).

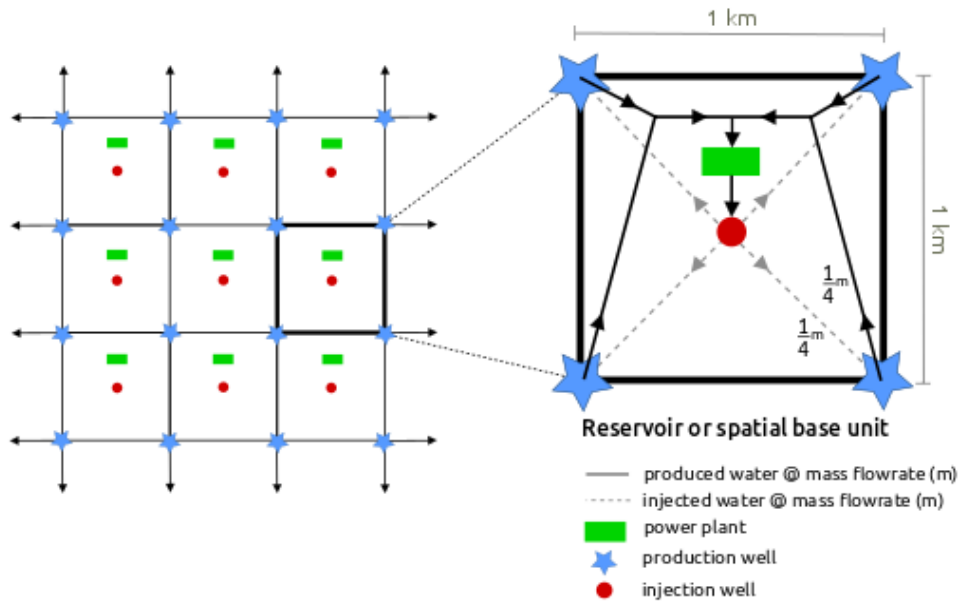


Figure 16. Spatial discretization and well pattern.

Figure 16 shows the five-spots well configuration repeated in each reservoir and zooms on one. Each reservoir has an injection well in the centre and four production wells in the corners. Each production well is shared with three other adjacent reservoirs. The simulation is done under the hypothesis that each reservoir is always surrounded by other reservoirs with the same five-spots well configuration. The distance between the production wells is 1 [km] and the footprint is 1 [km<sup>2</sup>]. This design results in a ratio of four production wells per injection well and a ratio of five wells per km<sup>2</sup> footprint. The distance between the production and the injection wells is 707 [m].

From an economic point of view, the sharing of the production wells, that allows the up-scaling of the basic pattern, reduces the number of required wells per km<sup>2</sup>. In the end, for each reservoir, only one injection well and one production well are paid. This and the use of economies of scale lead to the expectation of lowered capital costs (Sudhoff, Glos, Wechsung, 2019). This implies that in the simulation with GEOPHIRES, it is sufficient to evaluate the cost of just a doublet.

---

Also from a technical point of view, the five-spots configuration can be reduced to the simulation of a doublet. Given a reservoir as the one zoomed in figure 4, the injection well receives water from four production wells and then redistributes this water back to each of them. Considering 1 the total amount of water mass flow-rate exchanged in one reservoir, a fraction of  $\frac{1}{4}$  is exchanged between each production and injection well. GEOPHIRES calculates the power obtained from each reservoir using the total mass flow rate. However, the pump power needed depends on the pressure development between the injection well and one production well only. The pressure difference is linked to the mass flow-rate through the impedance. By reducing the impedance by a factor of 4, the pressure difference is estimated correctly. This is equal to considering each reservoir divided into four sub-reservoirs each of which exchanging  $\frac{1}{4}$  of the total water mass flow-rate through a doublet.

### 3.3 Simulation hypothesis

Three cases are simulated with the GEOPHIRES script:

- a. direct use and calculation of LCOH
- b. electric power production and calculation of the expected LCOE expected
- c. electric power production and calculation of LCOE using Lazards' economic hypotheses

For the a. case ThermoGIS heat power output and economic potential classes are used as a benchmark: GEOPHIRES is validated against existing results.

In the b. case, the existing economic hypotheses is used to evaluate an LCOE that could be expected given the Dutch reservoir conditions.

The case c. allows the comparison of the results with the LCOE of the other renewable and fossil fuel-based source of energy.

*Table 4* shows all the parameters used in the three simulations. The following paragraphs present the underlying hypothesis.

	<b>GEOPHIRES parameters</b>	<b>LCOH</b>	<b>LCOE expected</b>	<b>LCOE Lazard's'</b>
<b>Reservoir parameters</b>	Reservoir model	linear thermal drawdown model		
	Drawdown parameter [1/year]	No drawdown, constant temperature		
	Reservoir depth [m]	taken from the map		
	Reservoir temperature [°C]	taken from the map		
	Gradient [°C/km]	calculated from each value of reservoir temperature		
	Reservoir heat capacity [J/(kg K)]	1000		
	Reservoir thermal conductivity [W/(m K)]	3		
	Reservoir density [kg/m <sup>3</sup> ]	2500		
	Reservoir impedance [kPa s/kg]	calculated for each reservoir		
	Well pattern	5-spots		
	Number of production wells [-]	4 x 1/4 (a 5-spots share each production well with 3 adjacent 5-spots)		
	Number of injection wells [-]	1		
	Ramey production wellbore model	enabled		
	Injection wellbore temperature gain [°C]	0 as default		
	Injection temperature [°C]	30		
	Redrilling	no		
Water loss fraction [-]	no loss			
<b>Power plant parameters</b>	End-use option	Direct use	Electricity	
	Power plant type	-	Organic Rankine Cycle	
	End-use efficiency factor [%]	90	-	
	Well flow-rate [kg/s]	taken from the map as input	optimized by ad-hoc built function before applying GEOPHIRES	
	Well diameter [cm] (default values when selecting the well drilling cost correlation in the capital cost parameters)	21.59 (small diameter)	31.75 (large diameter)	
	Pump efficiency [%]	68	75	
	Utilization factor [%]	68	90	
	Surface temperature [°C]	10.5		
	Ambient temperature [°C]	10.5		

	<b>GEOPHIRES parameters</b>	<b>LCOH</b>	<b>LCOE expected</b>	<b>LCOE Lazards'</b>
<b>Economic parameters</b>	Economic model	Standard LCOH	Standard LCOE	
	Lifetime [years]	15	25	
	Inflation rate [%]	0		
	Discount rate [%]	5.4	9.6	
	Electricity rate [€ct/(kW h)]	8	-	
<b>Capital cost parameters</b>	Well drilling and completion [M\$]	built-in function		
	Well drilling cost correlation option	vertical-open hole, small diameter	vertical-open hole, large diameter	
	Reservoir stimulation [M\$]	no stimulation		
	Surface plant [M\$]	built-in function		
	Field gathering system [M\$]	built-in function		
	Exploration [M\$]	built-in function	1	built-in function
<b>O&amp;M cost param.</b>	Wellfield [M\$/year]	built-in function		
	Surface plant [M\$/year]	built-in function		
	Water cost [M\$/year]	built-in function		

Table 4. Simulation parameters.

### ***Reservoir parameters***

The reservoir parameters are the same for all the simulations as they represent the physical characteristics of the sedimentary basin and the well pattern. The Netherlands reservoirs can be modelled as porous media where the temperature distribution follows a local gradient. Among the GEOPHIRES reservoir options, the **thermal drawdown model** is the most suitable one and for the sake of simplicity no drawdown is considered. The **depth** of each reservoir is taken from the CSV file extracted by the maps as well as the **temperature** from which the **monodimensional gradient** is calculated as a function of the depth  $z$ :

$$\nabla T = \frac{\partial T}{\partial z} \hat{z} \quad (24)$$



$$\frac{\partial T}{\partial z} = \frac{T_{res} - T_{surf}}{z_{res}} \left[ \frac{^{\circ}\text{C}}{\text{km}} \right] \quad (25)$$

$T_{res}$  is the reservoir temperature taken from the maps [ $^{\circ}\text{C}$ ]

$T_{surf}$  is the surface temperature given by TNO [ $^{\circ}\text{C}$ ]

$z_{res}$  is the reservoir depth taken from the maps [km]

Reservoir **heat capacity**, **thermal conductivity** and **density** are related to one another through the reservoir diffusivity  $\alpha$  (H F Mijnlief et al., 2014).

$$\alpha = \frac{r_{res}}{\rho_{res} c_{p_{res}}} \left[ \frac{\text{m}^2}{\text{s}} \right] \quad (26)$$

$r_{res}$  is the reservoir thermal conductivity  $\left[ \frac{\text{W}}{(\text{m K})} \right]$

$\rho_{res}$  is the reservoir density  $\left[ \frac{\text{kg}}{\text{m}^3} \right]$

$c_{p_{res}}$  is the reservoir heat capacity  $\left[ \frac{\text{J}}{(\text{kg K})} \right]$

Using empirically derived data, TNO has set  $r_{res} = 3 \left[ \frac{\text{W}}{(\text{m K})} \right]$  and  $\alpha = 1.2 \cdot 10^{-6} \left[ \frac{\text{m}^2}{\text{s}} \right]$ . Then here the rock heat capacity is set to  $c_{p_{res}} = 1000 \left[ \frac{\text{J}}{(\text{kg K})} \right]$  according to a similar case of geothermal application in a porous medium (Randolph & Saar, 2011). The reservoir density is then derived  $\rho_{res} = 2500 \left[ \frac{\text{kg}}{\text{m}^3} \right]$ .

The **reservoir impedance** is defined as the ratio between the pressure difference between one injection and one production well  $\Delta P_{wells}$  and a given mass flow rate  $\dot{m}$ . It is calculated for each reservoir using a 1-D Darcy approximation as a function of water properties, reservoir properties and well configuration according to (Adams et al., 2020):

$$I = \frac{\Delta P_{wells}}{\dot{m}} = \frac{\mu_{water}}{\rho_{water,res} k_{res} h_{res}} \ln \left( \frac{4L}{D\pi} \right) \left[ \frac{\text{Pa s}}{\text{kg}} \right] \quad (27)$$

$\mu_{water}$  is the water dynamic viscosity as a function of the water temperature here assumed equal to the reservoir temperature [Pa s]

$\rho_{water,res}$  is the water density function as a function of the water temperature here assumed equal to the reservoir temperature  $\left[ \frac{\text{kg}}{\text{m}^3} \right]$

$k_{res}$  is the reservoir permeability taken from the maps [ $\text{m}^2$ ]

$h_{res}$  is the reservoir thickness taken from the maps [m]

$L$  is the production-injection wells spacing set at 707 [m]

$D$  is the well diameter [m]

Using this equation of the impedance allows including explicitly the information about the well spacing (and so about the well configuration). At the same time, it

---

characterizes punctually each reservoir refining the simulation, instead of having one impedance value for all the sedimentary basin.

As explained in paragraph 3.2 and according to the symmetry of the five-spots configuration, it is enough to simulate just one **injection well** and one **production well**. This eases the comparison with the results from ThermoGIS as well based on a doublet configuration.

**Ramey production wellbore model** is enabled to calculate the wellbore temperature drop.

The **injection temperature** is set to 30 [°C] to comply with the ThermoGIS hypothesis (Vrijlandt et al., 2019). The hypothesis of no **injection wellbore temperature gain**, no **redrilling** and no **water loss** are made.

### 3.4 Heat power simulation and LCOH

The purpose of the heat power simulation is to get a value of heat power and correspondent LCOH for each reservoir. This heat power can be compared reservoir by reservoir with the values obtained by TNO using DoubletCald1D. The LCOH values have to be compared with the four economic classes into which the reservoirs are grouped by TNO.

Having the ThermoGIS results as a benchmark, all the hypothesis are taken accordingly to the TNO work.

The **direct-use** option is selected and it does not require a power conversion plant. The **pump efficiency** and **utilization factor** are set as GEOPHIRES default. From the DoubletCalc1D manual, the yearly average **surface temperature** of 10.5 [°C] is selected (H F Mijnlief et al., 2014). The GEOPHIRES **ambient temperature** is considered equal to the surface temperature.

The **LCOH standard model** is selected with no **inflation rate** as the hypothesis of the overnight cost is assumed. The equation used by GEOPHIRES is:

$$LCOH = \frac{C_{cap} + \sum_{t=1}^{LT} \frac{C_{O\&M,t} - R_t}{(1+d)^t}}{\sum_{t=1}^{LT} \frac{E_t}{(1+d)^t}} \left[ \frac{\text{¢}}{MMBtu} \right] \quad (28)$$

$C_{cap}$  is the total capital cost [M\$]

$LT$  is the lifetime of 15 [years]

$C_{O\&M}$  is the O&M cost at each time step  $t$   $\left[ \frac{M\$}{year} \right]$

$t$  is the time step set equal to 1 year

$R_t$  is the secondary CHP revenue stream which is equal to 0 as no cogeneration is considered [M\$]

---

$d$  is the discount rate [-]

$E_t$  is the energy production per year  $\left[\frac{\text{MMBtu}}{\text{year}}\right]$

The results are then converted to €/ (MW h).

The Weighted Average Capital Cost calculated from the financial hypothesis made by TNO is used as the **discount rate**:

$$\begin{aligned} d = WACC &= \text{debt ratio} \times \text{interest on loan} \\ &+ (1 - \text{debt ratio}) \\ &\times \text{required return on equity} \\ &= 0.8 \times 0.05 + 0.2 \times 0.07 = 0.054 \text{ [-]} \end{aligned} \tag{29}$$

**Capital and O&M costs** are evaluated using the GEOPHIRES built-in functions.

### 3.5 Electric power simulation and LCOE

The purpose of the electric power simulation is to get a value of electric power and correspondent LCOE for each reservoir. There is no benchmark provided by TNO nor previous evaluation of this potential. For this reason, two simulations are proposed obtained by changing the discount rate which has a substantial impact on the economic simulation (see discussion in paragraph 1.4). The **LCOE expected** is evaluated using the same **discount rate** as the heat simulation that is 5.4% while the **LCOE Lazard** is evaluated using the **discount rate** proposed by Lazard for geothermal power plants, that is 9.6%. The **lifetime** of 25 years proposed by Lazard is considered for both cases. In the LCOH and LCOE Lazard cases, the built-in function for the **exploration cost** is used as default. This implies adding 15% of the exploration capital cost as a contingency. In the LCOE expected case, the **cost of exploration** is reduced to 1 M\$ without contingency as it is assumed that there is no need to further characterize the subsurface, given the amount of already existing exploration wells.

The **electricity** option is selected and the ORC (Organic Rankine Cycle) is set as a type of **power plant** which is suitable for low enthalpy geothermal sources (see discussion in paragraph 1.3). The **end-use efficiency**, **pump efficiency**, **well diameter**, **utilization factor**, **lifetime** and **electricity rate** are set equal to the TNO simulation (Vrijlandt et al., 2019). From the DoubletCalc1D manual, the yearly average **surface temperature** of 10.5 [°C] is selected (K. F. Beckers, 2016).

---

The GEOPHIRES **ambient temperature** is considered equal to the surface temperature.

The **well diameter** values are set once the well drilling cost correlation is chosen in the capital cost parameters: the small diameter corresponds to 21.59 cm, the large diameter to 31.75 [cm] (K. F. Beckers, 2016). Injection and production wells have the same diameter.

The **well flow-rate** is found in each reservoir by minimizing the LCOE. A first simulation was done using the same flow-rate as the heat simulation with a result of a very poor output both in terms of power and LCOE. The optimization script reported in the Appendix makes GEOPHIRES testing different flow-rate values chosen by varying an initial random value. Then the correspondent LCOE is calculated and compared to the one from the previous simulation until the minimum is found. The associated flow-rate is considered the optimal one.

*Figure 17* shows how the optimization works and proves the necessity of finding the optimal flow-rate. The plot is about one case, reservoir A presented later in the results. The LCOE is a parabolic shaped function of the flow-rate. When using the flow-rate provided by TNO, it is not guaranteed to choose the lowest LCOE either a positive net power value. The optimization (see Appendix) explores the parabola from the top left looking for the lowest LCOE. It starts with a small value of flow-rate and an initial very high value of LCOE. At each time-step, GEOPHIRES is run and the new LCOE is compared to the previous one. As long as the new LCOE is smaller than the previous one, GEOPHIRES is run again with a new flow-rate increased by  $5 \left[ \frac{kg}{s} \right]$ . When the new LCOE is higher than the previous one, it means the minimum has been crossed. At this point, the flow-rate is decreased by  $1 \left[ \frac{kg}{s} \right]$  going backwards on the blue parabola until the minimum LCOE is found.

The red dotted line intersects the lowest LCOE in  $149 \left[ \frac{\text{€}}{MWh} \right]$  and the optimal flow-rate in  $163 \left[ \frac{kg}{s} \right]$ . The correspondent net power is  $2.3 [MW_e]$ . The black dashed line crosses the maximum net power showing that the net power found is suboptimal. This results in a trade-off between the lowest LCOE and the maximum achievable net power. This should be taken into account when doing a more refined analysis within the reservoir during the power plant design phase. This issue is addressed in chapter 5.

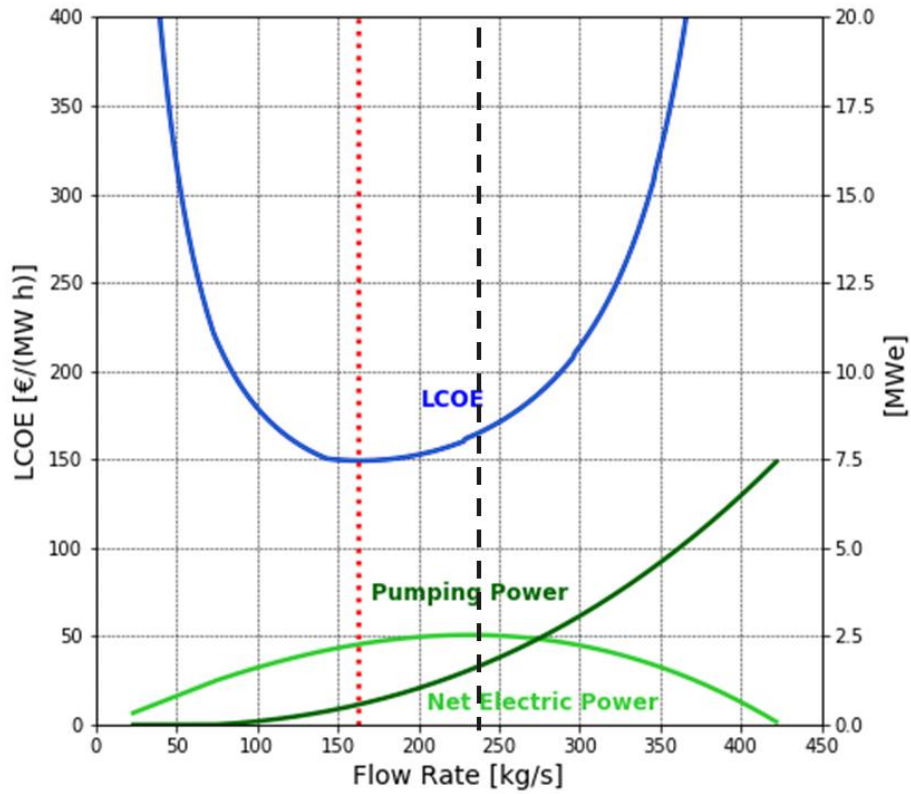


Figure 17. Optimization of the flow rate in the best reservoir. The red dotted line intersects the minimum LCOE while the black dashed line intersects the maximum net power.

The **LCOE standard model** is selected with no **inflation rate** as the hypothesis of the overnight cost is assumed. The equation used by GEOPHIRES is the same as in the LCOH case:

$$LCOE = \frac{C_{cap} + \sum_{t=1}^{LT} \frac{C_{O\&M,t} - R_t}{(1+d)^t}}{\sum_{t=1}^{LT} \frac{E_t}{(1+d)^t}} \left[ \frac{\text{€}}{\text{kWh}} \right] \quad (30)$$

$C_{cap}$  is the total capital cost [M\$]

$LT$  is the lifetime of 15 [years]

$C_{O\&M}$  is the O&M cost at each time step  $t$   $\left[ \frac{\text{M\$}}{\text{year}} \right]$

$t$  is the time step set equal to 1 year

$R_t$  is the secondary CHP revenue stream which is equal to 0 as no cogeneration is considered [M\$]

$d$  is the discount rate [-]

$E_t$  is the energy production per year  $\left[ \frac{\text{kWh}}{\text{year}} \right]$

The results are then converted to  $\left[ \frac{\text{€}}{\text{MWh}} \right]$ .

**Capital and O&M costs** listed in Table 4 are evaluated using the GEOPHIRES built-in functions.

---

## CHAPTER 4

### RESULTS

The results of the three simulations are discussed in this chapter.

In paragraph 4.1 the heat power production potential is compared to the results obtained by TNO. The comparison between the two different models, DoubletCalc1D and GEOPHIRES in chapter 2, is completed here with the analysis of the obtained results. The impact of the salinity, which is used in DoubletCalc1D but not considered in GEOPHIRES, is discussed. The economic indicators evaluated automatically with the GEOPHIRES simulation are compared to the economic classes obtained by TNO. The reservoirs classified according to their economic potential are rendered in a map which is compared to the one of ThermoGIS and the map of the existing development projects. The advantages of the maps built with this method are presented.

The expected LCOE results are discussed in paragraph 4.2. The relationship between LCOE and net electric power is examined with regard to the optimization implemented. The influence of the reservoir characteristics, especially temperature and transmissivity is highlighted.

In paragraph 4.3 the electric power potential is analysed at the regional scale and with a long term perspective. At the same time, the LCOE is compared to the ones of other renewable and conventional sources taken from the Lazard's (Lazard's, 2019) LCOE report.

---

## 4.1 Heat power potential and LCOH

The heat power potential is compared reservoir by reservoir by selecting the punctual values obtained from the GEOPHIRES simulation and the ThermoGIS dataset. The results of the comparison are plot in *Figure 18*. Each blue dot is one of the simulated reservoirs with the overlapped regression line. The black line would be the ideal regression line in case the simulated power were the same in each reservoir. They match with a 6% difference. GEOPHIRES appears to underestimate the heat power potential.

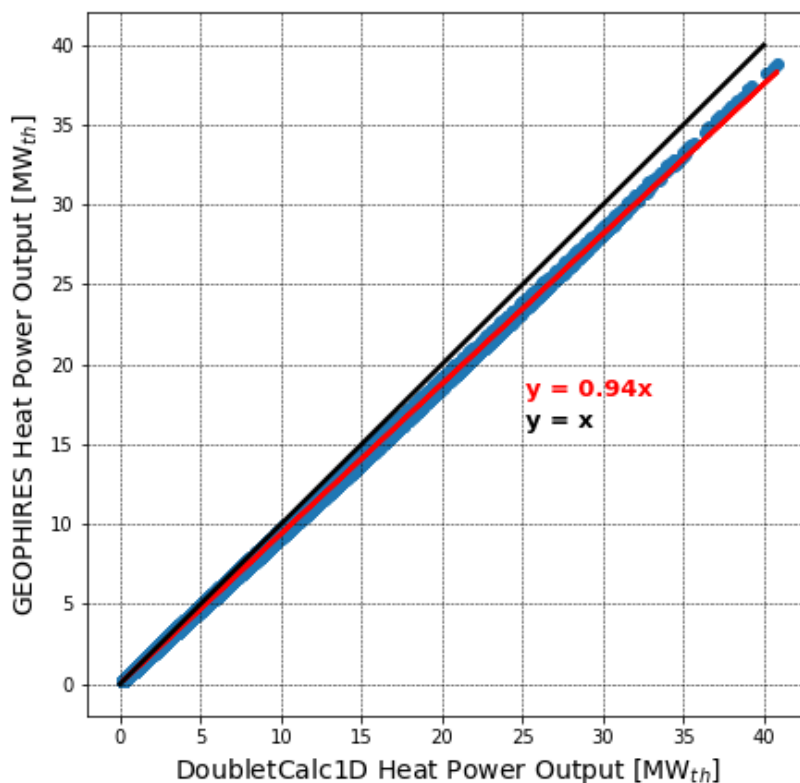


*Figure 18. Heat power comparison between TNO results and GEOPHIRES results. The actual regression line is in red, while the ideal regression line is in black and represent the ideal case where the results of the two models perfectly overlap.*

As already discussed in paragraph 2.4, the heat power potential is calculated in the same way by DoubletCalc1D and GEOPHIRES (equations 1 and 19). The mass flow-rate is the same as it is given as input to GEOPHIRES. The temperature difference accounts for the heat losses in the production well which are evaluated in the same way in both models as proven with equation 10. Then, the only difference might be in the correlation used for the water specific heat. In GEOPHIRES it is a function of the temperature only, while in DoubletCalc1D it is a function of the salinity as well.

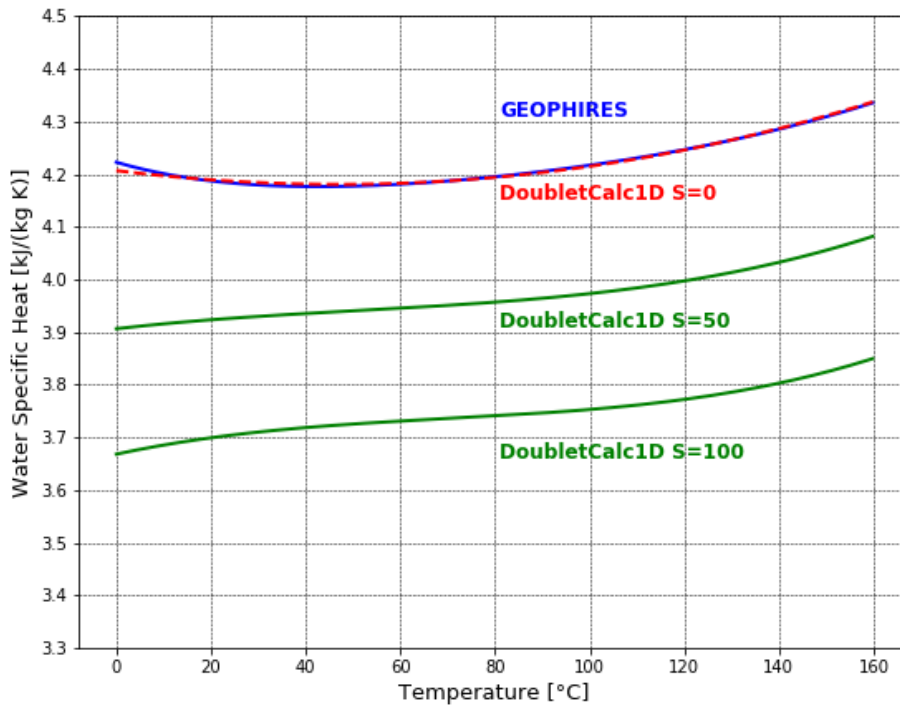


Figure 19. Comparison of the water specific heat correlations used in the two models (blue line and green line) as a function of reservoir temperature. The red dashed line is the DoubletCalc1D correlation considering salinity equal to 0  $\left[\frac{g_{NaCl_{eq}}}{kg_{water}}\right]$ .

Figure 19 shows the different correlation functions used for the water specific heat. When setting the salinity to 0 ppm, the DoubletCalc1D function overlaps with the one used in GEOPHIRES. Using average salinity values equal to 50  $\left[\frac{g_{NaCl_{eq}}}{kg_{water}}\right]$  and 100  $\left[\frac{g_{NaCl_{eq}}}{kg_{water}}\right]$  the green lines are obtained. The red dashed line overlapping with the blue one can be considered as an upper limit for the specific heat used in DoubletCalc1D. The higher the salinity, the lower the heat capacity. This means that the TNO simulation should give lower values of geothermal heat power which is exactly the contrary of what shown in Figure 18.

Comparing again the two manuals, it is found out that  $\Delta T_{he}$  has two different starting temperatures. DoubletCalc1D takes the reservoir temperature in the middle of the thickness, while GEOPHIRES takes it at the top depth. For example, given the gradient of 31  $\left[\frac{^{\circ}C}{km}\right]$ , a reservoir with 300 [m] thickness has a starting temperature for DoubletCalc1D almost 5 [°C] higher than the GEOPHIRES one. This could reasonably overcompensate for the smaller water heat capacity values, especially for low salinity rate. When simulating the reservoirs again in GEOPHIRES but using a reservoir temperature in the middle of each reservoir, the results perfectly overlap with the ones of TNO as proven in Figure 20.

The overall matching between the heat power output is satisfactory, always noting that GEOPHIRES tends to underestimate the heat power compared to



DoubletCalc1D. Taking the reservoir temperature at the top depth can be then considered as a conservative hypothesis.

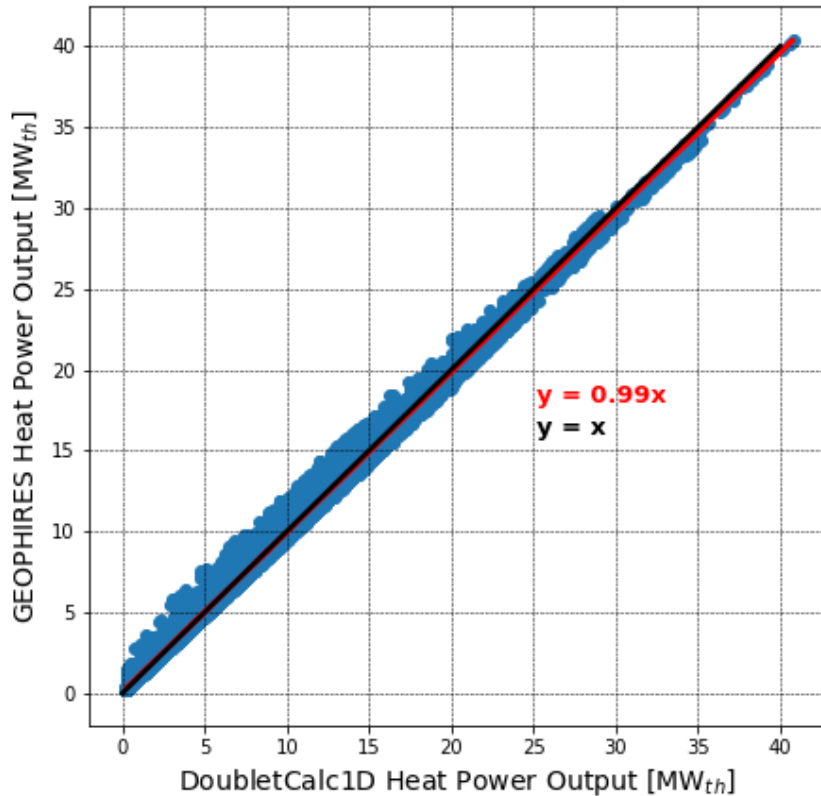


Figure 20. Comparison of the heat power obtained considering also in GEOPHIRES the reservoir temperature in the middle of the thickness instead of the top depth.

The economic potential found by TNO is difficult to be compared with the LCOH values. The main problem is that on the TNO side there are classes that group numerous reservoirs, while after the GEOPHIRES simulation, each reservoir is given a specific LCOH punctual value. Even if TNO has evaluated UTC (Unit Technical Cost), with the same dimension of LCOH, for each reservoir, these values are not available. The classes and the classification rules are (see again paragraph 2.2):

- Unknown: UTC P10 > reference price → class 1
- Indication: UTC P10 < reference price → class 2
- Moderate: UTC P30 < reference price → class 3
- Good: UTC P50 < reference price → class 4

The reference price is  $5.1 \left[ \frac{\text{€ct}}{\text{kWh}} \right]$  equivalent to  $51 \left[ \frac{\text{€}}{\text{MWh}} \right]$ , which corresponds to the threshold set by the SDE+ (Dutch subsidy scheme presented in paragraph 2.1) for geothermal energy. P10 is the 10% probability given to the occurrence of that UTC, P30 is the 30% probability, P50 is the 50% probability and reflect the stochasticity of the input used by TNO.

A way to compare them is presented here and imply applying the TNO threshold set for the UTC to the found LCOH. The reservoirs with a power capacity equal to or greater than 100 [ $kW_{th}$ ] are analysed which are a sample of 91908. To overcome the difficulty given by the TNO classes based on a probabilistic assessment, a comparison criterion is set. LCOH values below 51 [ $\frac{\text{€}}{MWh}$ ] are seen as more promising reservoirs and should belong to classes 3 and 4 (Moderate and Good). LCOH greater than 51 [ $\frac{\text{€}}{MWh}$ ] are seen as less promising and should belong to class 1 or 2 (Unknown and Indication).

Figure 21 shows the results of this analysis. The orange slice represents the reservoirs considered promising both by TNO and this assessment. In green, there are the reservoirs classified as not promising both by TNO and this assessment. It can be said that 93.6% of the reservoirs is classified unanimously by the two analysis. Just 0.3% is classified as not promising by TNO even if they have an LCOH lower than 51 [ $\frac{\text{€}}{MWh}$ ] according to GEOPHIRES. They are 266 reservoirs with an average temperature of 56 [ $^{\circ}C$ ] and an average transmissivity of 156 [ $Dm$ ]. TNO might have privileged a temperature criterion so classifying it as too low and the reservoirs as not promising. On the other hand, GEOPHIRES might compensate for it with high transmissivity. 4.1% reservoirs are classified as promising even if their LCOH is greater than 51 [ $\frac{\text{€}}{MWh}$ ]. However, their average LCOH is 68 [ $\frac{\text{€}}{MWh}$ ] so they are still close to the threshold.

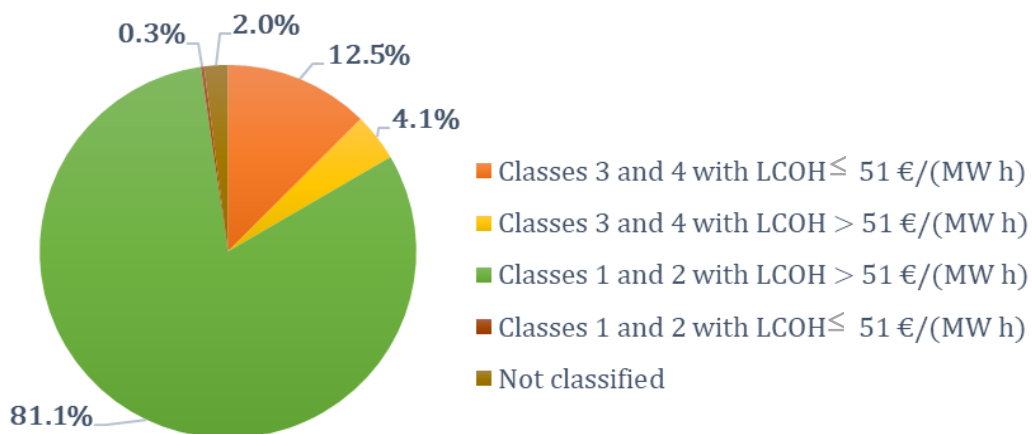
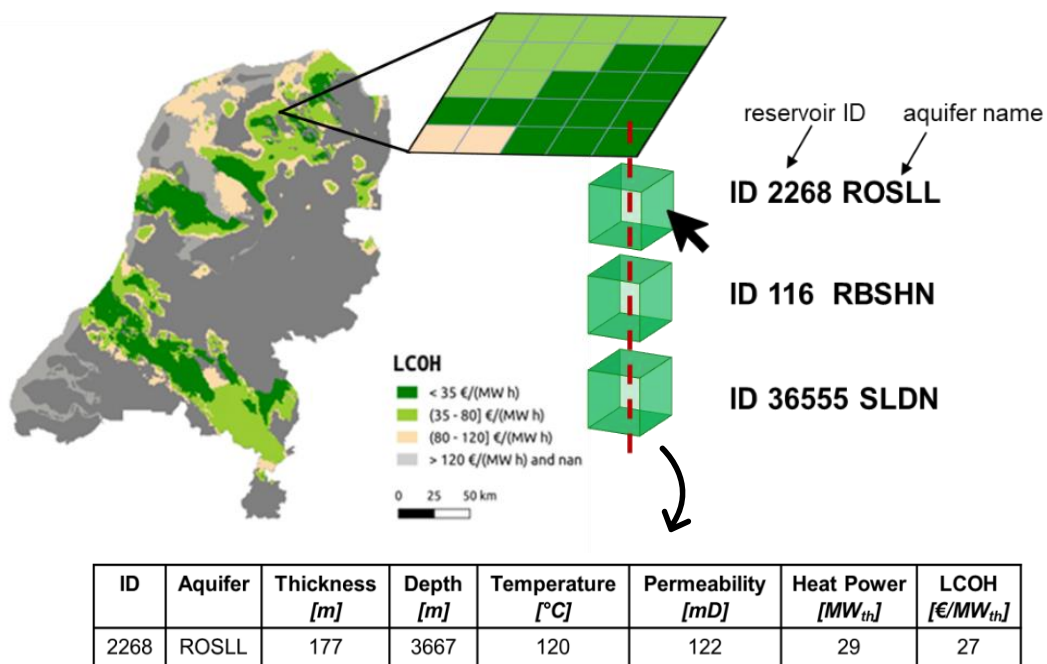


Figure 21. Comparison between the TNO classification and the LCOH obtained with GEOPHIRES. Only reservoirs with heat power equal or greater than 0.1 [ $MW_{th}$ ] are considered. Green and orange areas represent the percentage of reservoirs where the economic classifications of GEOPHIRES and TNO are in accordance.

Among the two economic potential assessment method, TNO versus GEOPHIRES, there is more agreement in excluding not promising reservoirs than classifying them as good. However, the misclassified ones are just 4.4% of the total sample.

This is nice evidence that GEOPHIRES LCOH is a good indicator of the economic potential in the Netherlands context as it gives the same results as the TNO classification. *Figure 23* shows this graphically: the map on the right is based on the LCOH calculated with GEOPHIRES and matches nicely with the ThermoGIS map on the left.

These results about the technical heat power and its economic opportunity represent a mutual validation of the geothermal potential in the Netherlands. On one side, GEOPHIRES technical and economic simulation components are validated against existing data. The LCOH is proved to be a reliable economic indicator and allows a refined ranking of the reservoirs. Moreover, giving an LCOH value for each reservoir and stacking them all together brings some advantages to the analysis as shown in *Figure 22*. Differently from ThermoGIS, all the input and output parameters for each reservoir are available by clicking on them. Then all the reservoirs are accessible in the same map and not distributed in different map files according to the aquifer they belong to. Finally, each reservoir has its cost indicator so reservoirs with specific costs can be targeted.



*Figure 22. Advantages of the LCOH map configuration proposed with this work.*

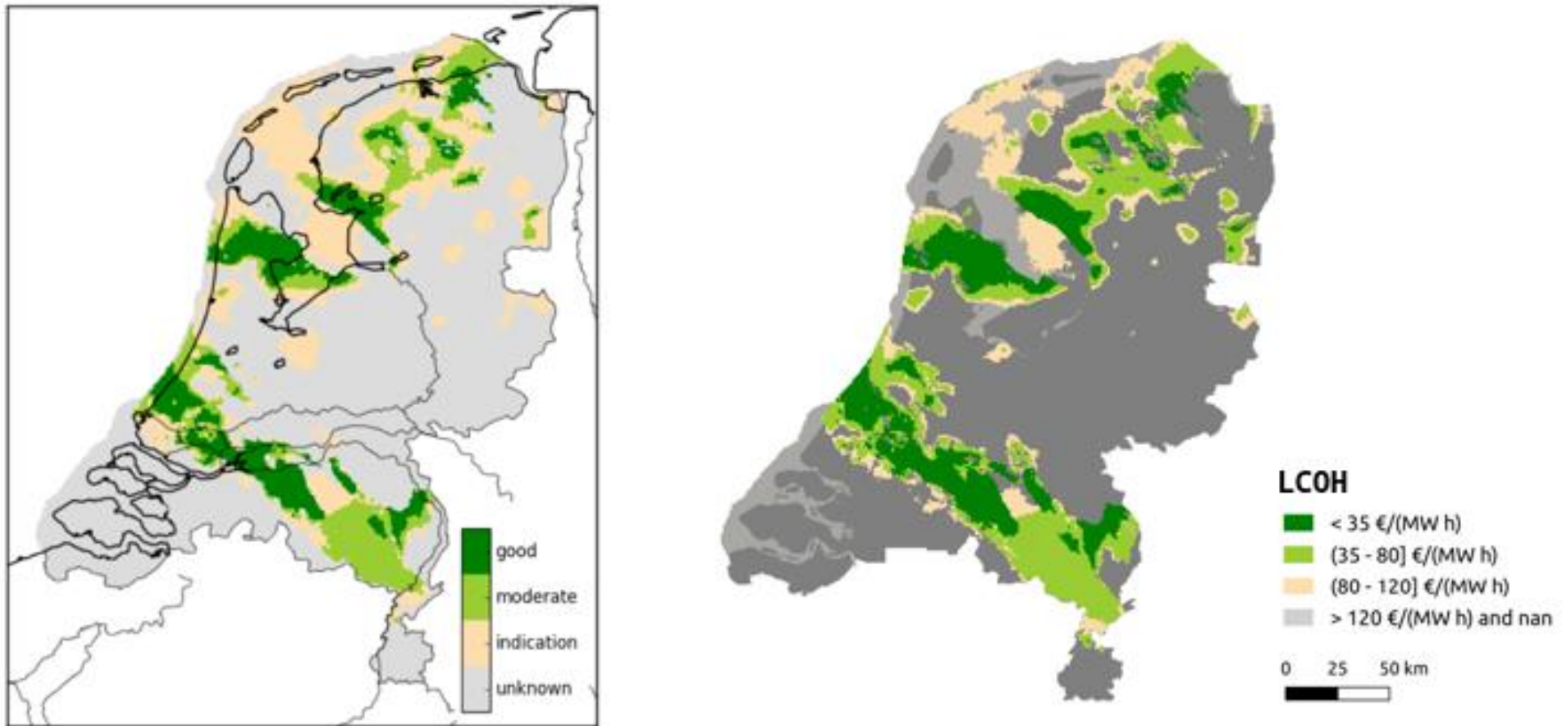


Figure 23. Geothermal economic potential map of the Netherlands. On the left, the map produced by TNO taken from (Vrijlandt et al., 2019). After the technical simulation with DoubletCalc1D, TNO has assigned an economic potential class to each reservoir. The legend shows the classes going from “good” to “unknown”. On the right, the map of LCOH values obtained after the GEOPHIRES simulation. The LCOH values are grouped manually to resemble the TNO classes, as the UTC values calculated by TNO for each reservoir are not available.

---

## 4.2 Electric power potential and LCOE expected

Compared to the results of the heat power potential, there is less available power at a higher cost. Among the 364742 simulated reservoirs, only 8% of them have a net power greater than 100 [kW] and only 238 reservoirs, which are the 0.07% of the total, have a net power equal or greater than 1 [MWe] with a range of LCOE between 149  $\left[\frac{\text{€}}{\text{MWh}}\right]$  and 301  $\left[\frac{\text{€}}{\text{MWh}}\right]$ . These results are not surprising as the geothermal resource of the Netherlands has already been classified as low temperature with a maximum  $T_{\text{res}}$  around 160 [°C]. This implies a low utilization efficiency for ORC between 18% and 32% as can be seen in *Figure 10*.

On the other hand, the technical simulation shows that this potential is in place. In *Figure 24* the LCOE is plotted against the correspondent net electric power for the reservoir with a capacity greater than 1 [MWe] as this is the minimum size for ORC as discussed in paragraph 1.3. The red line is the polynomial regression and shows the general trend according to which it is cheaper building power plant with higher capacity. The variability of the data, that is represented by the blue horizontal spikes, is greater for higher LCOE and lower capacity.

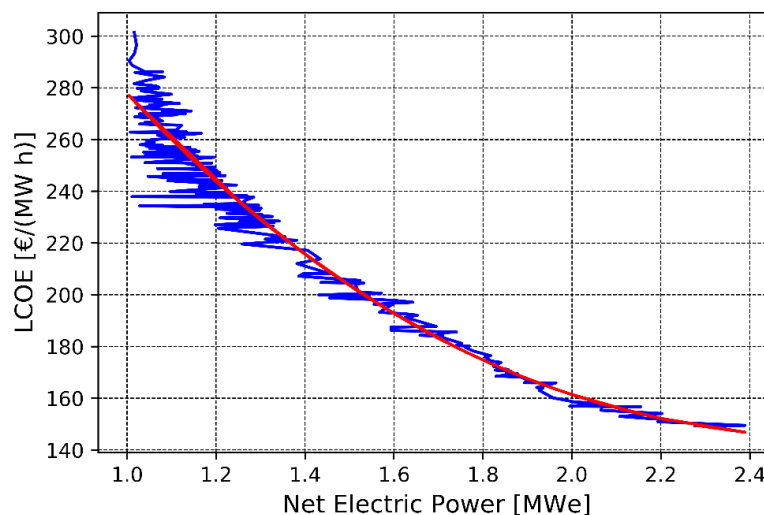


*Figure 24. LCOE and correspondent net electric power for the reservoirs where this is greater than 1 [MWe].*

This means that lower power capacity can be obtained at a higher variable cost. To understand why there are so few reservoirs providing enough power at a relatively low cost, it is worth analysing the geothermal characteristics that make this possible. The economic success of a doublet is driven by the fluid temperature and the transmissivity (Stober & Bucher, 2013). In *Figure 25* they are plotted against the LCOE, each dot representing one of the 238 reservoirs with a power capacity higher than 1

[ $MW_e$ ]. They are arranged on parallel hyperbolas with subsequent bands coloured according to increasing costs along the bottom-left direction. The majority of the reservoirs is spread on the green-dotted band. Fewer reservoirs with low LCOE, the red dots in the dashed box, are concentrated in the plot area where both temperature and transmissivity are high. Their temperature ranges from 117 [ $^{\circ}C$ ] to 125 [ $^{\circ}C$ ], the transmissivity between 16 [ $Dm$ ] and 27 [ $Dm$ ]. These reservoirs conditions can be considered the most favourable ones in the Dutch basin. The red reservoirs distribution shows that higher temperatures compensate for lower transmissivities to get low LCOE values and vice-versa, thus validating the complementary roles of transmissivity and temperature already shown by *Figure 8*.

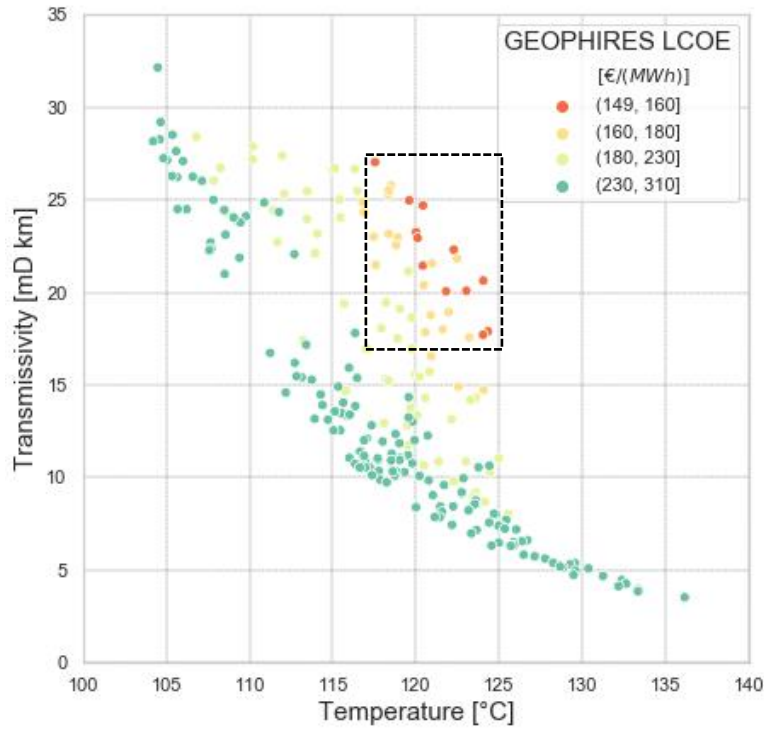


*Figure 25. LCOE and characteristics of the 238 reservoirs above 1  $MW_e$  capacity. The black dashed box highlights the best reservoirs that are the ones with the lowest LCOE values.*

Of course, transmissivity and temperature influence the power as well. To show their complementary role, it is useful to look at the net electric power equation (23) arranged as a function of the mass flow rate as this is the perturbed input variable to get the lowest LCOE. Getting to the highest power capacity, even if constrained by the cost, is directly dependent on the reservoir characteristics, especially temperature and transmissivity.

Starting from the net electric power equation (23), the electric power (20) and pumping power (18) are explicitly written while factoring the mass flow-rate. The



simulations with Ramey's model prove that after a few months of operation, the temperature difference between the top and bottom of each well is typically less than 10 [°C] so  $\Delta T_{prod}$  (equation 3) is considered as a constant (Ramey, 1962).

$$\begin{aligned}
P_{el,net} &= P - P_{pump,net} = \dot{m} \eta_u B - \frac{\Delta p \dot{m}}{\rho_{water,inj} \eta_{pump}} = & (31) \\
&= \dot{m} \eta_u f(T_{res} - \Delta T_{prod}) - \frac{\dot{m}}{\rho_{water,inj} \eta_{pump}} (\Delta p_{prod,inj} + \Delta p_{well,hydro} + \Delta p_{res}) = \\
&= \dot{m} \eta_u f(T_{res} - \Delta T_{prod}) - \frac{\dot{m}}{\rho_{water,inj} \eta_{pump}} \left( \Delta p_{prod,inj} + \Delta p_{well,hydro} + \frac{I \dot{m}}{\rho_{water,res}} \right) = \\
&= \dot{m} \left[ \eta_u f(T_{res} - \Delta T_{prod}) - \frac{(\Delta p_{prod,inj} + \Delta p_{well,hydro})}{\rho_{water,inj} \eta_{pump}} \right] - \dot{m}^2 \frac{I}{f(T_{res})} = \\
&= \dot{m} \left[ \eta_u f(\boxed{T_{res}} - \Delta T_{prod}) - \frac{(\Delta p_{prod,inj} + \Delta p_{well,hydro})}{\rho_{water,inj} \eta_{pump}} \right] - \dot{m}^2 \frac{\mu_{water}}{\boxed{k_{res} h_{res} f(\boxed{T_{res}})} \rho_{water,inj} \eta_{pump}} \ln\left(\frac{4L}{D\pi}\right)
\end{aligned}$$

The orange box highlights the reservoir temperature contribution, while the green one highlights the transmissivity. Their complementary role is clear in the impedance equation: they are both at the denominator and contribute to reducing the mass flow-rate at the second power which negatively impacts on the overall net electric power. As their product is influencing the reduction of the negative part of the equation (31), if transmissivity is low, an high value of temperature could compensate for it and get the same amount of net electric power and vice versa.  $T_{res}$  is also in the first part of the equation and positively contributes to the net electric power.

However, such a combination of temperature and transmissivity is not that common among the Dutch reservoirs as it can be seen in the map in *Figure 26*. Given the general trend of LCOE and net electric power analysed in *Figure 25*, the reservoirs providing a good power capacity at a reasonable cost are very few. The areas under 300  $\left[\frac{\text{€}}{MWh}\right]$ , thus having a minimum capacity of 1 [MW<sub>e</sub>], are clustered following the same pattern as the dark green zones in *Figure 23* which are the core areas of the reservoirs good for heat extraction. The majority of the Netherlands is in grey, meaning that the electric power production capacity is low with a high cost.

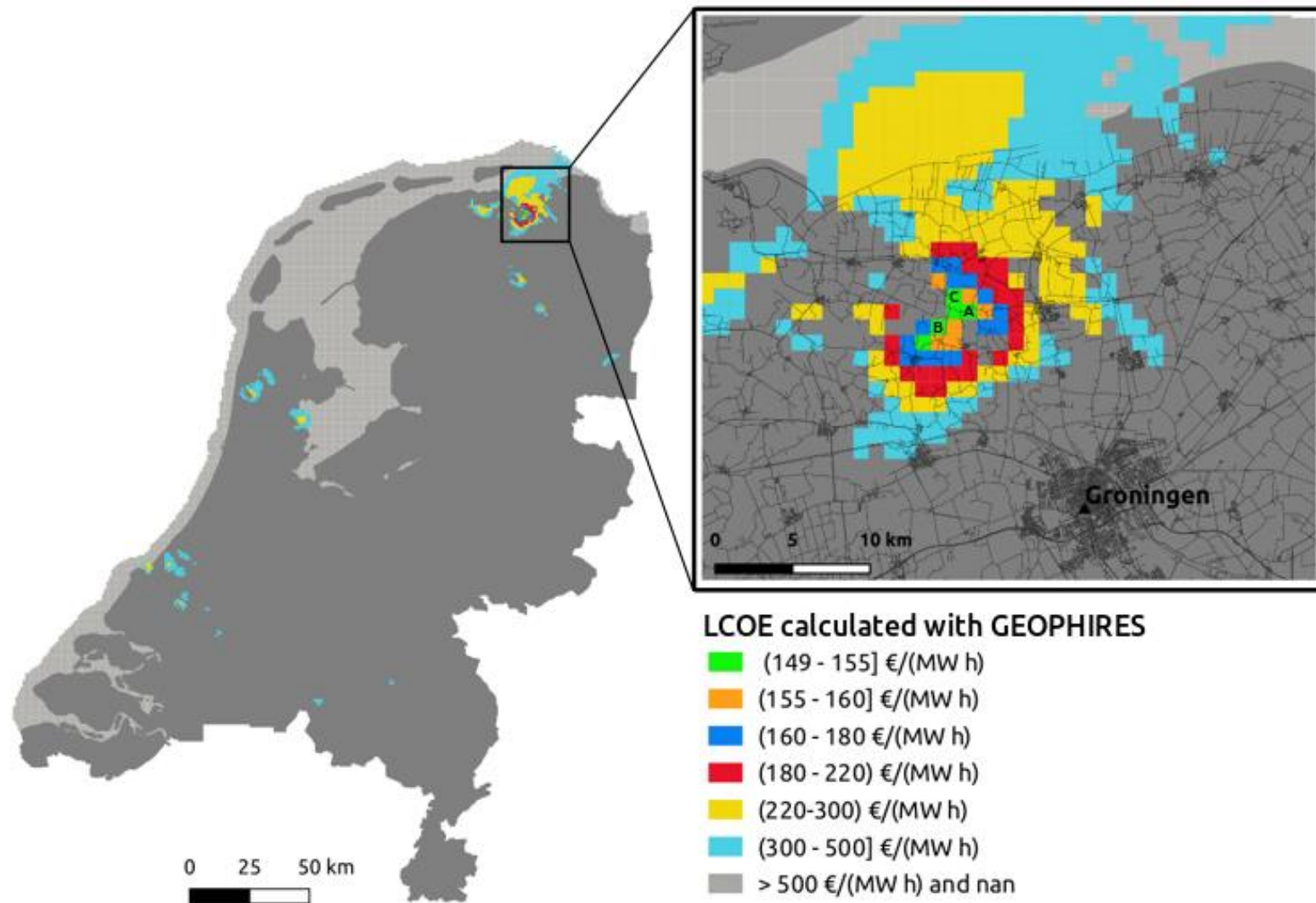


Figure 26. LCOE expected map of the Netherlands. On the left, the map of the whole Netherlands showing a few places where the LCOE is below 500 €/ (MW h). On the right, the zoom on the more promising area, 20 km north from Groningen. The reservoirs A, B and C have the lowest LCOE and their characteristic are summarized in the following table. They all belong to the Upper Rotliegend Group, the RO STACKED basin.



The zoom on *Figure 26* shows the most promising area for electric production potential which is well-populated with low LCOE reservoirs. Each pixel is a reservoir of 1 [km<sup>2</sup>] characterized by their simulation attributes accessible by clicking on them. In QGIS the analysis can be more interactive as one can access the information about all the reservoirs at different depths that share the same location. On this map, only the reservoir with the lowest LCOE for each location is rendered. A section of the attribute table of the best three reservoirs in the whole Netherlands is reported in

*Table 5.* The three reservoirs A, B and C are surrounded by concentric circles of gradually increasing LCOE values. This means there are homogeneous characteristics of the subsurface for a quite extended area supporting the most promising reservoirs. They all belong to the Upper Rotliegend Group, the RO STACKED basin. Both reservoir input and power and cost output are similar among the three reservoirs. They are all around 3700 [m] depth, qualifying for deep geothermal reservoirs. The complementary role of temperature and transmissivity is confirmed once again: the lowest temperature (reservoir C) is linked to the highest transmissivity and vice versa (reservoir B).

<b>RO STACKED</b>	<b>A</b>	<b>B</b>	<b>C</b>
<b>Thickness [m]</b>	243	234	241
<b>Depth [m]</b>	3701	3835	3666
<b>Temperature [°C]</b>	122	124	120
<b>Permeability [mD]</b>	92	88	103
<b>Transmissivity [D m]</b>	22	20	25
<b>LCOE [€/ (MW h)]</b>	149	150	151
<b>Net electric power [MW<sub>e</sub>]</b>	2.3	2.4	2.2
<b>Flow-rate [kg/s]</b>	163	164	164

*Table 5.* Characteristics of the three best reservoirs, having the lowest expected LCOE.

The Rotliegend Group covers almost the entire Netherlands area at a variable depth around 3 [km]. The Slochteren Formation of the Rotliegend Group is the main gas reservoir in the Netherlands. In the north of the dashed line in *Figure 27*, the gas is caught in the Rotliegend Slochteren Sandstone reservoir under the Zechtein seal. To the south of that line, the seal of the Rotliegend petroleum play is absent. Eight geothermal systems are in the Slochteren Sandstone and they are all situated around the structural geological domain, the TYH. The average reported permeability of the

reservoir is in the order of 50–350 [mD] and thickness values of 100–250 [m]. These result in transmissivity values of up to 50 [Dm] (Figure 27), which leads to a possible installed power of up to more than 30 [MW<sub>th</sub>] for direct use (Harmen F. Mijnlief, 2020). These characteristics prove well in the case of ORC power production as well in the detected area of this study.

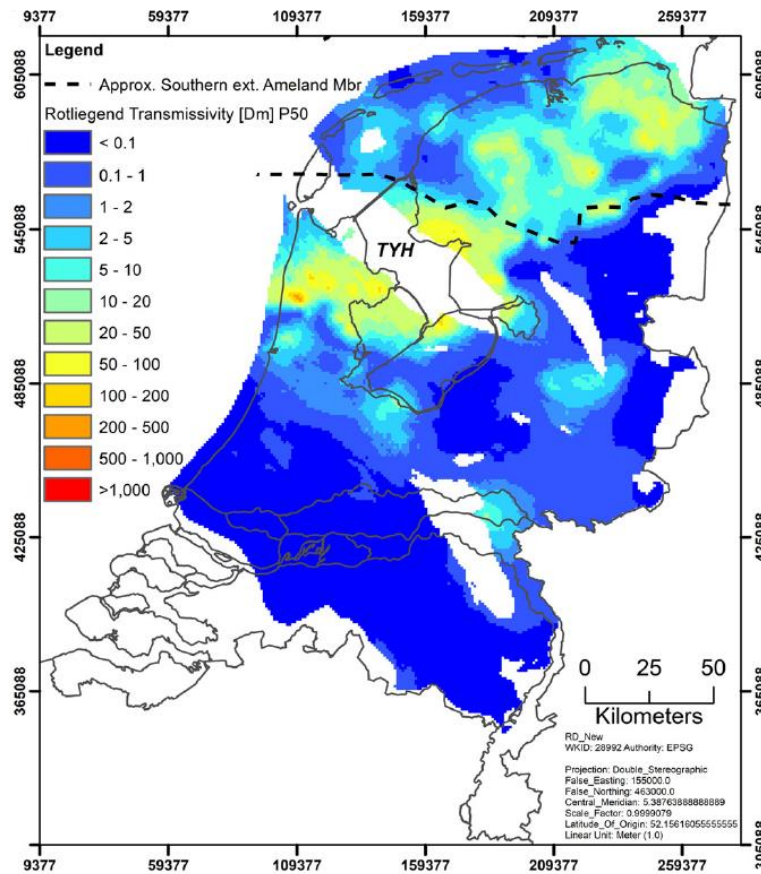
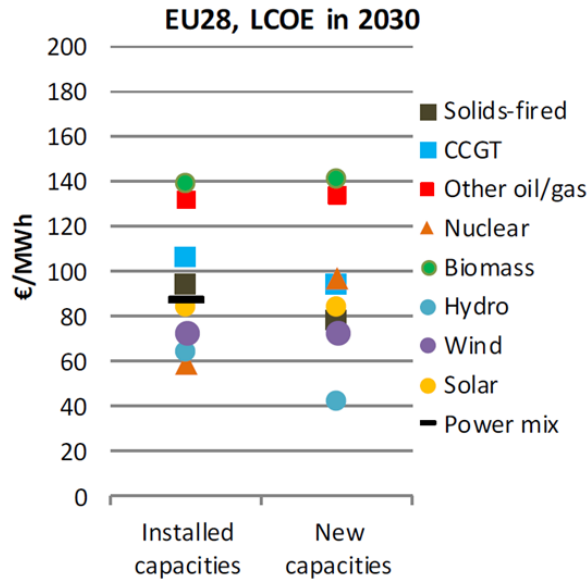


Figure 27. Transmissivity of the Rotliegend Group taken from Mijnlief (2020). TYH is the structural geological domain. The dashed line separates the Zechtein seal area from the rest of the basin.

Given the technical potential for electric power generation, the LCOE analysis provides a first useful insight into the economic potential. When approaching the LCOE evaluation, it is good to bear in mind that it provides only a partial answer to the preferred technology for new baseload generation. For example, it does not address exactly when capacity is needed. It might understate the rates of decline for existing stock, changes in transmission capacity, or even location impactation (limits to land use expansion). Other externalities, including market financial risks and short-term price volatility, are difficult to portray in the overall LCOE question and comparative analysis (see paragraph 1.4).

While being careful when comparing the LCOE with literature values, such analysis still gives useful information. *Figure 28* shows the cost projection for the European countries in 2030 by type of source. The upper limit is  $140 \left[ \frac{\text{€}}{\text{MWh}} \right]$  and is related to conventional fossil fuel and biomass. The best LCOE expected values in the Netherlands are a bit over this threshold. The other renewables are below  $100 \left[ \frac{\text{€}}{\text{MWh}} \right]$ .



*Figure 28. Electricity cost projection for European countries in 2030, taken from (Energy prices and costs in Europe., 2019).*

### 4.3 Electric power potential and LCOE Lazard

To partially overcome the difficulty in comparing LCOE evaluated with different hypotheses, the LCOE Lazard simulation is put in place. To evaluate the electric power potential at a regional scale it is better considering the cumulative capacity. *Figure 29* shows the LCOE obtained after simulation two and three as a function of the cumulative capacity. The LCOE expected is in green while the LCOE Lazard is in blue. They have the same shape, the Lazard being shifted upward. This is mainly due to the higher discount rate used in Lazard, 9.6% instead of 5.4%, which has a substantial impact on the LCOE (see equation 30). Both functions have a linear grow up to almost 2200  $[MW_e]$  capacity and then it becomes exponential. This can be interpreted as the maximum capacity is reached. However, the convenience of the implementation might have already faded away in the first hundreds of cumulative capacity.

That is why a more realistic analysis can be done focusing on the first linear part of this plot. *Figure 30* is a zoom of the functions up to 650 [MW<sub>e</sub>] capacity and LCOE of 650  $\left[\frac{\text{€}}{\text{MWh}}\right]$ . The linear growth is interrupted around 130 [MW<sub>e</sub>] where the lines change the slope: LCOE Lazard slope goes from 0.8 to 0.6, expected LCOE from 0.5 to 0.3. 100 [MW<sub>e</sub>] capacity is available under 200  $\left[\frac{\text{€}}{\text{MWh}}\right]$  using TNO financial hypothesis, under 320  $\left[\frac{\text{€}}{\text{MWh}}\right]$  using Lazard's hypothesis. 100 [MW<sub>e</sub>] capacity turns into an energy production of 600000 [MW<sub>th</sub>] (considering annual load hours of 6000, (Vrijlandt et al., 2019)). That corresponds to 2.16 [PJ] which is 0.5% of 2018 electric consumption (435 [PJ]) and 7.5% of 2018 electric import (28.7 [PJ]), (cbs.nl, 2018)).

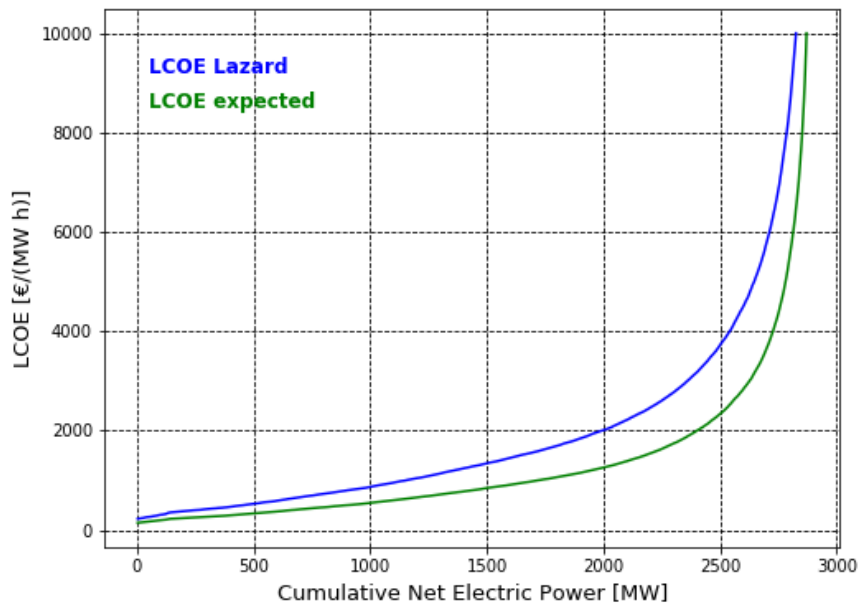


*Figure 29. LCOE obtained with Lazard economic hypothesis and with TNO hypothesis as a function of the cumulative capacity.*

The LCOE Lazard range for cumulative capacity up to 100 [MW<sub>e</sub>] goes from 228  $\left[\frac{\text{€}}{\text{MWh}}\right]$  to 320  $\left[\frac{\text{€}}{\text{MWh}}\right]$ . Converted into  $\left[\frac{\text{\$}}{\text{MWh}}\right]$ , it is plotted in *Figure 31*. This interval is the highest one compared to both conventional and renewable energy sources. However, it has to be noticed that the reported LCOE ranges for renewables already include the subsidies while the simulated LCOE Lazard for the Netherlands does not consider them. In principle, there might be a margin to reduce cost.

According to these economic indicators, a geothermal development project for electric power production purposes might be not yet competitive in the actual market. This consideration should not prevent from thinking that in the future the costs could decrease due to technological improvements and subsidies to CO<sub>2</sub>-free

resources. It is good to stress again that this is a regional analysis where the LCOE acts as a good proxy to assess the overall economic potential and to rank the reservoirs but that might not be exhaustive for a site-specific evaluation.

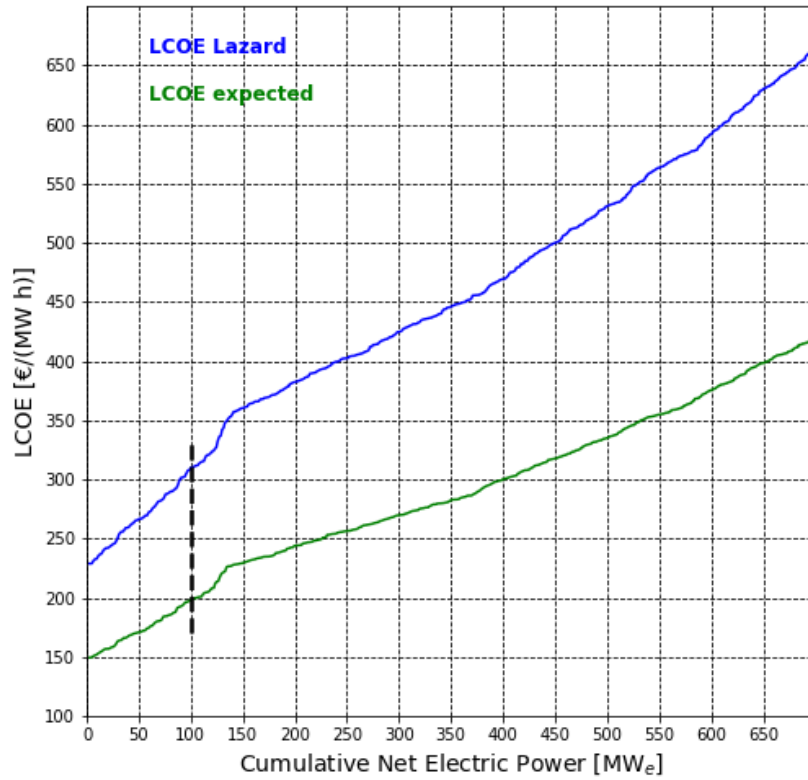


Figure 30. Zoom of the previous figure.

		\$0	\$30	\$60	\$90	\$120	\$150	\$180	\$210	\$240	\$270	\$300	\$330	\$360	\$390
LCOE Lazard	Geothermal ORC in the Netherlands											\$251			\$352
	Gas Combined Cycle		\$44		\$68										
Conventional	Coal		\$66										\$152		
	Nuclear				\$118										\$192
	Gas Peaking											\$150			\$199
	Wind		\$28		\$54										
Renewable Energy	Solar PV-Thin Film Utility Scale		\$32		\$42										
	Solar PV-Rooftop C&I				\$75										\$154
	Solar PV-Rooftop Residential													\$151	\$242

Figure 31. LCOE Lazard for the Netherlands and comparison with other sources. Adapted from Lazard's (2019).

---

---

## CHAPTER 5

# ORC OPTIMIZATION

In this chapter, the ORC configuration for the most promising reservoir, reservoir A found in paragraph 4.2, is optimized with respect to the net power output. As presented in paragraph 3.5, the minimization of the cost implemented in GEOPHIRES implies the acceptance of a suboptimal solution for the net power output. A trade-off is identified between the lowest achievable cost and the highest available net power (see again *Figure 17*). At the regional scale of the resource assessment presented with this work, the minimum cost is the driving criteria chosen. This is because the main goal is to identify the most promising reservoirs among the other ones. To this purpose, a tool like GEOPHIRES has proven well as it allows a quick and straightforward evaluation of both power and cost thanks to its built-in correlation based on existing power plants. But what might happen when the analysis is brought forward to a specific reservoir? What are the key cycle parameters for the conversion of thermal power into electric power? And finally, how much the ORC optimization will change the results already obtained with a regional assessment?

In this chapter, this issue is addressed giving an insight into the ORC cycle parameters. The calculations are made in an Excel spreadsheet coupled with FluidProp (*FluidProp*, n.d.). This allows having control over all the thermodynamic stages in the cycle and performing the desired optimization of the cycle performances. This is not possible with GEOPHIRES as it relies on correlations between the utilization efficiency, the geofluids wellhead temperature and ambient temperature (see again *Figure 10*). While building these functions, they have been already optimized for a specific working fluid (K. F. Beckers, 2016). In GEOPHIRES only the final correlation function is used, as the code is not designed for optimizing a particular cycle but gives different correlations depending on the desired cycle (see

---

again paragraph 2.4). In this way, there is no control over the cycle parameters which is instead the necessary condition to the preliminary design of a power plant.

For example, one of the ORC parameters that would be interesting to know is the reinjection temperature of the geothermal fluid. In GEOPHIRES the reinjection temperature is an input and does not influence the ORC power output. However, this temperature influences the reinjected water density modifying the pressure balance (see equations 14, 15, 16, 17). This affects the needed pump power (see equation 18). The pump power is then subtracted to the useful power  $P_e$  to obtain the net electric power (see equation 23). According to the equations, the higher the reinjection temperature, the higher the pump power, the lower the net electric power. In the regional assessment done, the reinjection temperature of 30 [°C] is kept for the ORC simulation as well to be compliant with the hypothesis set by TNO for the heat. As there are no constraints for the reinjection temperature, this choice would assure higher net power and lower cost. However, in real cycles, the reinjection temperature is linked to the useful power as well.

The optimization done in Excel maximizes the net power output by changing the evaporation temperature of the working fluid for a given pinch point temperature difference (which is a cycle parameter explained later). The reinjection temperature is then a function of the evaporation temperature and becomes physically linked to the modelled process. The optimal net power is compared to the one found with the regional assessment in GEOPHIRES (paragraph 5.2).

Given the found optimal reinjection temperature, reservoir A is simulated back in GEOPHIRES to see the changes in the power and cost output (paragraph 5.3).

## 5.1 Geothermal ORC typical configurations

The ORC configuration chosen for this work is the subcritical single-pressure-level using the refrigerant R245fa as the working fluid.

The single-pressure-level system is the simplest ORC configuration possible. The geothermal fluid, either in liquid or both phases, provides heat to the organic fluid through the tubes of heat exchangers, where the organic fluid is vaporized and fed to the turbine (Macchi, 2016).

The critical point of a substance is the temperature and pressure at which that substance can behave like a gas and a liquid at the same time, hence indistinguishable gas and liquid phases occur. A subcritical cycle has a maximum pressure that is lower than the critical one. Working fluid passes through an evaporation process that is isothermal if the fluid is a pure compound. If the working fluid has a critical temperature higher than the heat source maximum temperature,



---

the use of superheating is generally detrimental since it entails a reduction of the working fluid mass flow rate and the power production (Macchi, 2016). A supercritical or transcritical cycle is a cycle with a maximum pressure higher than the critical one. Working fluid is heated up from subcooled liquid to superheated vapour with a smooth transition above the critical point. The phase change is gradual and all the physical and thermodynamic properties vary without discontinuity in the heat introduction process (Macchi, 2016). Despite the higher attainable efficiencies, supercritical cycles generally have higher pressures than the subcritical cycles and more expensive devices are required. For this reason, the subcritical ORC is considered here.

In GEOPHIRES there is no indication about the working fluid used. So, for this analysis, the refrigerant R245fa is chosen as it is widely used in the literature and proves well in simulations (Bamgbopa, 2012) (Astolfi et al., 2014) (Liu et al., 2013). Besides, it belongs to the refrigerant group of hydrofluorocarbon (HFC). Most of HCFs are safe being non-toxic and flammable only under extreme conditions, differently from other working fluids such as hydrocarbons.

## 5.2 Reservoir A: ORC simulation hypothesis and results

Reservoir A is the best reservoir identified in paragraph 4.2 and described in *Table 5*. This is the target reservoir for the ORC optimization here carried out both as an example of what a further analysis of viability could be for the specific case and a check on the GEOPHIRES performances.

The cycle scheme is presented in *Figure 32*. The geothermal fluid is pumped up from the ground (bottom left well) at the temperature of the reservoir A which is 122 [°C]. In this case the heat losses in the production well are neglected. The water releases heat to the working fluids through two heat exchangers stages from A to C (evaporator and economizer). It is then reinjected back to the ground at the temperature  $T_c$ . R245fa circulates on the right from points 1 to 5. It is pumped as liquid phase from 1 to 2, heated up in the economizer until it changes phase and evaporates in the economizer.  $T_4$  is the evaporation temperature  $T_{eva}$  which is changed until the maximum net power is found. *Figure 33* shows the cycle points already optimized. It is introduced here to show the heat exchange process and the constraint quantity such as the pinch point temperature difference  $\Delta T_{pinch\ point}$ . It is the difference between  $T_B$  and  $T_{eva}$  and it is the point where the temperature difference between the hot fluid (geothermal water) and the cold fluid (R245fa) is minimum in the heat exchanger (economizer and evaporator). As listed in

*Table 6*, this is set to 10 [°C]. Between  $T_{eva}$  and  $T_3$  there is the subcooling temperature difference here set as 3 [°C]. During the evaporation, the temperature is constant and the working fluid receives heat from the geothermal water to change phase and

evaporate. At the same time, the geothermal fluid cools down from  $T_A$  to  $T_C$ . Once the working fluid is evaporated, it enters the turbines and generates mechanical power turned into electricity. From 5 to 1 there is the condenser. Here the working fluid changes phase again into liquid by releasing heat to the air at ambient temperature flowing from a to b.

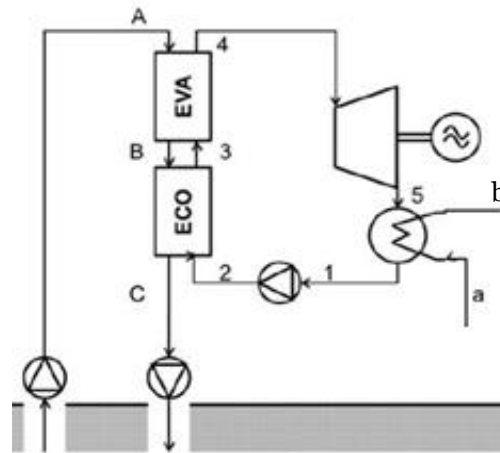


Figure 32. Scheme of the ORC cycle configuration optimized for the reservoir A. This is a subcritical ORC where the working fluid is condensed with air at ambient temperature. Adapted from (Astolfi et al., 2014)

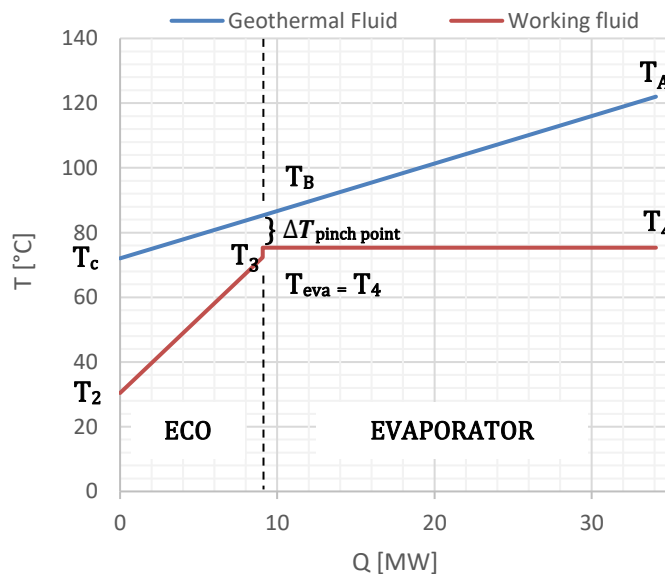


Figure 33. Plot of the heat exchanged between the geothermal fluid and the working fluid.

All the simulation hypothesis are listed in Table 6. Besides the parameters already presented, the pressure losses are included, the condensing conditions are specified and the turbomachinery efficiency listed. The power consumption of the auxiliaries is estimated to be 1.5 % of the obtained ORC gross power.

<b>Reservoir A: ORC using R245fa refrigerant</b>			
<b><i>Geothermal pressurized water from the doublet</i></b>			
Geothermal fluid flow rate	$\dot{m}$	[kg/s]	163
Geothermal fluid temperature	$T_A$	[°C]	122
<b><i>Evaporator and economizer</i></b>			
Sub-cooling at the economizer exit	$\Delta T_{\text{sub}}$	[°C]	3
Pinch point temperature difference	$\Delta T_{\text{pinch point}}$	[°C]	10
Relative pressure losses in the economizer	$(\Delta p/p)_{\text{eco}}$	[-]	0.2
<b><i>Condenser</i></b>			
Cooling air entering the condenser	$T_{\text{air,in}}$	[°C]	15
Temperature rise in the condenser	$\Delta T_{\text{cond}}$	[°C]	5
Condensing temperature	$T_{\text{cond}}$	[°C]	25
Condenser pressure losses	$\Delta p$	[bar]	2
<b><i>Machine efficiencies and consumption</i></b>			
Turbine isentropic efficiency	$\eta_{\text{is-T}}$	[%]	80
Generator mechanical-electrical efficiency	$\eta_{\text{m-el,g}}$	[%]	95
Pumps hydraulic efficiency	$\eta_{\text{hyd}}$	[%]	70
Pumps mechanical-electrical efficiency	$\eta_{\text{m-el,p}}$	[%]	90
Auxiliaries power consumption as a percentage of the ORC gross power		[%]	1.5

Table 6. ORC simulation parameters in reservoir A.

The thermodynamic properties (pressure, temperature, enthalpy, entropy) of the fluids, both the geothermal one and R245fa are calculated with FluidProp for each point in the scheme.

The heat power entering the cycle  $Q_{in}$ :

$$Q_{in} = \dot{m} c_{p_{\text{water}}} (T_A - T_C) [MW_{th}] \quad (32)$$

The gross power  $P_e$  is defined as:

$$P_e = m_{R245fa} \left[ (h_4 - h_5) \eta_{\text{m-el,g}} - \frac{h_2 - h_1}{\eta_{\text{m-el,p}}} \right] [MW_e] \quad (33)$$

$$m_{R245fa}: \text{mass flow rate of the working fluid } \left[ \frac{\text{kg}}{\text{s}} \right]$$

$h_i$ : enthalpy of the correspondent fluid in the thermodynamic point  $i$   $\left[\frac{kJ}{kg}\right]$

The mass flow rate of the working fluid  $m_{R245fa}$  is calculated as:

$$m_{R245fa} = \dot{m}c_{p_{water}}T_A \frac{h_A - h_B}{h_4 - h_3} \left[\frac{kg}{s}\right] \quad (34)$$

$c_{p_{water}}$ : heat capacity of water set equal to  $4.186 \left[\frac{kJ}{kg}\right]$

$h_i$ : enthalpy of the correspondent fluid in the thermodynamic point  $i$   $\left[\frac{kJ}{kg}\right]$

Particularly,  $h_4$  is the enthalpy of saturated vapour for R245fa at the evaporation temperature  $T_{eva}$ .  $h_3$  is the enthalpy of saturated liquid for R245fa at  $T_3$  which is the difference between  $T_{eva}$  and  $\Delta T_{sub}$ .

The ORC power  $P_{ORC}$  is obtained by subtracting the auxiliaries power consumption to the gross power obtained:

$$P_{ORC} = (1 - 0.015)P_e [MW_e] \quad (35)$$

With the Excel solver,  $P_{ORC}$  is maximized by varying  $T_{eva}$ . The first law efficiency  $\eta_l$  is defined as:

$$\eta_l = \frac{P_e}{Q_{in}} [-] \quad (36)$$

**Error! Reference source not found.** shows the variation of  $P_{ORC}$  (orange line) depending on the evaporation temperature.

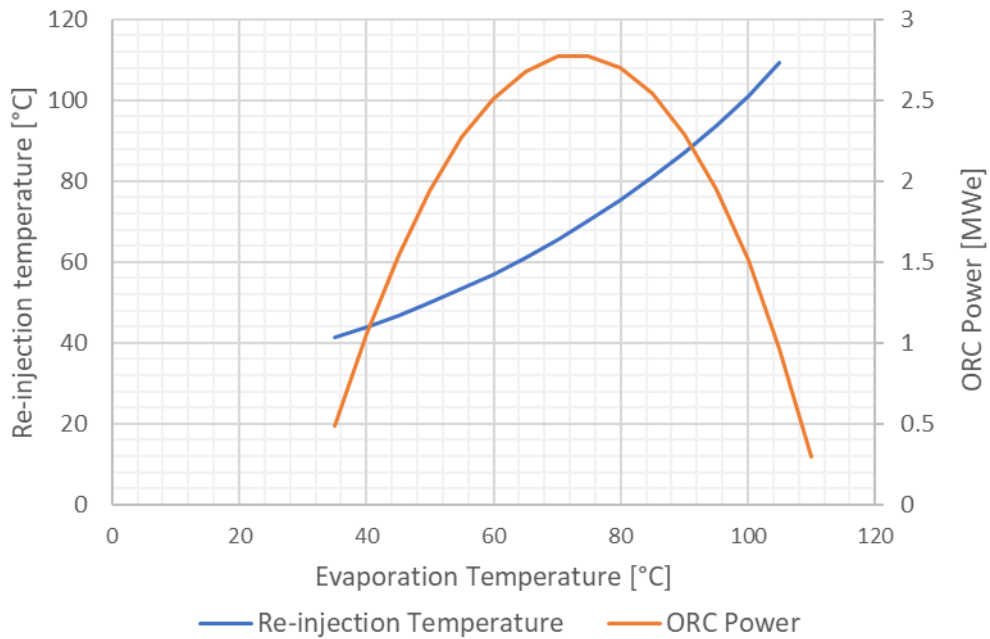


Figure 34. Plot of the ORC power and re-injection temperature as functions of the evaporation temperature.

The maximum is  $P_{ORC} = 2.78 [MW_e]$  for a  $T_{eva} = 72.88 [^{\circ}C]$ . The blue line shows that the injection temperature depends on the evaporation temperature. The corresponding re-injection temperature is equal to  $T_c = 68.15 [^{\circ}C]$ . Compared to the ORC power obtained with GEOPHIRES it is found that they are very close, being  $P_{ORC-GEOPHIRES} = 2.84 [MW_e]$ . The discrepancy could be due to some of the simulation hypothesis set in

Table 6 which might be different from the ones of GEOPHIRES that unfortunately are not available. The utilization efficiency  $\eta_u$  defined in equation 22 is close to the one calculated here as well. In fact,  $\eta_{u-Excel} = 24.4 [\%]$  with the correspondent exergy (see equation 21) calculated using the geothermal fluid flow rate and its enthalpies and entropies in point A and for a  $T_{amb} = 10.5 [^{\circ}C]$ . The utilization efficiency in GEOPHIRES is obtained through the correlation (purple line) for the ORC in *Figure 10*. Given the wellhead temperature of  $122 [^{\circ}C]$  and interpolating for an ambient temperature of  $10.5 [^{\circ}C]$ , the correspondent  $\eta_{u-GEOPHIRES} = 24.2 [\%]$ . This comparison is reported in Table 7.

	Electric power output	
	EXCEL	GEOPHIRES
Heat power entering the cycle $[MW_{th}]$	36.74	-
Gross power $P_e [MW_e]$	3.25	-
Auxiliaries power consumption $[MW_e]$	0.47	-
ORC power $P_{ORC} [MW_e]$	2.78	2.84
Utilization efficiency $\eta_u [\%]$	24.4	24.2

Table 7. Power output comparison between the optimization done in Excel and the results already obtained with GEOPHIRES.

All the thermodynamic points of the cycle are shown in *Figure 35*. Their properties are calculated in *Table 8* and used to evaluate the desired output of Table 7. The blue line is the ORC cycle. The circulating mass flow rate is the working fluid R245fa (equation 34).  $T_4$  is the evaporation temperature  $T_{eva}$  changed by the solver to get the maximum ORC power. The evaporation is made possible by the heat exchanged with the geothermal fluid (orange line). Its mass flow rate is an input and it is set to the optimal one found by GEOPHIRES.  $T_c$  is the new re-injection temperature found once solving the optimization. Between 5\* and 1 the working fluid condenses by releasing heat to the condensing airflow from the outside. The condensation area is not considered in the optimization and there is no constraint

on the amount of air needed. That is why the air mass flow rate is not specifically calculated.

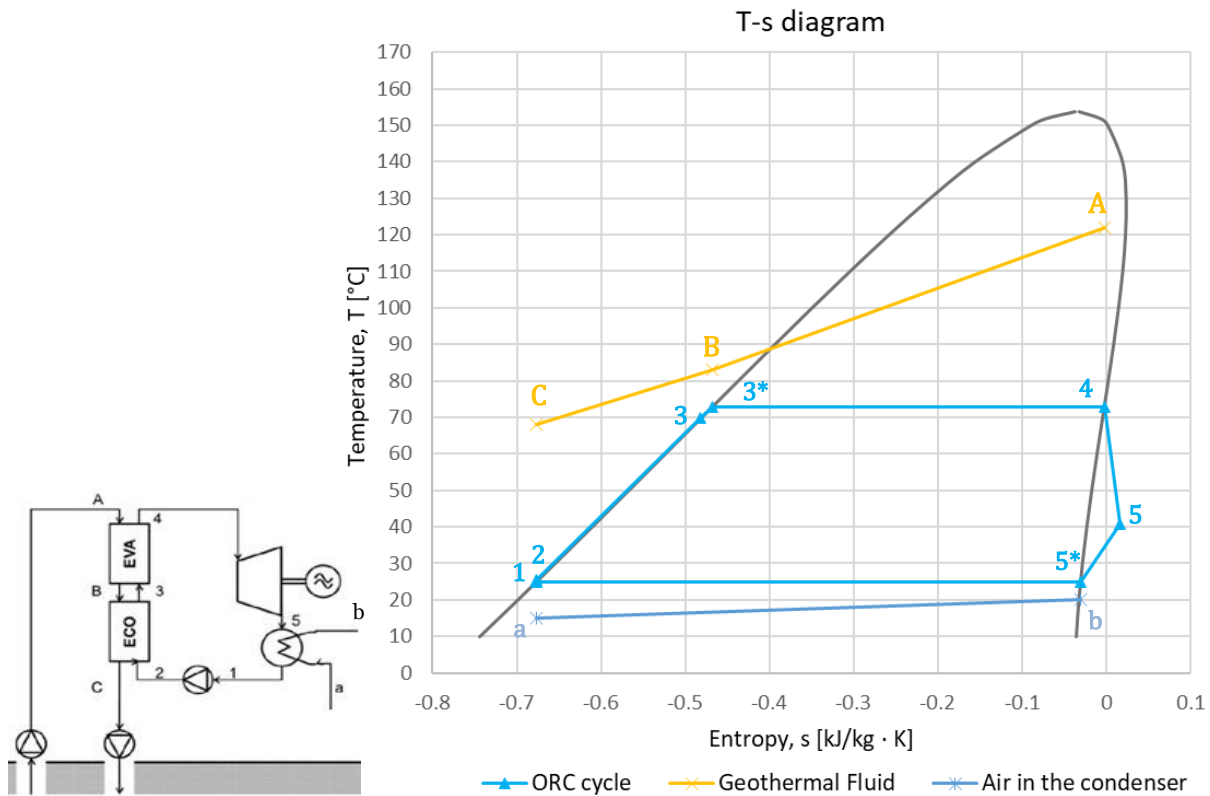


Figure 35. T-s diagram of the ORC cycle in reservoir A.

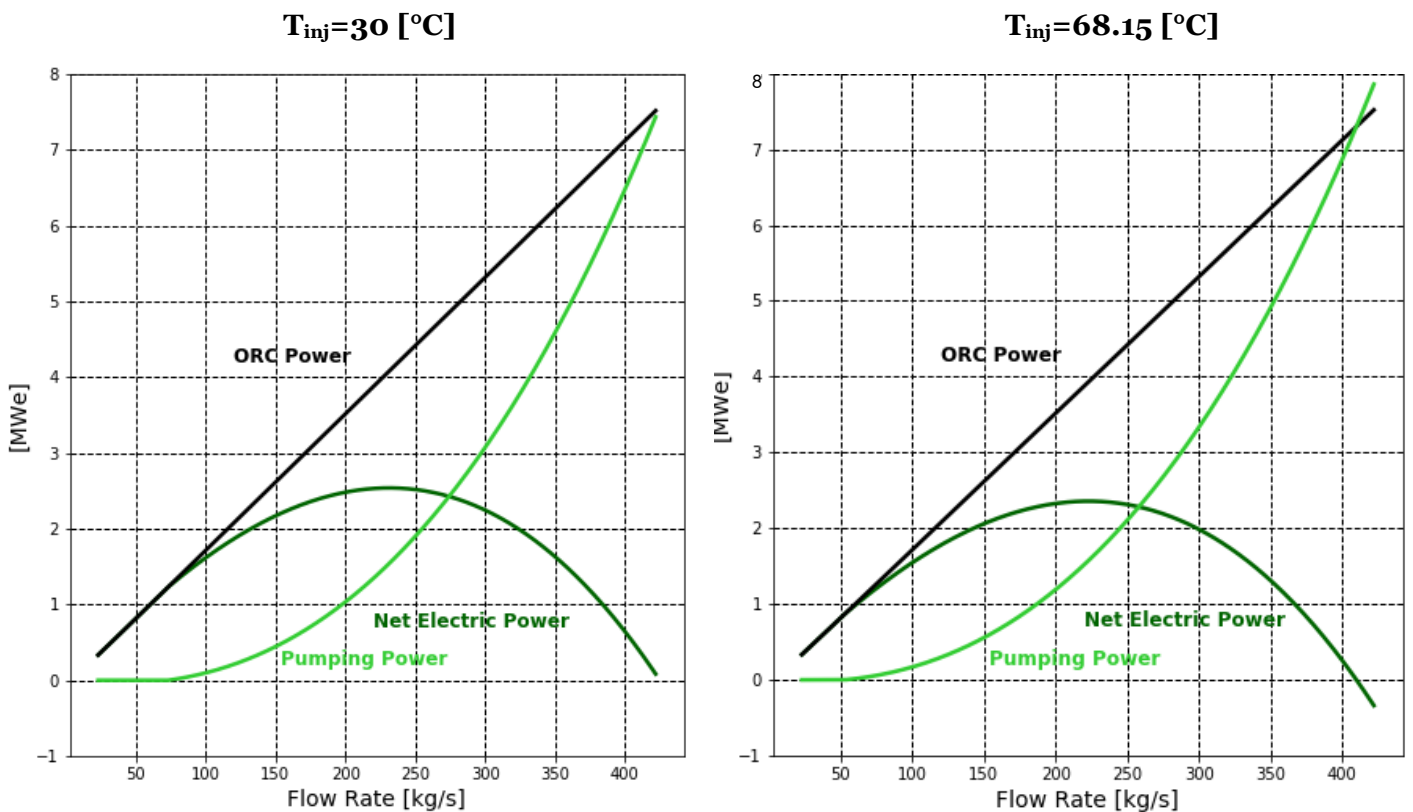
Cycle points	Mass flow rate [kg/s]	Pressure [bar]	Temperature [°C]	Enthalpy [kJ/kg]	Entropy [kJ/kg K]	Vapour quality [-]
<b>1</b>	160.91	1.49	25.00	-195.47	-0.68	0
<b>2</b>	160.91	8.26	25.40	-194.76	-0.68	0
<b>3</b>	160.91	6.60	69.88	-132.33	-0.48	0
<b>3*</b>	160.91	6.60	72.88	-127.80	-0.47	0
<b>4</b>	160.91	6.60	72.88	33.57	0.00	1
<b>5</b>	160.91	1.49	40.81	11.51	0.02	1
<b>5*</b>	160.91	0.03	25.00	-2.53	-0.03	1
<b>A</b>	163	2.12	122.00	512.29	1.55	0
<b>B</b>	163	0.53	82.88	347.03	1.11	0
<b>C</b>	163	0.29	68.15	285.28	0.93	0
<b>a</b>	-	0.02	15.00	62.98	0.22	0
<b>b</b>	-	0.02	20.00	83.92	0.30	0

Table 8. Thermodynamic properties of each point in the cycle.

---

### 5.3 Reservoir A: comparison with GEOPHIRES results

Once obtained the reinjection temperature in the optimal case, it is worth checking how the GEOPHIRES results would change when including this new information. *Figure 36* shows the power variations depending on the geothermal mass flow rate in the case of the original re-injection temperature (on the left) and with the new one (on the right). The ORC power increases linearly with the flow-rate being the same in the two plots. This confirms that in GEOPHIRES the re-injection temperature set as input by the user does not affect the gross power. The pumping power curve is shifted upwards. As the net power is the difference between the ORC power and the pumping power and being the ORC the same curve, the net electric power is reduced for a higher reinjection temperature, given the same flow rate. The net power curve on the right is shifted downwards. This behaviour confirms that in GEOPHIRES the higher the reinjection temperature, the higher the pump power, the lower the net electric power.



*Figure 36. Reservoir A: simulation in GEOPHIRES of the ORC power, pumping power and net electric power varying the flow rate. On the left the simulation done in the regional assessment using a re-injection temperature of 30 [°C]. On the right reservoir A is simulated again using the new re-injection temperature of 68.15 [°C] found with the Excel optimization.*

However, the changes in the results don't appear substantial. Table 9 lists the actual values obtained for the optimal flow rate found for reservoir A. GEOPHIRES and the Excel spreadsheet are used in cascade to refine the power and cost optimization. The first row is the optimization of the LCOE expected which gives as results the minimum LCOE and the corresponding optimal flow rate. This value is used as input for the ORC power optimization done in Excel which gives as output the maximum ORC power and the corresponding re-injection temperature. When the re-injection temperature of 68.15 [°C] is used back in GEOPHIRES, the actual decrease in the net electric power is 0.16 [MW<sub>e</sub>]. The LCOE is then increased up to 159 [ $\frac{\text{€}}{\text{MWh}}$ ]. This last simulation gives a new optimal flow-rate that can be used again in the Excel spreadsheet to find a new ORC power maximum. This iteration shows again the trade-off between the minimum LCOE that can be reached and the maximum available power. The ORC power values are close to each other and the net electric power (the ORC power minus the pump power) is decreased a little when using the re-injection temperature given by the Excel optimization.

<b>Reservoir A: power and cost optimization</b>					
	<b>Flow rate [kg/s]</b>	<b>Re-injection temperature [°C]</b>	<b>ORC power [MW<sub>e</sub>]</b>	<b>Net electric power [MW<sub>e</sub>]</b>	<b>LCOE [€/MWh]</b>
<b>GEOPHIRES</b> <i>LCOE expected</i>	163	30	2.84	2.28	149
<b>EXCEL</b> <i>ORC optimized</i>	163	68.15 *	2.78	-	-
<b>GEOPHIRES</b> <i>T<sub>inj</sub> from Excel *</i>	158 **	68.15	2.76	2.12	159
<b>EXCEL</b> <i>Flow rate from GEOPHIRES **</i>	158	68.15	2.70	-	-

Table 9. Results of the local analysis in reservoir A. The first row is the GEOPHIRES regional assessment done using the same re-injection temperature of the heat simulation. The second row presents the results of the ORC optimization results. In the third row, there are the new results obtained using the new re-injection temperature back in GEOPHIRES. In the last one, the ORC power is optimized again using the newly optimized mass flow rate from GEOPHIRES.

The results show that there is accordance between the regional analysis done with the proposed method and a preliminary ORC optimization done for a specific reservoir. Both power and LCOE values are of the same order of magnitude. The power shows smaller variations compared to the LCOE. However, the variation in LCOE can be assumed to be proportional to the same extent in every reservoir. This means that the correspondent ranking of the reservoirs is not going to be modified.



---

An increase in the LCOE range might affect only the comparison with other sources of energy production.

---

## CHAPTER 6

# CONCLUSIONS

This work has benefitted from the availability of numerous subsurface data publicly available in the ThermoGIS project. The key data of temperature, thickness and permeability at a resolution of 1 km<sup>2</sup> reservoir at a certain depth have made it possible an assessment of the geothermal potential for the whole Netherlands at a refined scale.

- *The set-up procedure to overcome the difficulty in using GIS-based data with a Python source code has enabled the techno-economic simulator to run over more than three hundred thousands of reservoirs, instead of just one. The great advantage of using GEOPHIRES is the possibility to simulate both direct-use of heat and electricity generation. Moreover, it evaluates the cost indicator simultaneously.*
- *Given the availability of the crucial input data that are reservoir temperature, depth, thickness and permeability, this assessment method can be applied to other regions or countries.*
- *The method presented is reliable at a regional scale and provides accurate results when compared to a case-specific analysis as well. A specific ORC power optimization is done for the best reservoir identified with the regional analysis. The ORC power results in the two cases are very close: 2.84 [MW<sub>e</sub>] obtained with GEOPHIRES and 2.78 [MW<sub>e</sub>]. When simulating the reservoir back in GEOPHIRES with the newfound conditions, the net electric power goes from 2.28 [MW<sub>e</sub>] to 2.12 [MW<sub>e</sub>] and the LCOE increases from 149  $\left[\frac{\text{€}}{\text{kWh}}\right]$  to 159  $\left[\frac{\text{€}}{\text{kWh}}\right]$ .*

- 
- *The geothermal heat power assessment has confirmed the results previously obtained by TNO and GEOPHIRES technical and economic simulation components has been validated against existing data.* At the same time, assigning one LCOH value to each reservoir has allowed for a refined ranking of the promising reservoirs. The corresponding maps become powerful tools for land planning and private investments.
  - *The technical potential for electric power production with Organic Rankine Cycle technology in the Netherlands is proven.* This has been possible thanks to the optimization of the flow-rate and the concurrent evaluation of temperature and transmissivity. This one is present in the impedance parameter which is calculated reservoir by reservoir before becoming an input into GEOPHIRES. The electric power potential assessment hasn't been done before in the Netherlands because the geothermal source is classified as low temperature. However, this work has identified 238 reservoirs with power capacity between 1 [ $MW_e$ ] and 2.4 [ $MW_e$ ]. This proves that it is not always advisable to classify a reservoir as not suitable for electric power production based only on the temperature criteria.
  - *The economic viability of ORC power plants in the Netherlands seems to be challenged by the high cost at the moment.* Both LCOE expected and Lazard's ones have higher values compared to the ones of the other renewables. However, there is a cumulative power capacity of 100 [ $MW_e$ ] which might generate energy correspondent to 7.5% of 2018 electric import, under 200 [ $\frac{\text{€}}{\text{kWh}}$ ]. It is worth remembering that the LCOE does not include environmental costs, for example, CO<sub>2</sub> emissions. In the case of conventional energy sources, these costs need to be added, while for geothermal binary plants there are avoided emissions. Moreover, the LCOE does not represent the advantage of the geothermal energy which is both renewable and a source of baseload electricity. Further studies could be focussed on evaluating complementary indicators to include these aspects in the assessment as well. Even if LCOE is a good first-hand indicator of the economic potential, this might improve as well, given future changes in the market, technological development and greater support from government subsidies.

---

## Bibliography

- Adams, B. M., Sutter, D., Mazzotti, M., & Saar, M. O. (2020). Combining Direct Air Capture and Geothermal Heat and Electricity Generation for Net-negative Carbon Dioxide Emissions. *World Geothermal Congress*.
- Aldersey-Williams, J., & Rubert, T. (2019). Levelised cost of energy – A theoretical justification and critical assessment. *Energy Policy*, *124*, 169–179. <https://doi.org/10.1016/J.ENPOL.2018.10.004>
- Anderson, A., & Rezaie, B. (2019). Geothermal technology: Trends and potential role in a sustainable future. *Applied Energy*, *248*, 18–34. <https://doi.org/10.1016/J.APENERGY.2019.04.102>
- Arnórsson, S., Thórhallsson, S., & Stefánsson, A. (2015). Utilization of Geothermal Resources. In *The Encyclopedia of Volcanoes* (pp. 1235–1252). Academic Press. <https://doi.org/10.1016/B978-0-12-385938-9.00071-7>
- Astolfi, M., Romano, M. C., Bombarda, P., & Macchi, E. (2014). Binary ORC (organic Rankine cycles) power plants for the exploitation of medium–low temperature geothermal sources – Part A: Thermodynamic optimization. *Energy*, *66*, 423–434. <https://doi.org/10.1016/J.ENERGY.2013.11.056>
- Bamgbopa, M. O. (2012). *Modeling and performance evaluation of an organic Rankine cycle (ORC) with R245FA as working fluid*. <https://www.researchgate.net/publication/314735013>
- Beckers. (2020). *GEOPIHRES*. <https://github.com/NREL/GEOPIHRES-v2>
- Beckers, K. F. (2016). *Low-Temperature Geothermal Energy: Systems Modeling, Reservoir Simulation, And Economic Analysis*. <https://www.qoppa.com/pdfstudio>
- Beckers, Koenraad F., & McCabe, K. (2019). GEOPIHRES v2.0: updated geothermal techno-economic simulation tool. *Geothermal Energy*, *7*(1). <https://doi.org/10.1186/s40517-019-0119-6>
- Bertani, R. (2016). Geothermal power generation in the world 2010-2014 update report. *Geothermics*, *60*, 31–43. <https://doi.org/10.1016/j.geothermics.2015.11.003>
- CanGEA. (n.d.). <https://www.cangea.ca/britishcolumbiageothermal.html>
- cbs.nl. (2018). Centraal Bureau Voor de Statistiek (Central Agency for Statistics). <https://longreads.cbs.nl/trends18-eng/economy/figures/energy/>
- Ciriaco, A. E., Zarrouk, S. J., & Zakeri, G. (2020). Geothermal resource and reserve assessment methodology: Overview, analysis and future directions. *Renewable and*

- 
- Sustainable Energy Reviews*, 119, 109515.  
<https://doi.org/10.1016/J.RSER.2019.109515>
- Craig, J., Gerali, F., Macaulay, F., & Sorkhabi, R. (2018). The history of the European oil and gas industry (1600s-2000s). In *Geological Society Special Publication* (Vol. 465, Issue 1, pp. 1–24). Geological Society of London. <https://doi.org/10.1144/SP465.23>
- Data.gov*. (n.d.). <https://catalog.data.gov/dataset/geothermal-resources-of-alaska>
- de Vries, J. J. (2007). Groundwater. In D. A. J. B. & J. de J. Th.E. Wong (Ed.), *Geology of the Netherlands* (pp. 295–315). Royal Netherlands Academy of Arts.
- DiPippo, R. (2016). Binary Cycle Power Plants. In *Geothermal Power Plants* (pp. 193–239). Elsevier. <https://doi.org/10.1016/B978-0-08-100879-9.00008-2>
- Dutch Mining Act*. (n.d.). [https://wetten.overheid.nl/BWBR0014168/2020-03-18/#Hoofdstuk7\\_Artikel123](https://wetten.overheid.nl/BWBR0014168/2020-03-18/#Hoofdstuk7_Artikel123)
- ebn.nl*. (2019). [www.ebn.nl/wp-content/uploads/2019/03/EBN\\_Infographic-2019\\_18-MAART\\_Engels.pdf](http://www.ebn.nl/wp-content/uploads/2019/03/EBN_Infographic-2019_18-MAART_Engels.pdf) (2019)
- Edenhofer, Ottmar., Pichs Madruga, R., & Sokona, Y. (2012). *Renewable energy sources and climate change mitigation : special report of the Intergovernmental Panel on Climate Change*. Cambridge University Press.
- Energy Agenda Towards a low-carbon energy supply*. (2017).
- Energy prices and costs in Europe*. (2019).
- FluidProp*. (n.d.). <http://www.asimptote.nl/software/fluidprop>
- Garcia-Gutierrez, A., Espinosa-Paredes, G., & Hernandez-Ramirez, I. (2002). Study on the flow production characteristics of deep geothermal wells. *Geothermics*, 31(2), 141–167. [https://doi.org/10.1016/S0375-6505\(01\)00032-3](https://doi.org/10.1016/S0375-6505(01)00032-3)
- Garg, S. K., & Combs, J. (2015). A reformulation of USGS volumetric “heat in place” resource estimation method. *Geothermics*, 55, 150–158. <https://doi.org/https://doi.org/10.1016/j.geothermics.2015.02.004>
- Ge, S., & Gorelick, S. M. (2015). HYDROLOGY, FLOODS AND DROUGHTS | Groundwater and Surface Water. In *Encyclopedia of Atmospheric Sciences* (pp. 209–216). Academic Press. <https://doi.org/10.1016/B978-0-12-382225-3.00171-7>
- govenment.nl*. (2018). <https://www.government.nl/latest/news/2018/03/29/dutch-cabinet-termination-of-natural-gas-extraction-in-groningen>
- Gudmundsson, J.-S. (1988). *The elements of direct uses*. 17(1), 119–136.
- Holm, A., Jennejohn, D., & Blodgett, L. (2012). *Geothermal Energy and Greenhouse Gas Emissions*.
- International Renewable Energy Agency. (2017). *Geothermal power: Technology brief*. [www.irena.org](http://www.irena.org)
- Lazard’s. (2019). *Lazard’s Levelized Cost Of Energy Analysis – Version 13.0*.
- Liu, Q., Duan, Y., & Yang, Z. (2013). Performance analyses of geothermal organic Rankine cycles with selected hydrocarbon working fluids. *Energy*, 63, 123–132. <https://doi.org/10.1016/J.ENERGY.2013.10.035>
-

- 
- Lund, J. W., & Boyd, T. L. (2016). Direct utilization of geothermal energy 2015 worldwide review. *Geothermics*, 60, 66–93. <https://doi.org/10.1016/j.geothermics.2015.11.004>
- Macchi, Ennio. (2016). *Organic Rankine Cycle (ORC) Power Systems*. Elsevier Science.
- Mijnlieff, H F, Obdam, A. N. M., van Wees, J. D. A. M., Pluymaekers, M. P. D., & Veldkamp, J. G. (2014). *Oil and Gas Princetonlaan 6 3584 CB Utrecht DoubletCalc 1.4 manual English version for DoubletCalc 1.4.3*. [www.tno.nl](http://www.tno.nl)
- Mijnlieff, Harmen F. (2020). Introduction to the geothermal play and reservoir geology of the Netherlands. In *Geologie en Mijnbouw/Netherlands Journal of Geosciences* (Vol. 99). Cambridge University Press. <https://doi.org/10.1017/njg.2020.2>
- Moya, D., Aldás, C., & Kaparaju, P. (2018). Geothermal energy: Power plant technology and direct heat applications. *Renewable and Sustainable Energy Reviews*, 94, 889–901. <https://doi.org/10.1016/J.RSER.2018.06.047>
- Muffler, P., & Cataldi, R. (1978). Methods for regional assessment of geothermal resources. *Geothermics*, 7(2), 53–89. [https://doi.org/https://doi.org/10.1016/0375-6505\(78\)90002-0](https://doi.org/https://doi.org/10.1016/0375-6505(78)90002-0)
- Musch, E. (2018). The Energy Agreement (Energieakkoord) of the Netherlands in the European context. *ECPR General Conference*, August 22-25. [NLOG.nl](https://www.nlog.nl/en). (n.d.). <https://www.nlog.nl/en>
- Norden, B. (2011). *Geothermal Energy Utilization in Low-Enthalpy Sedimentary Environments*. [www.gfz-potsdam.de](http://www.gfz-potsdam.de)
- Onajite, E. (2014). Sedimentation and Oil/Gas Formation. In *Seismic Data Analysis Techniques in Hydrocarbon Exploration* (pp. 3–16). Elsevier. <https://doi.org/10.1016/B978-0-12-420023-4.00001-0>
- Ormat. (n.d.). <https://www.ormat.com/en/home/a/main/>
- Paris Agreement. (n.d.). [https://ec.europa.eu/clima/policies/international/negotiations/paris\\_en](https://ec.europa.eu/clima/policies/international/negotiations/paris_en)
- QGIS. (n.d.). <https://www.qgis.org/en/site/>
- Ramey, H. J. (1962). Wellbore Heat Transmission. *Journal of Petroleum Technology*.
- Randolph, J. B., & Saar, M. O. (2011). Coupling carbon dioxide sequestration with geothermal energy capture in naturally permeable, porous geologic formations: Implications for CO<sub>2</sub> sequestration. *Energy Procedia*, 4, 2206–2213. <https://doi.org/10.1016/J.EGYPRO.2011.02.108>
- Renewable Energy Agency, I. (2019). *Global Energy Transformation: A Roadmap to 2050 (2019 Edition)*. [www.irena.org](http://www.irena.org)
- rvo.nl. (2019). [english.rvo.nl/sites/default/files/2019/10/Brochure%20SDE%20plus%20ENG%20Autumn%202019.pdf](http://english.rvo.nl/sites/default/files/2019/10/Brochure%20SDE%20plus%20ENG%20Autumn%202019.pdf)
- Schütz F., Huenges E., Spalek A., Paloma Pérez D. B., de G. M. (2013). *Geothermal Electricity: Potential for CO<sub>2</sub> Mitigation*.
- spyder-IDE. (n.d.). <https://www.spyder-ide.org/>
-

- 
- Stefánsson, A., & Kleine, B. I. (2017). Hydrothermal Alteration. In *Encyclopedia of Geochemistry* (pp. 1–3). Springer International Publishing. [https://doi.org/10.1007/978-3-319-39193-9\\_65-1](https://doi.org/10.1007/978-3-319-39193-9_65-1)
- Stimac James, Goff Fraser, & Goff Cathy J. (2015). *Intrusion-related Geothermal Systems* (Dr Jim Stimac, Ed.). Elsevier.
- Stober, I., & Bucher, K. (2013). *Geothermal Energy From Theoretical Models to Exploration and Development* (Springer-Verlag, Ed.). <https://doi.org/10.1007/978-3-642-13352-7>
- Sudhoff, Glos, Wechsung, A. & S. (2019). Next Level Geothermal Power Generation (NGP) – A new sCO<sub>2</sub>-based geothermal concept. *German Geothermal Congress DGK. The European Green Deal*. (2019). European Commission.
- ThermoGIS*. (n.d.). <https://www.thermogis.nl/en>
- TNO.nl*. (n.d.). <https://www.tno.nl/en/about-tno/organisation/>
- TOUGH*. (n.d.). <https://tough.lbl.gov/>
- van der Zwaan, B., & Dalla Longa, F. (2019). Integrated assessment projections for global geothermal energy use. *Geothermics*, 82, 203–211. <https://doi.org/10.1016/J.GEOTHERMICS.2019.06.008>
- vigor-geothermia.it*. (n.d.). [http://www.vigor-geothermia.it/index.php?option=com\\_content&view=article&id=16&Itemid=23&lang=it](http://www.vigor-geothermia.it/index.php?option=com_content&view=article&id=16&Itemid=23&lang=it)
- Vrijlandt, M. A. W., Struijk, E. L. M., Brunner, L. G., Veldkamp, J. G., Witmans, N., Maljers, D., & van Wees, J. D. (2019). *ThermoGIS update: a renewed view on geothermal potential in the Netherlands*. 11–14. [www.thermogis.nl](http://www.thermogis.nl)
- Walraven, D., Laenen, B., & D'Haeseleer, W. (2013). Comparison of thermodynamic cycles for power production from low-temperature geothermal heat sources. *Energy Conversion and Management*, 66, 220–233. <https://doi.org/10.1016/j.enconman.2012.10.003>





---

## **APPENDIX**

# **PROGRAM SCRIPTS AND INPUT FILES**

Here are presented the scripts written to read the CSV file from the maps, to take the parameters of interest and to arrange them into an input file suitable for GEOPHIRES. At the same time, it makes GEOPHIRES run automatically all over the reservoirs. This is possible because GEOPHIRES is turned into a function which can be called by the main script returning the desired output.

The first script is the one I wrote for the LCOH calculation. The second script is the one for the LCOE calculation and includes the LCOE minimization described in paragraph 2.3. It is followed by the correspondent general input file. The LCOH general input file has the same structure with different values as reported in the simulation parameter table in paragraph 2.5. For this reason, it is reported only the LCOE general input file.

Each script is commented to help the understanding of the process. I wrote the general input file from the scratch reporting and organizing all the variables listed in the GEOPHIRES manual. The source code does not provide any comprehensive input file but each user has to set it up on their own.

## *Main Python script for the LCOH calculation*

```
1. # HEAT_TAKE_INPUT.py
2.
3. #!/usr/bin/env python
4. # coding: utf-8
5. """
6. @author: selene
7. """
8.
9. # Import libraries and GEOPHIRES written as a function.
10. import pandas as pd
11. import math
12. import numpy as np
13. import GEOPHIRES_Test
14.
15.
16. # CSV files exported from the QGIS maps. Each file corresponds to one basin.
17. basins = ['RBSHN', 'DC_STACKED', 'KN_STACKED', 'KNGLG_KNGLS', 'KNNSB', 'KNNSF_',
            'KNNSP', 'KNNSG', 'KNNSL', 'KNNSR', 'KNNSY', 'N_STACKED', 'NLFFD', 'NLFFS', 'NLLFR', '
            NLLFS', 'NMRFT', 'NMRFV', 'NMVFS', 'NMVFV', 'RBMDL', 'RBMDU', 'RBMH', 'RBMVL', 'RB
            MVU', 'RNROF', 'RNSOB', 'RO_STACKED', 'ROSL_ROSLU', 'ROSL', 'SLDN_STACKED', 'TR
            _STACKED', 'DCD', 'DCH', 'DC_STACKED']
18.
19.
20. # This cycle makes the simulation automatic for all the basins.
21. for k in basins:
22.
23.     # Read csv input file.
24.     rows=pd.read_csv("01_CSV_input_for_GEOPHIRES/{}.csv".format(k), header=0)
25.
26.     # Look for empty items and replace with nan.
27.     rows.replace(np.nan, np.nan)
28.
29.     # Define the vectors where saving the simulation results.
30.     LCOH=[]
31.     Hpower=[]
32.
33.
34.     # This cycle makes the simulation automatic for each row in the CSV files (so for each reserv
        oir).
35.     for i in range(rows["THICKNESS"].size):
36.
37.         # Take the reservoir parameters from each row and convert to unit of measurements suitb
            ale for GEOPHIRES.
38.         thickness=rows["THICKNESS"][i]*rows["net_to_gro"][i]
39.         depth_Neth=rows["DEPTH"][i]
40.         depth=depth_Neth/1000
41.         Trock=rows["TEMPERATUR"][i]
42.         permeability=rows["PERMEABILI"][i]
43.
44.         Twater=Trock
45.         T=Twater+273.15
46.         rhewater=(.7983223+(1.50896E-3-2.9104E-6*T)*T)*1E3
47.         prodwellflowrate=((rows["flow_rate_"][i])/3600)*rhewater #convert m3/h to kg/s
48.
49.         # Discharge not reliable input data.
50.         if rows["economic_p"][i]<1 or rows["economic_p"][i]>4:
51.             rows["economic_p"][i]=np.nan
```

```

52.     LCOH.append(np.nan)
53.     Hpower.append(np.nan)
54.
55.     elif thickness==0 or depth==0 or Trock==0 or permeability==0 or prodwellflowrate==
0:
56.         LCOH.append(np.nan)
57.         Hpower.append(np.nan)
58.
59.     else:
60.
61.         # Calculate the impedance to be used in the Ramey model.
62.         muwater=2.414E-5*np.power(10,247.8/(Twater+273.15-140))
63.         wellsep=707
64.         prodwelldiam=8.5*0.0254
65.         impedance=((muwater/(thickness*permeability))*np.log((4*wellsep)/(math.pi*prodw
elldiam)))*100000)/4 #divided by 4 to consider one doublet in the 5-spots.
66.
67.         Tsurf=10.5
68.         gradient=((Trock-Tsurf)/depth)
69.
70.
71.         # Search for the variable input values in the intermediate input text file and replace the
m with the reservoir parameters.
72.         fin=open("geoINPUTheat.txt", "rt")
73.         data=fin.read()
74.         data=data.replace('@depth', depth.astype('str'))
75.         data=data.replace('@gradient', gradient.astype('str'))
76.         data=data.replace('@prodwell', prodwellflowrate.astype('str'))
77.         data=data.replace('@impedance', impedance.astype('str'))
78.
79.         fin.close()
80.
81.         #Save the updated intermediate input file as the proper input file for GEOPHIRES.
82.         fin=open("H_Input.txt", "wt")
83.         fin.write(data)
84.         fin.close()
85.
86.         #Run GEOPHIRES.
87.         simulation=GEOPHIRES_Test.MainFunction()
88.         LCOH.append((simulation[0]/2.931)*0.91)#convert from $/MBTU to c/ kWth (in Eur
os)
89.         Hpower.append(simulation[1])
90.
91.
92.         # Save simulation results both in CSV and XLSX format.
93.         rows["basin"]=str(k)
94.         rows["LCOH"]=LCOH
95.         rows["Hpower"]=Hpower
96.
97.         rows.to_excel("Heat_Output_xls/HEAT_{}.xlsx".format(k))
98.         rows.to_csv("Heat_Output_csv/HEAT_{}.csv".format(k))
99.
100.
101. # Save all the results into a CSV file and a XLSX file.
102. df_list=[]
103.
104. basins = ['RBSHN', 'DC_STACKED', 'KN_STACKED', 'KNGLG_KNGLS', 'KNNSB', 'KNNSF_
KNNSP', 'KNNSG', 'KNNSL', 'KNNSR', 'KNNSY', 'N_STACKED', 'NLFFD', 'NLFFS', 'NLLFR', '
NLLFS', 'NMRFT', 'NMRFV', 'NMVFS', 'NMVfV', 'RBMDL', 'RBMDU', 'RBMH', 'RBMVL', 'RB
MVU', 'RNROF', 'RNSOB', 'RO_STACKED', 'ROSL_ROSLU', 'ROSL', 'SLDN_STACKED', 'TR
_STACKED', 'DCD', 'DCH', 'DC_STACKED']

```

```
105.  
106. for k in basins:  
107.  
108.     df_list.append(pd.read_csv("Heat_Output_csv/HEAT_{}.csv".format(k)))  
109.  
110. fullH_df = pd.concat(df_list)  
111.  
112. fullH_df.to_csv("Heat_Output_Plot/TOT_heat_output.csv")  
113. fullH_df.to_excel("Heat_Output_Plot/TOT_heat_output.xlsx")
```

### ***Main Python script for the LCOE calculation***

```
1. # ELECTRICITY_TAKE_INPUT.py  
2.  
3. #!/usr/bin/env python3
```

```

4. # -*- coding: utf-8 -*-
5. """
6. @author: selene
7. """
8.
9. # Import libraries and GEOPHIRES written as a function.
10. import pandas as pd
11. import math
12. import numpy as np
13. import GEOPHIRES_Test2
14.
15.
16. # CSV files exported from the QGIS maps. Each file corresponds to one basin.
17. basins = ['RBSHN', 'DC_STACKED', 'KN_STACKED', 'KNGLG_KNGLS', 'KNNSB', 'KNNSF_
KNNSP', 'KNNSG', 'KNNSL', 'KNNSR', 'KNNSY', 'N_STACKED', 'NLFFD', 'NLFFS', 'NLLFR', '
NLLFS', 'NMRFT', 'NMRFV', 'NMVFS', 'NMVSV', 'RBMDD', 'RBMDDU', 'RBMH', 'RBMVL', 'RB
MVU', 'RNROF', 'RNSOB', 'RO_STACKED', 'ROSL_ROSLU', 'ROSL', 'SLDN_STACKED', 'TR
_STACKED', 'DCD', 'DCH', 'DC_STACKED']
18.
19.
20. # This cycle makes the simulation automatic for all the basins.
21. for k in basins:
22.
23.     # Read csv input file.
24.     rows=pd.read_csv("o1_CSV_input_for_GEOPHIRES/{}.csv".format(k), header=0)
25.
26.     # Look for empty items and replace with nan.
27.     rows.replace(np.nan, np.nan)
28.
29.     # Define the vectors where saving the simulation results.
30.     LCOE=[]
31.     Epower=[]
32.     FlowOPT=[]
33.
34.
35.     # This cycle makes the simulation automatic for each row in the CSV files (so for each reser
voir).
36.     for i in range(rows['THICKNESS'].size):
37.
38.         # Take the reservoir parameters from each row and convert to unit of measurements suitb
ale for GEOPHIRES.
39.         thickness=rows['THICKNESS'][i]*rows['net_to_gro'][i]
40.         depth_Neth=rows['DEPTH'][i]
41.         depth=depth_Neth/1000
42.         Trock=rows['TEMPERATUR'][i]
43.         permeability=rows['PERMEABILIT'][i]
44.
45.         Twater=Trock
46.         T=Twater+273.15
47.         rhewater=(.7983223+(1.50896E-3-2.9104E-6*T)*T)*1E3
48.         prodwellflowrate=((rows['flow_rate_'][i])/3600)*rhewater #convert m3/h to kg/s
49.
50.         # Discharge not reliable input data.
51.         if thickness==0 or depth==0 or Trock==0 or permeability==0 or prodwellflowrate==0:
52.             LCOE.append(np.nan)
53.             Epower.append(np.nan)
54.             FlowOPT.append(np.nan)
55.
56.         else:
57.

```

```
58.     # Calculate the impedance to be used in the Ramey model.
59.     muwater=2.414E-5*np.power(10,247.8/(Twater+273.15-140))
60.     wellsep=707
61.     prodwelldiam=12.25*0.0254 #convert inches to cm
62.     impedance=((muwater/(thickness*permeability))*np.log((4*wellsep)/(math.pi*prodw
    elldiam)))*1000000)/4 #divided by 4 to consider one doublet in the 5-spots.
63.
64.     Tsurf=10.5
65.     gradient=((Trock-Tsurf)/depth)
66.
67.     # LCOE and FLOW-RATE OPTIMIZATION.
68.     # Define the variable of STOP for the while loop.
69.     found_flowrate=False
70.
71.     # Assign a random value to the first flow-rate to be tested.
72.     prodwellflowrate=np.float64(1.0)
73.
74.     # Assign a very high value to the first LCOE.
75.     oldLCOE=1000000
76.
77.     # Assign the boolean 0 to the variable that test when the new LCOE is higher than the la
    st found (this means that the minimum has been passed).
78.     boundary_crosses=0
79.
80.     # This cycle keeps on testing different values of flow-
    rate until the minimum LCOE is found.
81.     while found_flowrate==False:
82.
83.         # Search for the variable input values in the intermediate input text file and replace t
    hem with the reservoir parameters.
84.         fin=open("geoINPUTel.txt", "rt")
85.         data=fin.read()
86.         data=data.replace('@depth', depth.astype('str'))
87.         data=data.replace('@gradient', gradient.astype('str'))
88.         data=data.replace('@prodwell', prodwellflowrate.astype('str'))
89.         data=data.replace('@impedance', impedance.astype('str'))
90.
91.         fin.close()
92.
93.         #Save the updated intermediate input file as the proper input file for GEOPHIRES.
94.         fin=open("E_Input.txt", "wt")
95.         fin.write(data)
96.         fin.close()
97.
98.         # Run GEOPHIRES and save the found LCOE.
99.         simulation=GEOPHIRES_Test2.MainFunction()
100.        LCOE_res=(simulation[0])
101.
102.        # As long as the found LCOE is lower than the previous one, increase the flow-
    rate by 5 kg/s. When the found LCOE is higher than the previous one, decrease the flow-
    rate by 1 kg/s. Keep testing the flow-
    rate until the found LCOE is again higher than the previous one. Stop the simulation and save
    the found LCOE.
103.        if boundary_crosses==0:
104.            if LCOE_res>oldLCOE:
105.                boundary_crosses=1
106.                prodwellflowrate-=1
107.            else:
108.                prodwellflowrate+=5
109.        else:
110.            if LCOE_res>oldLCOE:
```

---

```

111.         found_flowrate=True
112.     else:
113.         prodwellflowrate-=1
114.
115.         oldLCOE=LCOE_res
116.         print('Current flowrate {}'.format(prodwellflowrate))
117.
118.         # The optimization stops when the flow-rate value is not acceptable as well.
119.         if prodwellflowrate <=0:
120.             found_flowrate=True
121.
122.
123.         if prodwellflowrate <= 0:
124.             LCOE.append(np.nan)
125.             Epower.append(np.nan)
126.             FlowOPT.append(np.nan)
127.         else:
128.             LCOE.append(LCOE_res*0.91) #convert from c/kWh in Dollars to c/ kWth in Euros
129.
130.             Epower.append(simulation[1])
131.             FlowOPT.append(prodwellflowrate)
132.
133.         # Save simulation results both in CSV and XLSX format.
134.         rows["basin"]=str(k)
135.         rows["LCOE"]=LCOE
136.         rows["Epower"]=Epower
137.         rows["GEOflow"]=FlowOPT
138.
139.         rows.to_excel("El_Output_xls/EL_{}.xlsx".format(k))
140.         rows.to_csv("El_Output_csv/EL_{}.csv".format(k))
141.
142.
143.
144. # Save all the results into a CSV file and a XLSX file.
145. df_list=[]
146.
147. basins = ['RBSHN', 'DC_STACKED', 'KN_STACKED', 'KNGLG_KNGLS', 'KNNSB', 'KNNSF_
KNNSP', 'KNNSG', 'KNNSL', 'KNNSR', 'KNNSY', 'N_STACKED', 'NLFFD', 'NLFFS', 'NLLFR', '
NLLFS', 'NMRFT', 'NMRFV', 'NMVFS', 'NMVfV', 'RBMDL', 'RBMDU', 'RBMH', 'RBMVL', 'RB
MVU', 'RNROF', 'RNSOB', 'RO_STACKED', 'ROSL_ROSLU', 'ROSL', 'SLDN_STACKED', 'TR
_STACKED', 'DCD', 'DCH', 'DC_STACKED']
148.
149. for k in basins:
150.
151.     df_list.append(pd.read_csv("El_Output_csv/EL_{}.csv".format(k)))
152.
153. fullH_df = pd.concat(df_list)
154.
155. fullH_df.to_csv("El_Output_Plot/TOT_el_output.csv")
156. fullH_df.to_excel("El_Output_Plot/TOT_el_output.xlsx")

```

### ***Input file for LCOE calculation***

```
#####  
#@author: selene  
#####  
#This general GEOPHIRES input text file contains all the input variables #either used or not used for  
the simulation of the Dutch basins. The used #parameters are the ones always required plus the ones  
needed for our #project purposes. The not used parameters are all optional.  
#With the term 'BASIN' I refer to each formation which is represented by a #map (put together from  
the ThermoGIS dataset) and a correspondent CSV file.  
#With the term 'RESERVOIR' I refer to each of the 1x1km squares in which #each basin is discretized.  
It corresponds to one single record in a CSV #input file.  
#The number before each parameter corresponds to the ones given in the #GEOPHIRES Manual.  
#Note from GEOPHIRES manual: The GEOPHIRES v2.0 python code scans the input #file for each  
necessary "parameter, value". Therefore, the user cannot #change the string before the parameter value  
and the comma is the required #delimiter. Each parameter string may only appear once in this input  
file. #However, the parameters can be in any order and comments can be added #either by including
```



---

extra lines or by typing it after the parameter value, #separated by a comma. If a necessary parameter is not provided, a default #value is assumed, and a warning message is printed to the console.

-----  
-----  
#\*\*\*\*\*  
#\*\*\*A) Subsurface Technical Parameters\*\*\*  
#\*\*\*\*\*

1. Reservoir Model,4, #---[-] dflt 4 - range[1,6]  
#chosen this one because it is the closest  
to the Dutch sedimentary basins  
#1: Multiple parallel fractures model  
#2: 1D linear heat sweep model  
#3: m/a single fracture drawdown model  
#4: Linear thermal drawdown model  
#5: Generic user-provided temperature  
profile  
#6: TOUGH2
2. Drawdown Parameter,0.000, #---[1/year] no dflt  
#we make the hp of no drawdown T
5. Reservoir Depth,@depth, #---[km] dflt 3 - range[0.1,15]  
#taken from the CSV input file
6. Number of Segments,1, #---[-] dflt 1 - range[1,2,3,4]  
#because we analyze one reservoir per time
7. Gradient 1,@gradient, #---[°C/km] dflt 50 - range[0,500]  
#calculated from the CSV input file
14. Maximum Temperature,400, #---[°C] dflt 400 - range[50,1000]
15. Number of Production Wells,1,#---[-] dflt 2 - range[1,20]  
#because of the configuration: grid of 5  
spots (1 inj well serving 4 prod wells; each prod  
well receives from 4 inj wells)
16. Number of Injection Wells,1, #---[-] dflt 2 - range[1,20]  
#because of the configuration: grid of 5  
spots (1 inj #well serving 4 prod wells; each prod  
well receives from 4 inj wells)
17. Production Well Diameter,12.25,#---[inch] dflt 8 - range[1,30]  
#taken from GEOPHIRES manual
18. Injection Well Diameter,12.25,#---[inch] dflt 8 - range[1,30]  
#taken from GEOPHIRES manual
19. Ramey Production Wellbore Model,1,#---[-] dflt 1 - range 0(disable) or  
1(enable)  
#we decide to use it
21. Injection Wellbore Temperature Gain,0,#---[°C]dflt 0 - range[-5,50]  
#we make the hp of no T gain
22. Production Flow Rate per Well,@prodwell,#---[kg/s] dflt 50 -  
range[1,500]  
#taken from the CSV input file
27. Reservoir Volume Option,4, #---[-] dflt 4 if reservoir model 1 or  
2, 3 if reservoir model 3, 4, 5 or 6 -  
range[1,2,3,4]  
#because we don't consider fractures  
#1: Specify number of fractures and fracture separation  
#2: Specify reservoir volume and fracture separation  
#3: Specify reservoir volume and number of fractures  
#4: Specify reservoir volume only (sufficient for  
reservoir models 3, 4, 5 and 6)
30. Reservoir Volume,125000000, #---[m3] dflt 500x500x500 = 125000000 -  
range[10,1E12] - required if reservoir  
volume option 3 or 4

APPENDIX  
PROGRAM SCRIPTS AND INPUT FILES

---

```

#default
31. Water Loss Fraction,0, #---[-] dflt 0 - range[0,0.99] -
    required if reservoir volume option 3 or
    4
    #we make the hp of no water loss
32. Reservoir Impedance,@impedance,#---[GPa*s/m3] dflt 0.1 - range[1E-4,1E4]
    required if not specified productivity and
    injectivity indexes
    #calculated from the CSV input file for a pair of wells (so
    already divided by 4 to account for the flow distribution in
    the wells)
42. Reservoir Thermal Conductivity,3, #---[W/m/K] dflt 3 -
    range[0.01,100]- required if Ramey's
    model, or reservoir model = 1, 2 or 3, or
    reservoir model = 6 and use of built-in
    TOUGH2 model
    #taken from NL ThermoGIS Manual pag.32
38. Injection Temperature,30, #---[°C] dflt 70 - range[0,200]
    #taken from NL ThermoGIS paper
39. Maximum Drawdown,1, #---[-] dflt 1 - range[0,1] -
    required if reservoir model 1, 2, 3, 4
    #we make the hp not to consider redrilling
    #0: Redrilling considered
    #1: No redrilling considered
40. Reservoir Heat Capacity,1000,#---[J/kg/K] dflt 1000 - range[100,10000]
    #we take the default value
41. Reservoir Density,2500, #---[kg/m3] dflt 2700 - range[100,10000]
    #we choose the value to make it consistent
    with alpha - see NL ThermoGIS manual p.32

***not used A) parameters***
*****
#3. Reservoir Output File Name, ---dflt: ReservoirOutput.txt - required if reservoir model 5
#4. TOUGH2 Model/File Name, ---dflt: ReservoirOutput.txt - required if reservoir model 5
#8. Gradient 2, ---[°C/km] dflt 50 - range[0,500] - required if number of segments
> 1
#10. Gradient 3, ---[°C/km] dflt 50 - range[0,500] - required if number of segments
> 2
#12. Gradient 4, ---[°C/km] dflt 50 - range[0,500] - required if number of segments
> 3
#9. Thickness 1, ---[km] dflt 2 - range[0.01,100] - required if number of segments
> 1
#11. Thickness 2, ---[km] dflt 2 - range[0.01,100] - required if number of segments
> 2
#13. Thickness 3, ---[km] dflt 2 - range[0.01,100] - required if number of segments
> 3
#20. Production Wellbore Temperature Drop, ---[°C] dflt 5 - range[-5,50] - required if Ramey's
model is disabled
#23. Fracture Shape, ---[-] dflt 1 - range[1,2,3,4] - required if reservoir model 1 or 2
    # 1: Circular fracture with known area
    # 2: Circular fracture with known diameter
    # 3: Square fracture
    # 4: Rectangular fracture
#24. Fracture Area, ---[m2] dflt 250000 - range[1,1E8] - required if reservoir model 1
or 2 and fracture shape 1
#25. Fracture Height, ---[m] dflt 500 - range[1,10000] - required if reservoir model 1 or 2
and fracture shape 2, 3 or 4
#26. Fracture Width, ---[m] dflt 500 - range[1,10000] - required if reservoir model 1 or 2
and fracture shape 4
#28. Number of Fractures, ---[-] dflt 10 - range[1,20] - required if reservoir model 1 or 2 and
reservoir volume option 1 or 3
#29. Fracture Separation, ---[m] dflt 50 - range[1,1E4] - required if reservoir model 1 or 2 and
reservoir volume option 1 or 2

```

---

```

#33. Productivity Index,      ---[kg/s/bar] dflt 10 - range[1E-2,1E4] - required if not specifying
reservoir impedance and no flash power plant considered
#34. Injectivity Index,      ---[kg/s/bar] dflt 10 - range[1E-2,1E4] - required if not specifying
reservoir impedance
#35. Reservoir Hydrostatic Pressure, ---[kPa] dflt Built-in equation - range[1E2,1E5] - required
if specified productivity and #injectivity indexes
#36. Production Wellhead Pressure, ---[kPa] dflt WaterVapourPressure(at initial production
T+344.7) - range[0,1E4] - required #if specified productivity index
#37. Plant Outlet Pressure, ---[kPa] dflt 100 kPa if flash power plant
# Production wellhead pressure – 68.95 kPa (10 psi) in all other cases
# - range[0,1E4] - required if specified injectivity index
#43. Reservoir Porosity, ---[-] dflt 0.04 - range[0.001,0.99] - required if reservoir
model = 2, or reservoir model # = 6 and use of built-in TOUGH2 model
#44. Reservoir Permeability, ---[m2] dflt 1E-13 - range[1E-20,1E-5] - required if reservoir model =
6 and use of built-in TOUGH2 model
#45. Reservoir Thickness, ---[m] dflt 250 - range[10,10000] - required if reservoir model = 6 and
use of built-in TOUGH2 model
#46. Reservoir Width, ---[m] dflt 500 - range[10,10000] - required if reservoir model = 6 and
use of built-in TOUGH2 model
#47. Well Separation, ---[m] dflt 1000 - range[10,10000] - required if reservoir model = 6 and
use of built-in TOUGH2 model
#*****
#****B) Surface Technical Parameters****
#*****
48. End-Use Option,1, #---[-] dflt 1 -
range[1,2,31,32,41,42,51,52]
#the simulation is run twice: once for case
2 to compare the results and once for case 1 to
complete the analysis

# 1: Electricity (LCOE) in ¢/kWh e
# 2: Direct-Use Heat (LCOH) in $/MMBTU #here we convert it in ¢/kWh el
#31: CHP Topping Cycle with electricity as main product (LCOE) in ¢/kWh el
#32: CHP Topping Cycle with heat as main product (LCOH) in $/MMBTU
#41: CHP Bottoming Cycle with electricity as main product (LCOE) in ¢/kWh el
#42: CHP Bottoming Cycle with heat as main product (LCOH) in $/MMBTU
#51: CHP Parallel Cycle with electricity as main product (LCOE) in ¢/kWh el
#52: CHP Parallel Cycle with heat as main product (LCOH) in $/MMBTU
49. Power Plant Type,1, #---[-] dflt 1 - range[1,2,3,4] –
required if the end-use option is 1, 31,
32, 41, 42, 51 or 52
#we take the default value
#1: Subcritical ORC
#2: Supercritical ORC
#3: Single-flash
#4: Double-flash
50. Circulation Pump Efficiency,0.75,#---[-] dflt 0.75 - range[0.1,1]
#GEOPHIRES default
51. Utilization Factor,0.9, #---[-] dflt 0.90 - range[0.1,1]
#taken from LAZARD capacity factor
55. Surface Temperature,10.5, #---[°C] dflt 15 - range[-50,50]
#taken from NL ThermoGIS Manual pag.31

56. Ambient Temperature,10.5, #---[°C] dflt 15 - range[-50,50] –
required if the end-use option
is 1, 31, 32, 41, 42, 51, or 52
#we make the hp that surface T = ambient T

#***not used B) parameters***
#*****
#52. End-Use Efficiency Factor,0.9, #---[-] dflt 0.90 - range[0.1,1] - required if the end-use
option is 2, 31, 32, 41, 42, 51, or 52 #we take the default value
#53. CHP Fraction, #---[-] dflt 0.5 - range[0.0001, 0.9999] - required if the end-use
option is 51 or 52

```

---

APPENDIX  
PROGRAM SCRIPTS AND INPUT FILES

---

```
#54. CHP Bottoming Entering Temperature,    ---[°C]  dflt 150 - range[Injection Temperature,
Maximum Temperature] - required if the end-use option is 41 or 42
#*****
#*****C) Financial Parameters*****
#*****

57. Plant Lifetime,25,      #---[years] dflt 30 - range[1,100]
                               #taken from LAZARD

58. Economic Model,2,      # ---[-]  dflt 2 - range[1,2,3]
                               #we decide for standard LCOH and LCOE as
                               economic indicators
                               #1: Fixed Charge Rate Model
                               #2: Standard Levelized Cost Model
                               #3: BICYCLE Levelized Cost Model

60. Discount Rate,0.054,   #---[-]  dflt 0.07 - range[0,1] -
                               required if economic model 2
                               #taken from LAZARD for LCOE LAZARD and from
                               NL ThermoGIS paper as a Weighted Average Capital Cost
                               for LCOE expected

69. Inflation Rate During Construction,0,# ---[-]  dflt 0 - range[0,1]
                               #hp of overnight cost

#***not used C) parameters***
#*****
#59. Fixed Charge Rate,      ---[-]  dflt 0.1 - range[0,1] - required if economic model 1
#61. Fraction of Investment in Bonds,    ---[-]  dflt 0.5 - range[0,1] - required if economic model 3
#62. Inflated Bond Interest Rate,    ---[-]  dflt 0.05 - range[0,1] - required if economic model 3
#63. Inflated Equity Interest Rate,    ---[-]  dflt 0.1 - range[0,1] - required if economic model 3
#64. Inflation Rate,      ---[-]  dflt 0.02 - range[-0.1,1] - required if economic model 3
#65. Combined Income Tax Rate,    ---[-]  dflt 0.3 - range[0,1] - required if economic model 3
#66. Gross Revenue Tax Rate,    ---[-]  dflt 0 - range[0,1] - required if economic model 3
#67. Investment Tax Credit Rate,    ---[-]  dflt 0 - range[0,1] - required if economic model 3
#68. Property Tax Rate,      ---[-]  dflt 0 - range[0,1] - required if economic model 3
#*****
#***D) Capital and O&M Cost Parameters***
#*****

72. Well Drilling and Completion Capital Cost Adjustment Factor,1, #---[-]
    #dflt 1: use built-in correlation as it is - range[0,10] - required if no well drilling and
    completion capital cost number provided
    #we want to use the built-in correlations of GEOPHIRES

73. Well Drilling Cost Correlation,3, #---[-]  dflt 1 - range[1,2,3,4]
    #required if no valid fixed well drilling and completion
    capital cost is provided
    #1: vertical open-hole, small diameter (8.5 inch)
    #2: deviated liner, small diameter (8.5 inch)
    #3: vertical open-hole, large diameter (12.25 inch)
    #4: deviated liner, large diameter (12.25 inch)

74. Reservoir Stimulation Capital Cost,0, #---[M$]
    #dflt built-in capital cost correlations - range[0,100] - optional
    #we want to use the built-in correlations of GEOPHIRES

75. Reservoir Stimulation Capital Cost Adjustment Factor,1, #---[-]
    #dflt 1: use built-in correlation as is - range[0,10] - required if no reservoir stimulation capital
    cost number provided
    #we want to use the built-in correlations of GEOPHIRES

76. Surface Plant Capital Cost,, #---[M$]
    #dflt built-in capital cost correlations - range[0,1000] - optional
    #we want to use the built-in correlations of GEOPHIRES

77. Surface Plant Capital Cost Adjustment Factor,1, #---[-]
    #dflt 1: use built-in correlation as is - range[0,10] - required if no surface plant capital cost
    number provided
    #we want to use the built-in correlations of GEOPHIRES

78. Field Gathering System Capital Cost,, #---[M$]
    #dflt built-in capital cost correlations - range[0,100] - optional
```

---

```

#we want to use the built-in correlations of GEOPHIRES
79. Field Gathering System Capital Cost Adjustment Factor,1, #---[-]
#dflt 1: use built-in correlation as it is - range[0,10] - required if no field gathering system
capital cost number provided
#we want to use the built-in correlations of GEOPHIRES
80. Exploration Capital Cost,1, #---[M$]
#dflt built-in capital cost correlations - range[0,100] - optional
#we want to use the built-in correlations of GEOPHIRES

81. Exploration Capital Cost Adjustment Factor,1, #---[-]
#dflt 1: use built-in correlation as is - range[0,10] - required if no exploration capital cost
number provided
#we want to use the built-in correlations of GEOPHIRES
82. Total O&M Cost,, #---[M$/year]
#dflt built-in O&M cost correlations - range[0,100] - optional
#we want to use the built-in correlations of GEOPHIRES

83. Wellfield O&M Cost,, #---[M$/year]
#dflt built-in O&M cost correlations - range[0,100] - optional
#we want to use the built-in correlations of GEOPHIRES

84. Wellfield O&M Cost Adjustment Factor,1, #---[-]
#dflt 1: use built-in correlation as is - range[0,10] - required if no annual wellfield O&M cost
number provided
#we want to use the built-in correlations of GEOPHIRES
85. Surface Plant O&M Cost,, #---[M$/year]
#dflt built-in O&M cost correlations - range[0,100] - optional
#we want to use the built-in correlations of GEOPHIRES

86. Surface Plant O&M Cost Adjustment Factor,1, #---[-]
#dflt 1: use built-in correlation as is - range[0,10] - required if no annual surface plant O&M
cost number provided
#we want to use the built-in correlations of GEOPHIRES
87. Water Cost,, #---[M$/year]
#dflt built-in make-up water cost correlations - range[0,100] - optional
#we want to use the built-in correlations of GEOPHIRES
88. Water Cost Adjustment Factor,1, #---[-]
#dflt 1: use built-in correlation as is - range[0,10] - required if no annual make-up water cost
number provided
#we want to use the built-in correlations of GEOPHIRES
#***not used D) parameters***
#*****
#70. Total Capital Cost, ---[M$] dflt built-in capital cost correlations - range[0,1000] -
optional
#71. Well Drilling and Completion Capital Cost, ---[M$] dflt built-in capital cost correlations -
range[0,200] - optional
#89. Electricity Rate, ---[$/kWh] dflt 0.07 -range[0,1] - required if end-use option 2, 32,
42, or 52 #taken from #NL ThermoGIS paper and converted into dollars for LCOH
#90. Heat Rate, ---[$/kWh] dflt 0.02 -range[0,1] - required if end-use option 31, 41,
or 51
#*****
#*****E) Simulation Parameters*****
#*****
91. Print Output to Console,1, #---[-] dflt 1 - range 0 (disable) or
1(enable)

92. Time steps per year,1, # ---[-] dflt 4 - range[1,100]

```

